Summary of Magnetic Fusion plasma session

Ge Zhuang, Adi Liu

on behalf of all the MF session contributors

Outline

- Contributions to MF
- Major Progresses
  - Major progresses of machines
  - ELM control/simulation and RMP
  - MHD and EP physics
  - Transport and confinement
  - SOL/divertor/PMI physics
  - Scenario/Integrated model
  - Discharge Control/Diagnostics/Disruption

General Information for MF

- Plenary (4)
- Invited (44)
- Oral (41)
- Poster (32)
- Total : 121

Outline

- Contributions to MF
- Major Progresses
  - Major progresses of machines
  - ELM control/simulation and RMP
  - MHD and EP physics
  - Transport and confinement
  - SOL/divertor/PMI physics
  - Scenario/Integrated model
  - Discharge Control/Diagnostics/Disruption

PL20: KSTAR [Si-Woo Yoon]

Overview of KSTAR results and Plan

Important developments for advanced scenario have been achieved: early diverting, long-pulse capabilities and high Ti operation

Early Diverting at 0.5 sec

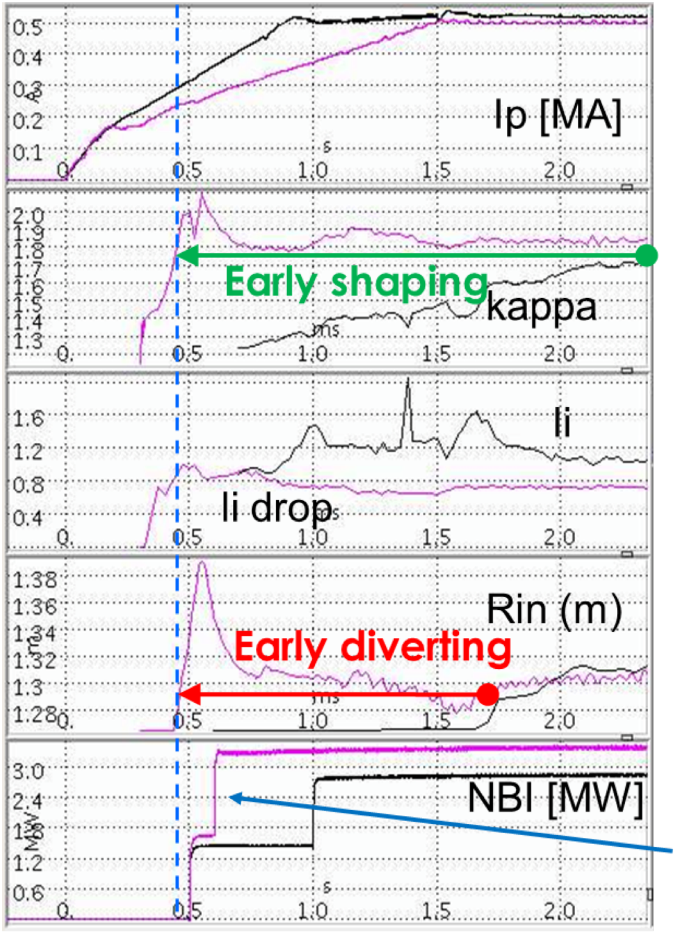

New record of pulse length ~90 sec (2018, #21735)

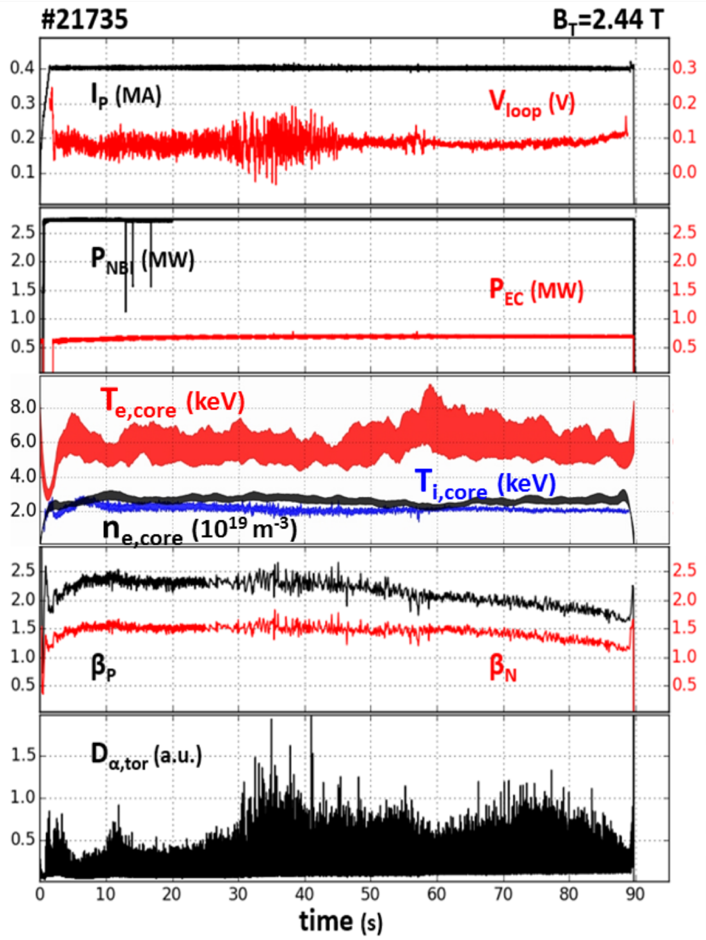

High T_i with stable ITB

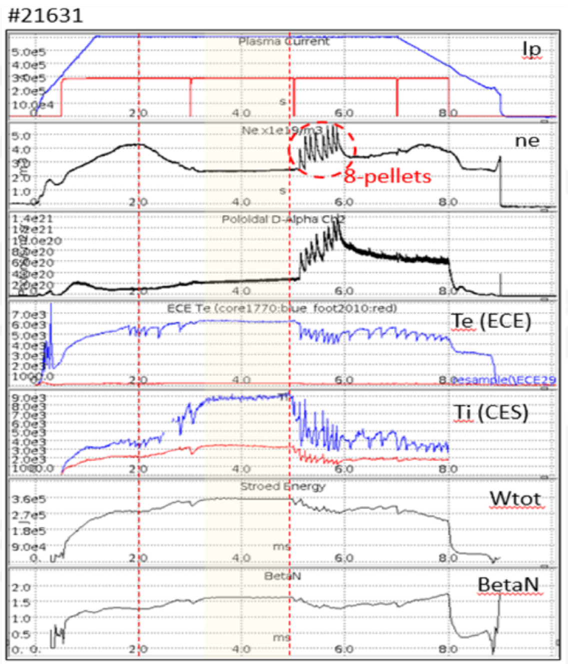

I26: KSTAR advanced operation [Jinil Chung]

Experimental studies on advanced operation scenarios in KSTAR

Early shaping & diverting (< 0.5 s)

#15433 : typical H-mode
#20812 : new scenario

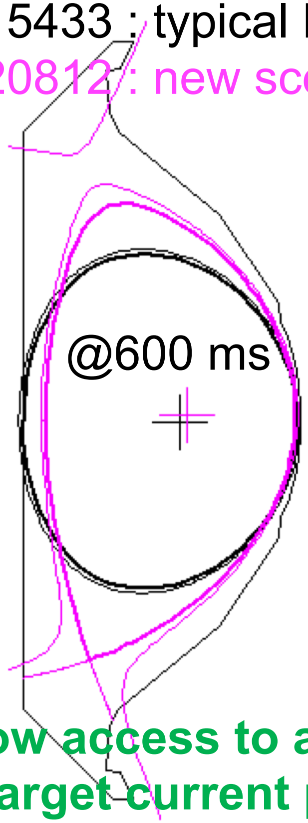

Allow access to a wide range of target current profiles

focused scenarios in KSTAR :
long pulse(~90s), high β_p, high q_{min}, high l_i, hybrid, ITB, low q_{95}

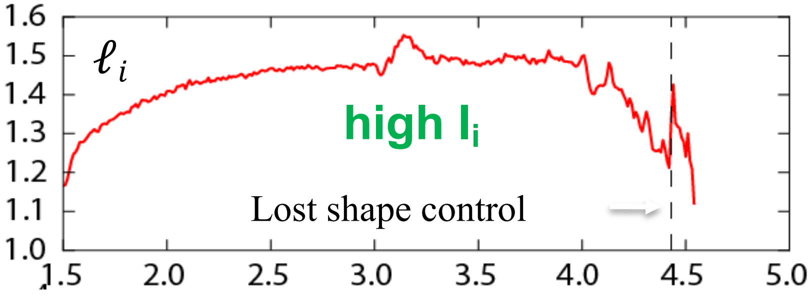

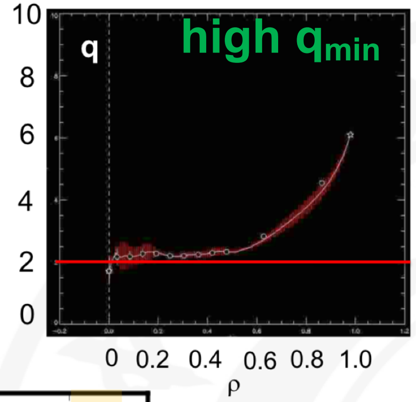

high β_p

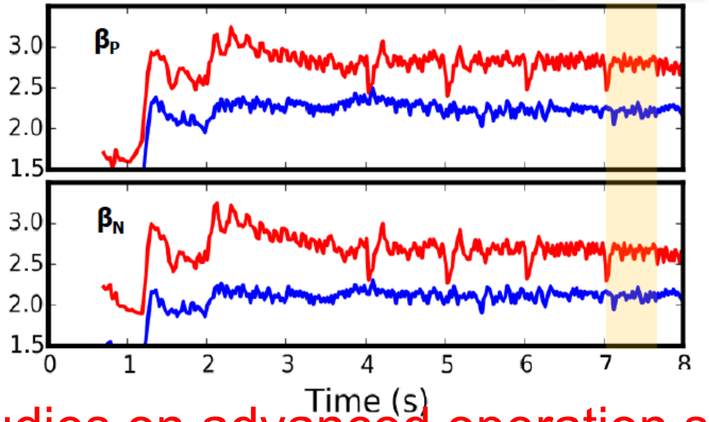

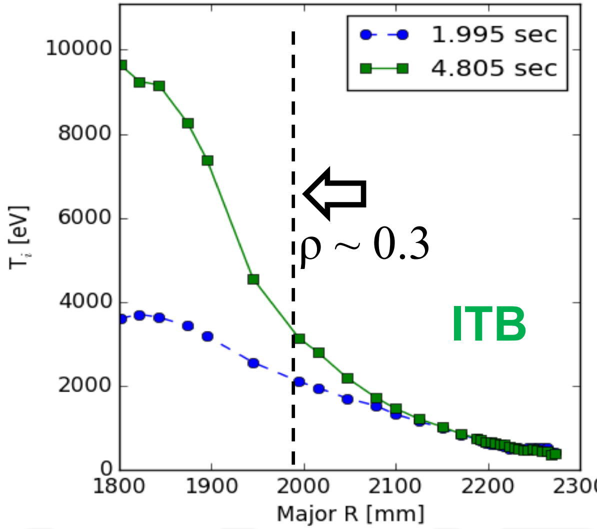

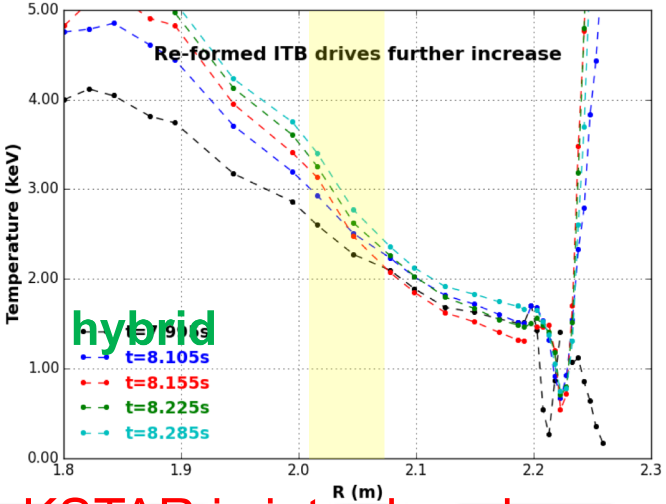

recent progress of experimental studies on advanced operation scenarios in KSTAR is introduced, such as high βp, high li, high q_{min}, hybrid, ITB and low q.

PL14: HL-2A [Min Xu]

Advances in understanding of turbulent transport and confinement improvement in HL-2A

- Modulation of **turbulence by MHD** has been systematically studied in the HL-2A tokamak
- It was found that residual stress drives an off-diagonal turbulent momentum flux and its divergence defines an **intrinsic poloidal torque**.
- The study reveals that the damped **zonal flow** results in edge cooling which excites MHD instability and even disruption.
- Radial **transport of impurity ions** is strongly enhanced in the plasma core region with the on-axis ECRH.
- The **pedestal dynamics** and the underlying physics have been extensively studied.
- The increase of the mean E×B **shear flow** plays a key role in L-H transition
- **ELM mitigation** realized by using LHCD, impurity seeding, RMP.
- Turbulence and transport, MHD and energetic particle physics under β_N high plasmas will be emphasized in the future.

Understandings of the multi-scale physics, the nonlinear coupling between flows, MHD and turbulences

PL23: EAST [Xianzu Gong]

Overview of experimental results in EAST Tokamak

- **Significant progress has been made in EAST SS long-pulse operation and physics research towards CFETR:**
  - Scenario development, H&CD, ELM control, PWI, D&SOL
- **SS scenarios demonstrated with extension of fusion performance:**
  - High f_{BS}~40-50% with improved confinement ($H_{98,y2}$ >1) at high-n_e;
  - Zero/low NBI torque, high performance experiments on EAST offer unique contributions toward ITER and CFETR.
- **Further research on core-edge integration for scenarios development and resolving heat flux issues is essential to extrapolate to SS reactor:**
  - **Lower divertor upgrade** for enhanced heat/particle exhaust compatible with high-performance SS operations.

I40: DIIID-EAST: High-β_P & SS scenario [Andrea Garofalo]

The high poloidal beta path towards steady state tokamak fusion

- **High-β_P regime optimizes at:**
  - low current → low disruption risks
  - high pressure → Shafranov shift suppression of turbulence
  - low pedestal → natural divertor solution
- **Projection of high-β_P scenario to ITER yields SS Q~6 with no rotation, day-one H&CD**
- **Extension of DIII-D high-β_P scenario to EAST achieves performance for SS Q~5 in CFETR**

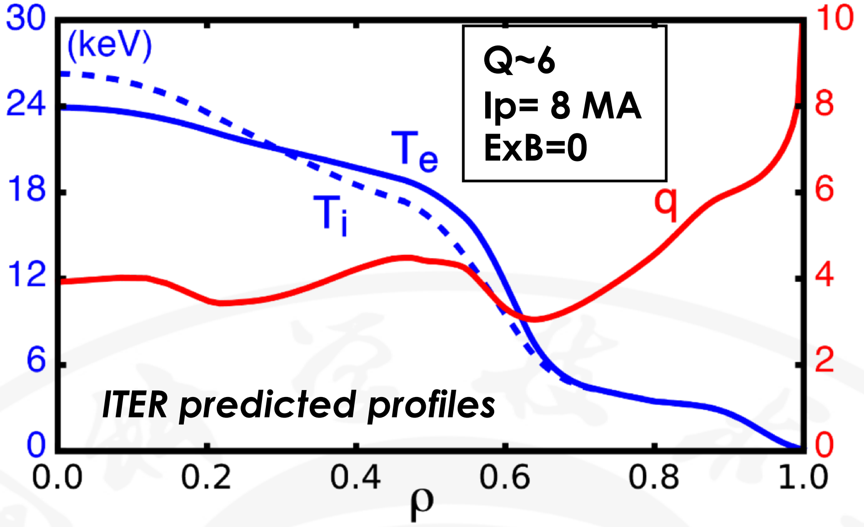

- β_p~2.0/β_N~1.6 using **RF-only**
- V_{loop}~ 0, f_{BS}~40-50% with **f_{GW}~0.6-0.8**

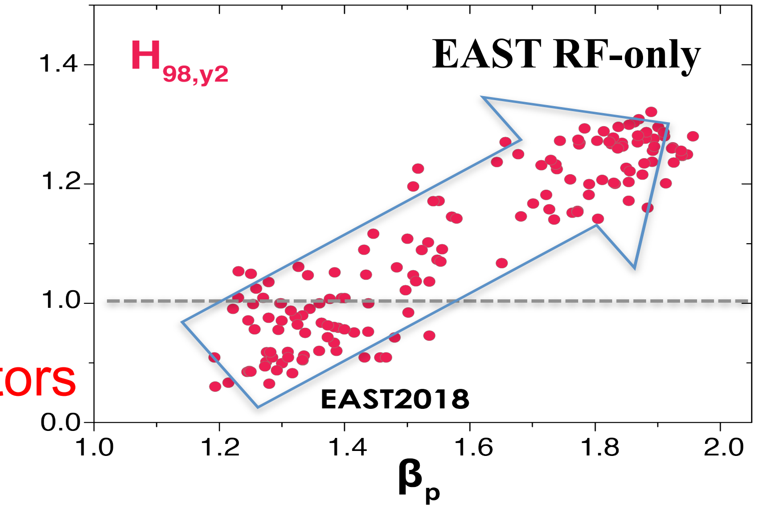

How high-β_P tokamaks provide promise for attractive fusion power reactors

I11: WEST: [Jerome Bucalossi]

First experiments in WEST with tungsten plasma facing components

Successful 1st experiments on WEST paving way for steady state operation in full W-environment

1st phase of operation with inertially cooled lower divertor elements and ITER-like prototypes

- 8 MW of RF power injected (5 LHCD + 3 ICRH)
  - 5 MW of LHCD alone
  - 5 MW of ICRH alone
- Tunsgten radiation dominates (~50% of P_{inj})
- Plasmas prone to tungsten induced MHD
- Intermittent LH-transition observed @ P_{loss}~3MW
- Long pulse achieved (30s+) in USN (actively cooled upper divertor)
- First damages observed on the ITER-like Plasma Facing Units (PFU)
  - Cracks, melting and droplets on the edges of the monoblocks of the misaligned PFU (0.79 mm)
  - Optical hot spot evidenced (local melting) on aligned PFU within ITER tolerance (<0.3mm)

2nd phase of operation (1000s pulses) to start in fall 2020

- Manufacturing of the fully actively cooled ITER-like lower divertor has started (456 PFUs)

B	Ip	R	A	P_{LHCD}	P_{ICRH}	Magnetic conf.
3.7 T	1 MA	2.5 m	5-6	7 MW	9 MW	LSN, USN, DN

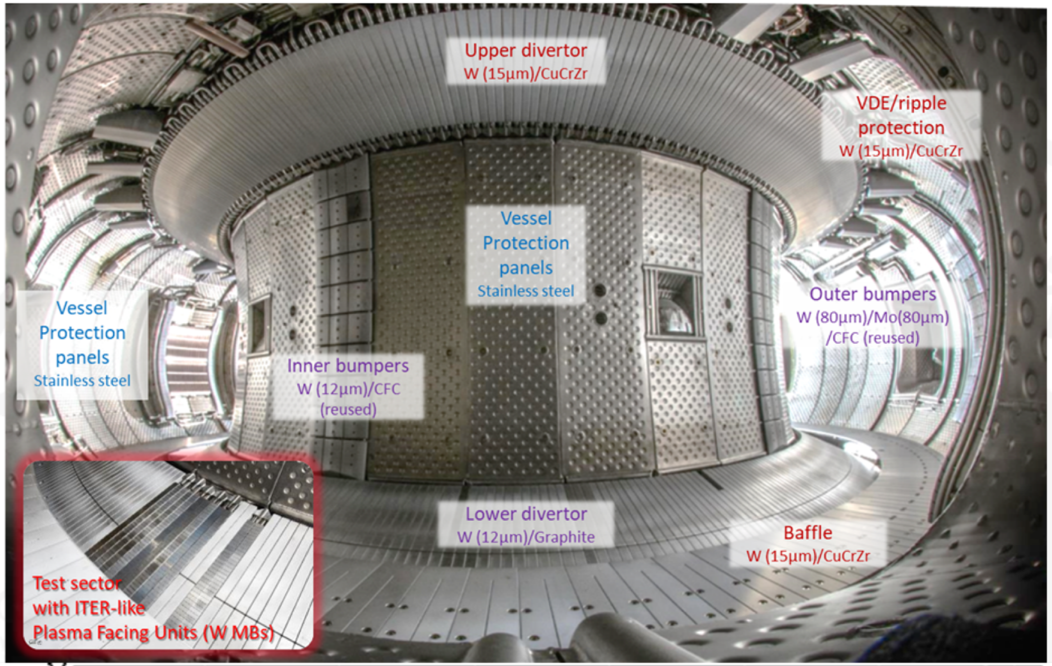

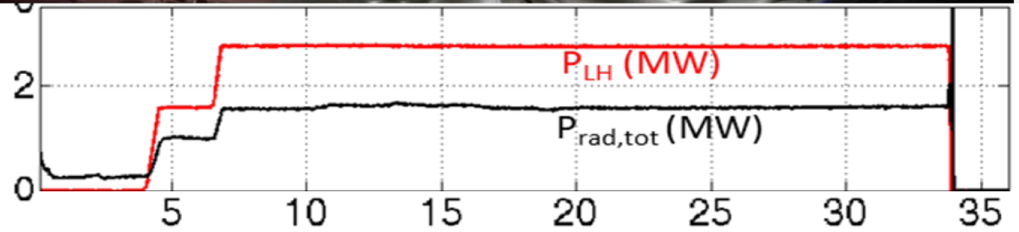

O25: MAST-U [Nick Walkden]

MAST Upgrade status and first results

Super-X Divertor

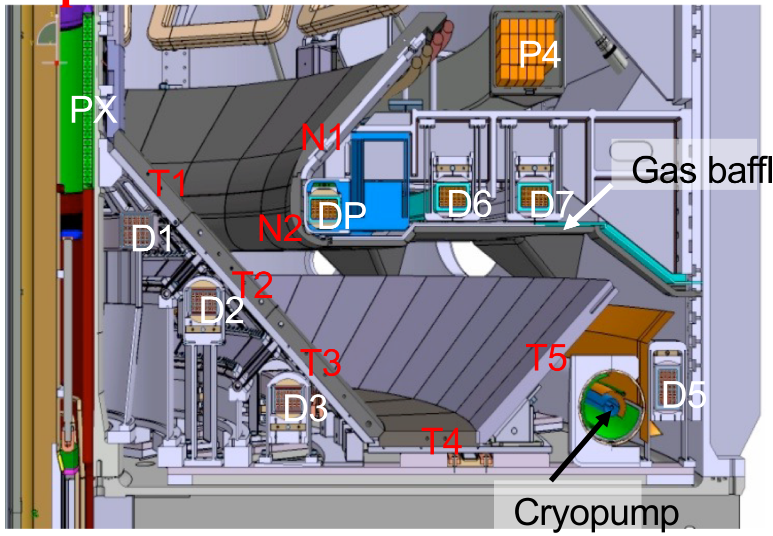

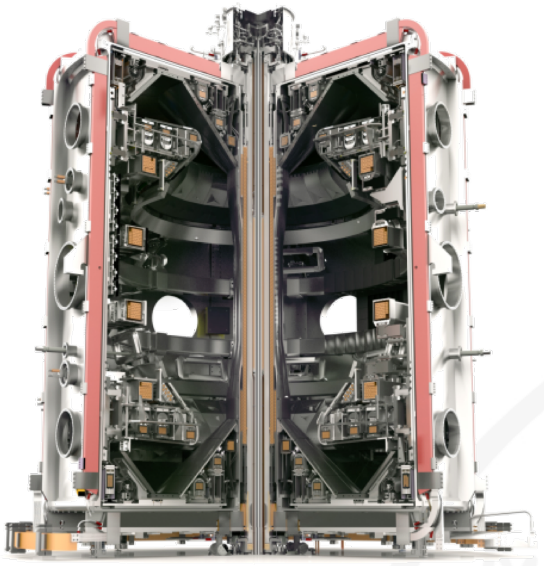

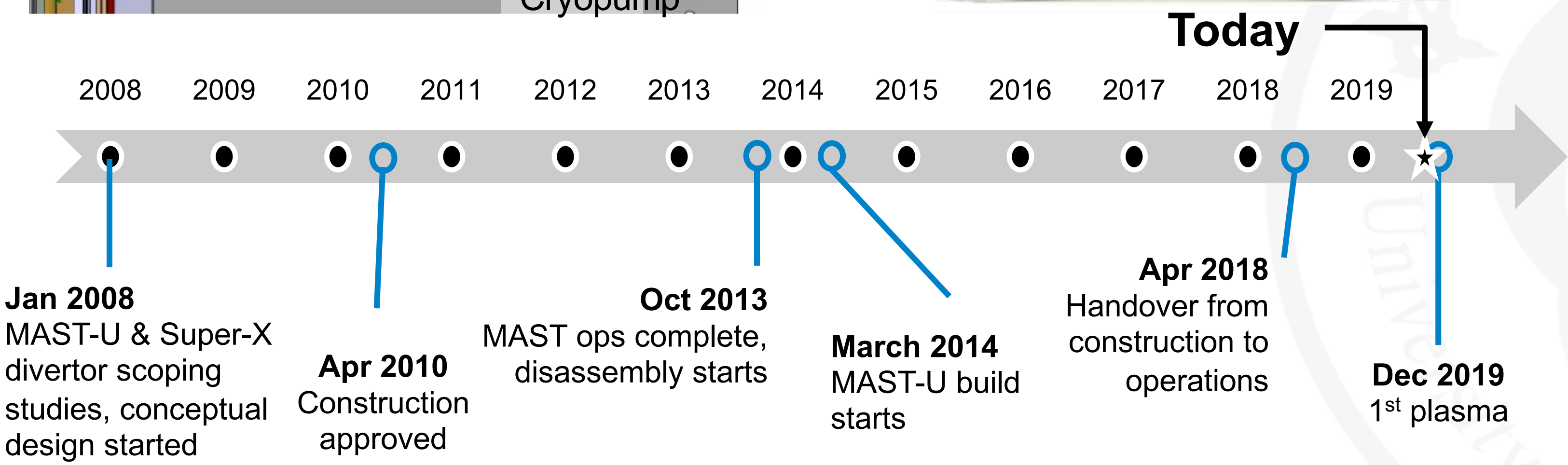

("core scope")

Increased TF
Improved confinement

New Solenoid
Greater I_p, pulse duration

19 New PF Coils
Improved shaping

Super-X Divertor
Improved power handling

Off-Axis NBI
Improved profile control

After upgrade, MAST would get greater Ip and Bt, improved shaping and power handling abilities.

Outline

- Contributions to MF
- Major Progresses
  - Major progresses of machines
  - ELM control/simulation and RMP
  - MHD and EP physics
  - Transport and confinement
  - SOL/divertor/PMI physics
  - Scenario/Integrated model
  - Discharge Control/Diagnostics/Disruption

I9: small/no ELM regime [Guosheng Xu]

Advances in understanding high-performance small/no ELM H-mode regimes

PRL 122 (2019) 255001

Parameter space of the EAST grassy-ELM regime overlaps with the projected 1GW scenario of CFETR

- q_{95} = 5.5-7
- $\beta_N \sim 2$
- $f_{bs} \sim 50\%$
- $n_{el}/n_{GW} \sim 0.8$

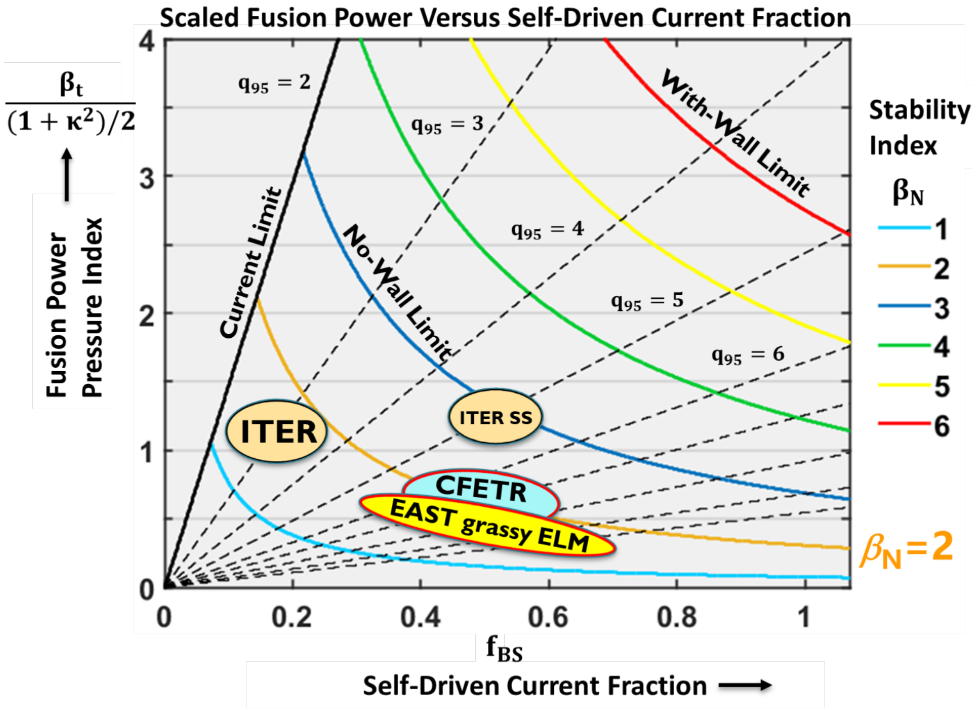

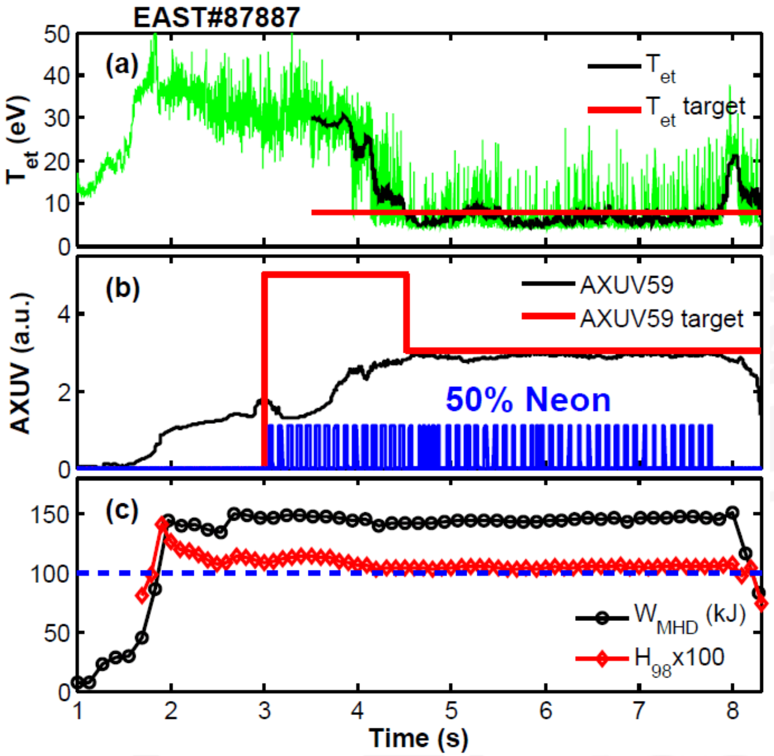

Detachment feedback control

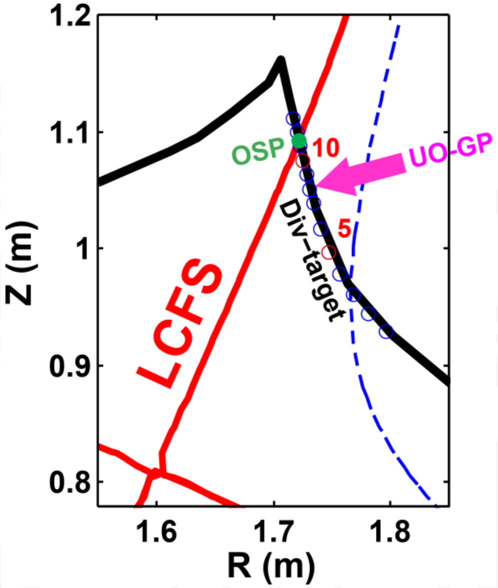

- **Strong particle exhaust capability makes the EAST grassy-ELM regime especially suitable for achieving steady-state operation with metal wall.**
- **Compatibility with partial detachment, high density and fully non-inductive operation has been demonstrated.**

The mechanism of EAST grassy-ELM regime has been revealed, could benefit the CFETR scenario

I32: ELM triggering [Julien Dominski]

Emerging Picture on the Pedestal Dynamics and Triggering Mechanism of ELMs

Study of a "mini-ELM" gives insight on the potential nonlinear mechanisms triggering an Edge Localized Mode (ELM).

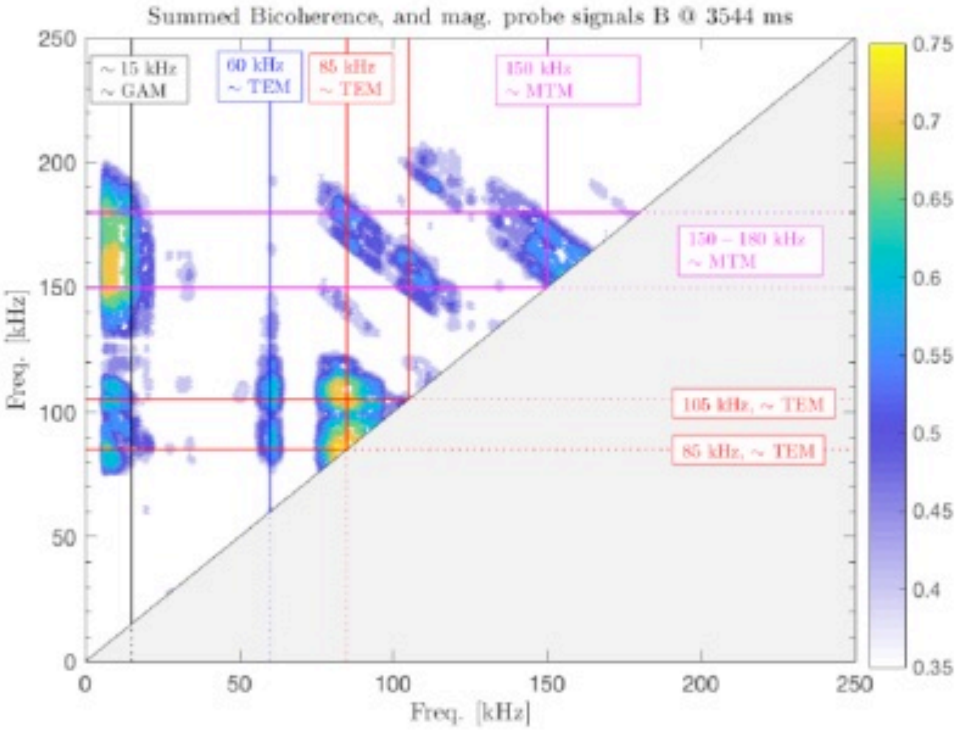

Figure: Bi-coherence during mini-ELM.

- Bi-coherence analysis reveals the nonlinear interactions at play between dominant modes of the mini-ELM.

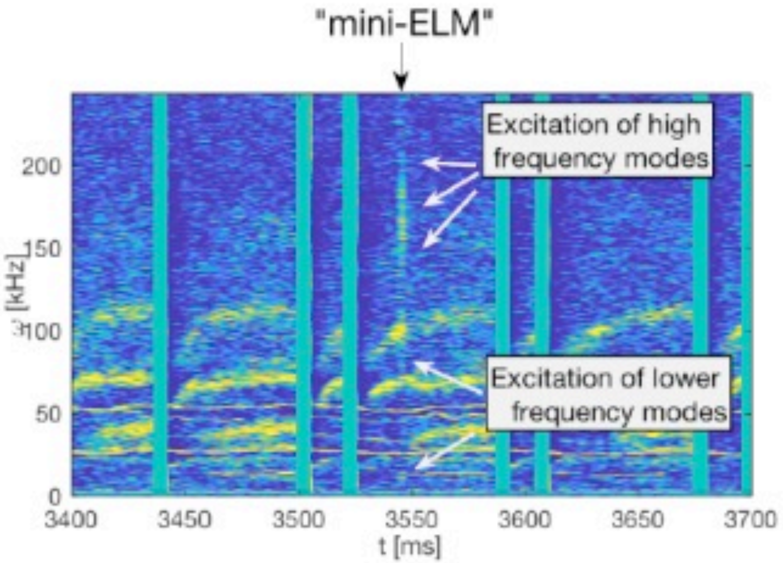

I19: ELM suppression exp. [Zhen Sun]

Real-time impurity powder injection for ELM and H-mode pedestal control in EAST

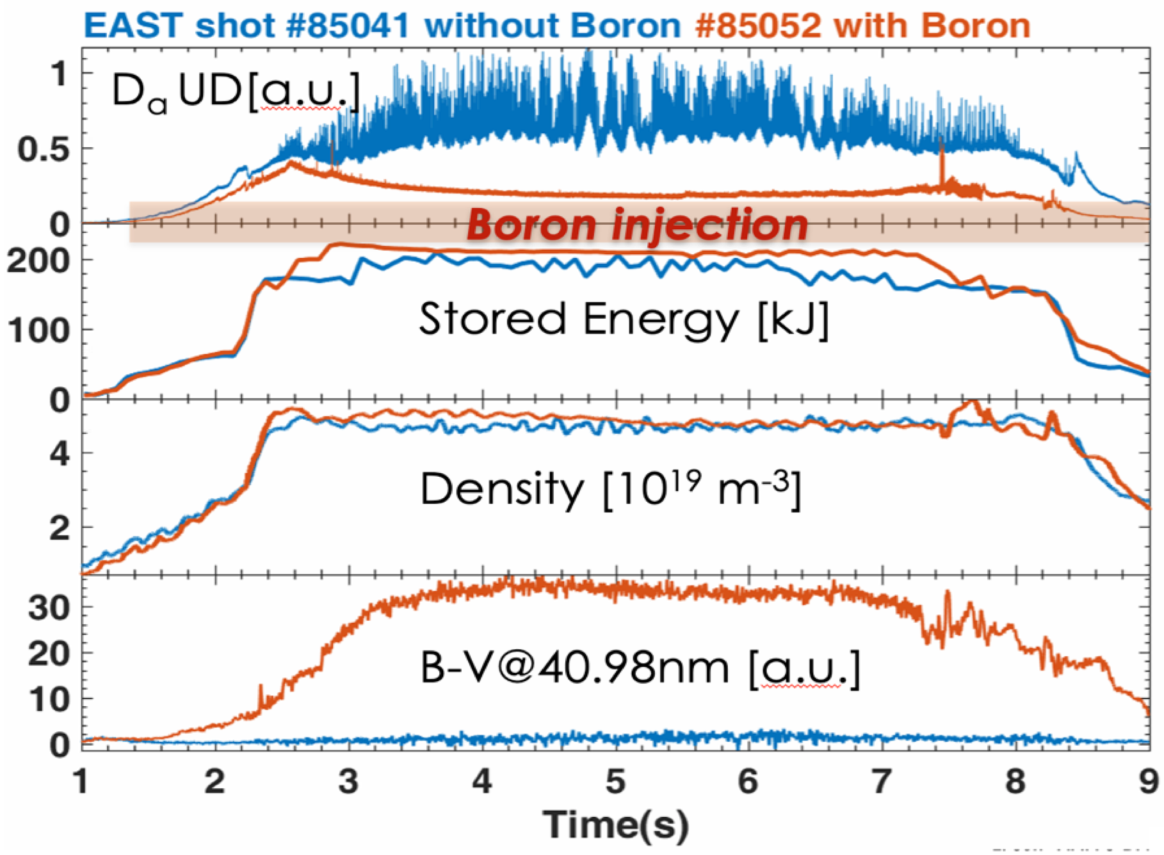

ELM in EAST were completely suppressed by boron powder injection into the X-point region of an upper-single null configuration plasma over a wide range of operating conditions (2.8 < Paux < 7.1 MW, 0.35 < n_e/n_{GW} < 0.82, RF-only and RF+NBI heating scenarios).

The injection of boron powder above the minimum amount for ELM suppression coincides with the occurrence of an edge oscillation with several harmonics in magnetics

boron powder injection into the X-point could achieve complete ELM suppression over a wide plasma parameters.

I31: ELM structure [Monica Spolaore]

Edge Localized Modes electromagnetic fine structure in the Scrape-Off Layer of tokamak discharges

ELM electrostatic and magnetic features were investigated in details in tokamak configurations of COMPASS and RFX-mod

COMPASS (Prague, Czech Rep.)   RFX-mod (Padova, Italy)

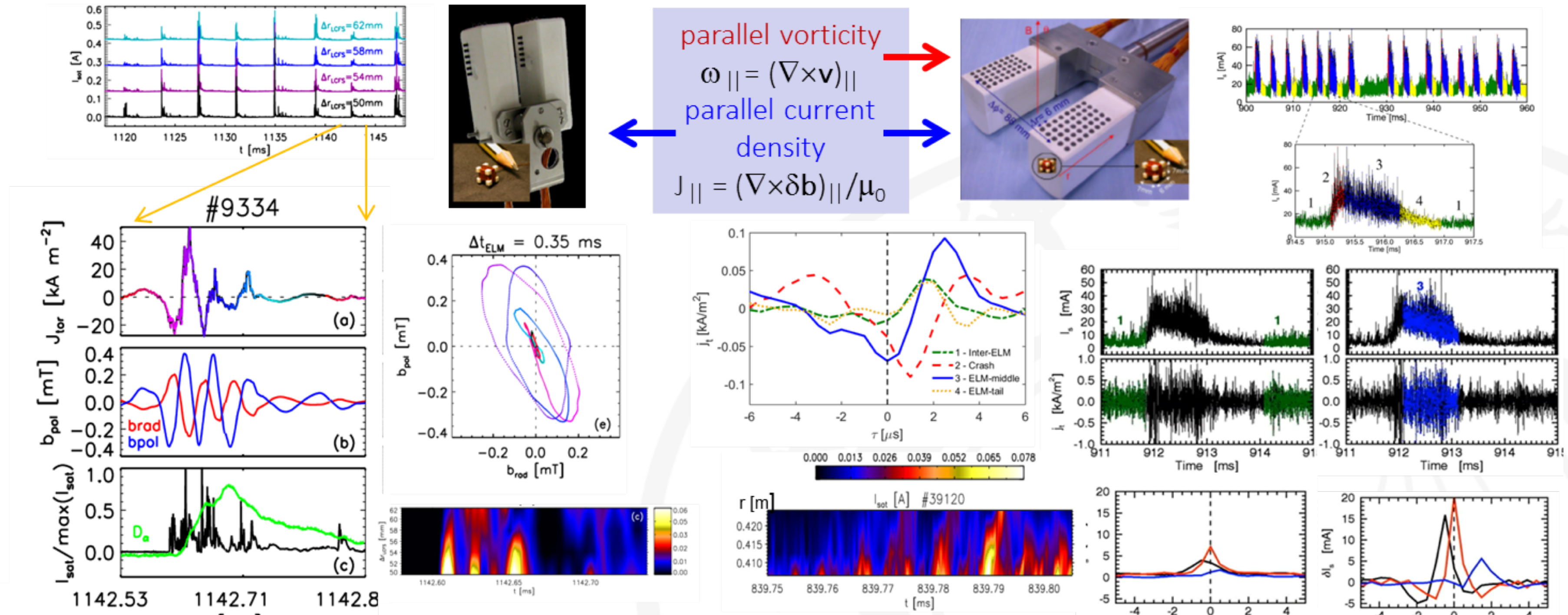

[Spolaore NME 2017]

- Complex fragmented and radially extended filamentary structures emerge within a single ELM. Strong peaks in parallel current density J_{tor} are observed to characterize the ELM bunch.
- Analogous features were observed in COMPASS and RFX-mod ELM structures.
- Within the ELM burst cycle (RFX-mod) the ejection phases were identified with the "crash" and "middle phase" where radial propagation of e.m. filaments recovers transiently the L-mode turbulent filament features.

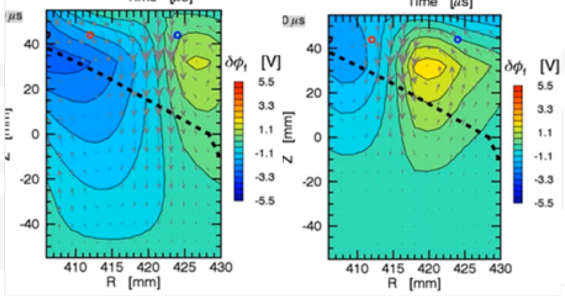

I25: ELM simulation [Zhanhui Wang]

Self-consistent multi-scale integrated modeling of ELM and transport

- One multi-scale self-consistent physical model of ELM turbulence and transport has been developed;
- Both transport *trans-neut* code and ELM *elm-pb/-6field* code have been integrated and coupling on OMFIT platform;
- Self-consistent multi-scale simulation results of ELM turbulence coupling with transport during ELM crash have been achieved;

Simulation on OMFIT platform

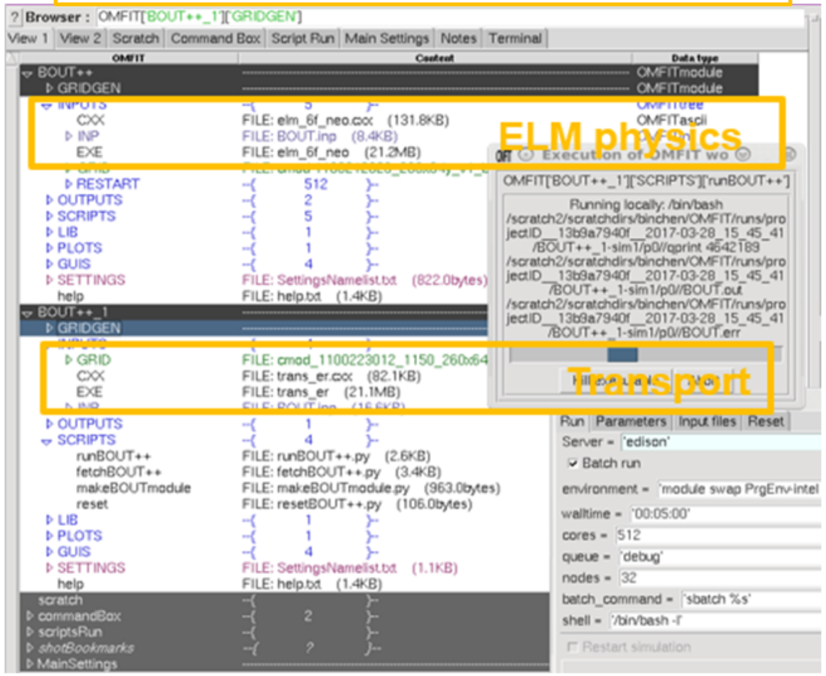

integrated modeling

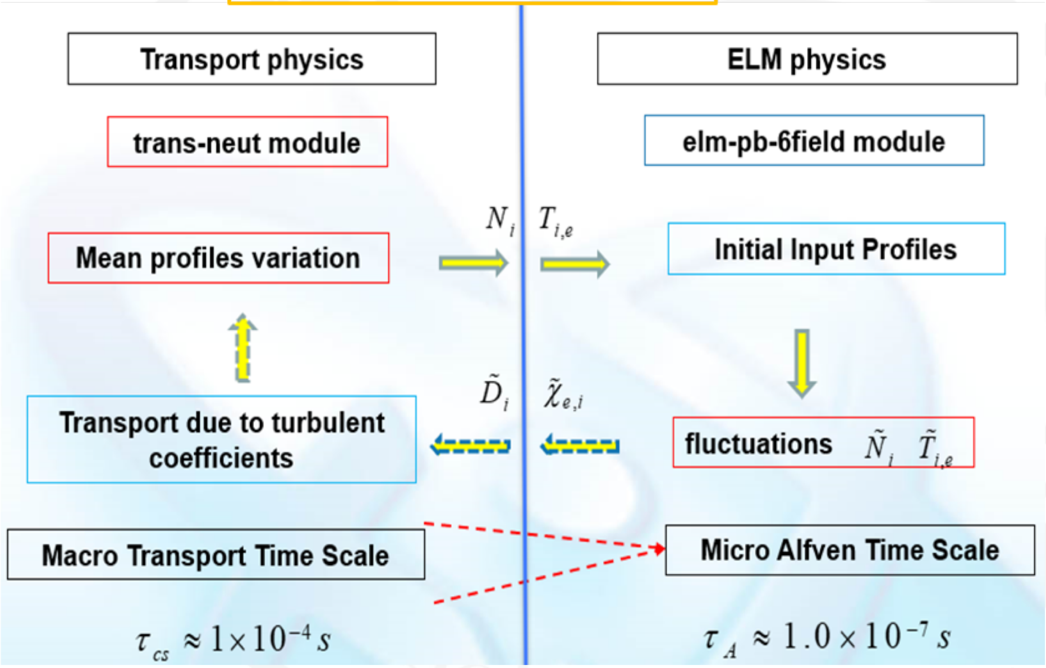

I14: RMP sim. [Juhyung Kim]

Effects of RMPs on nonlinear resistive reduced MHD simulations

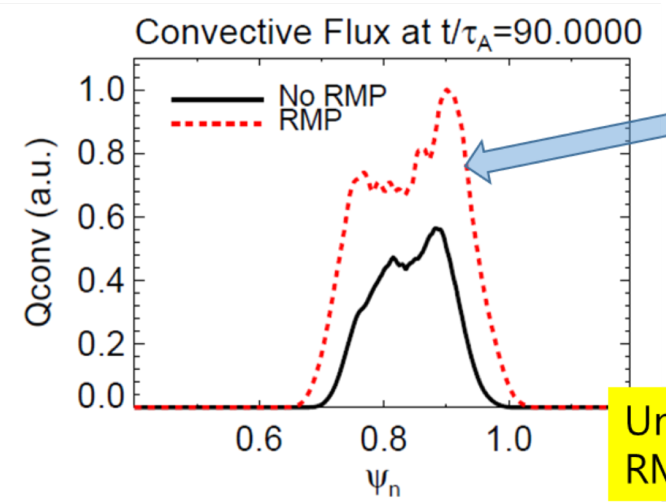

Enhanced convective transport

Enhanced fluctuation of low n

$$\gamma_{n=10} \simeq \gamma_{n=20,lin}$$

** max lin. growth rate at n ~ 20

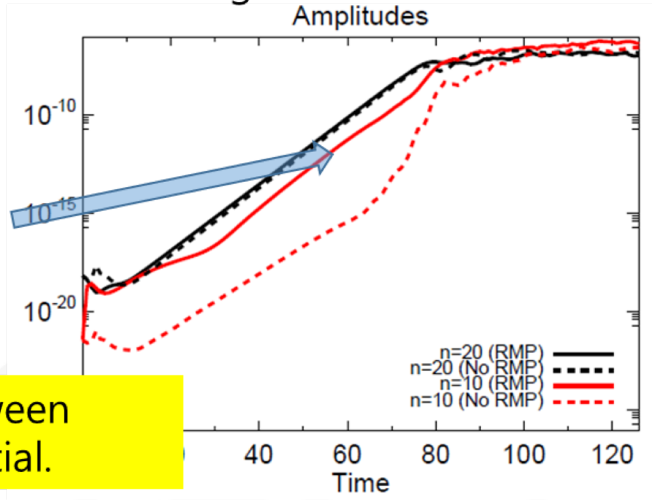

Understanding nonlinear coupling between RMP and turbulent fluctuation is essential.

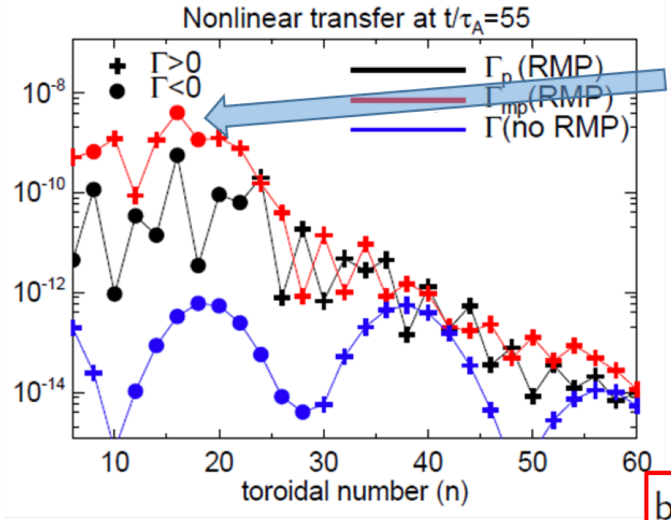

RMP mediated nonlinear transfer

$$\left\langle J_n \left[\psi^{\mathrm{RMP}}, \phi\right]_n^* \right\rangle$$

2nd tearing-parity generation*
Only possible with enhanced low n ballooning fluctuations, due to RMPs.

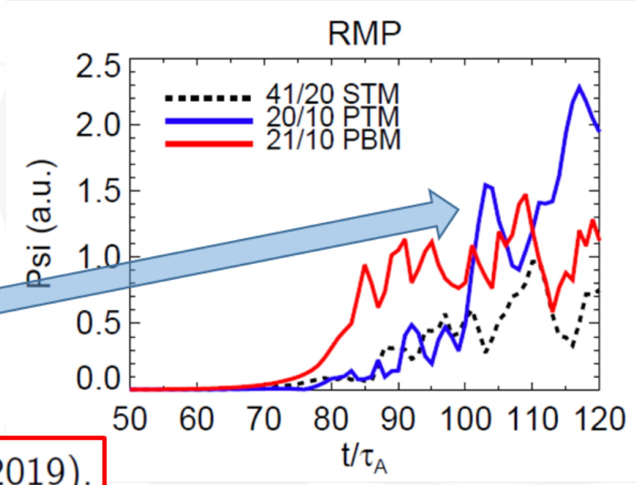

based on J. Kim *et al.*, NF 59, 096019 (2019).

RMPs are shown to expedite the magnetic field line stochastization process via the nonlinear energy transfer

O5: RMP; divertor flux control [Manni Jia]

3D divertor flux control using optimized dynamic RMP on EAST

- **Dynamic RMP application helps even 3D divertor flux distribution**
  - field rigid rotation
  - upper-lower current phase scan
- **Plasma response effects on the divertor power load were observed**
  - screening/amplifying → changing field line penetration depth → power load strength
  - confirmed by modeling: MARS-F + TOP2D + EMC3-EIRENE

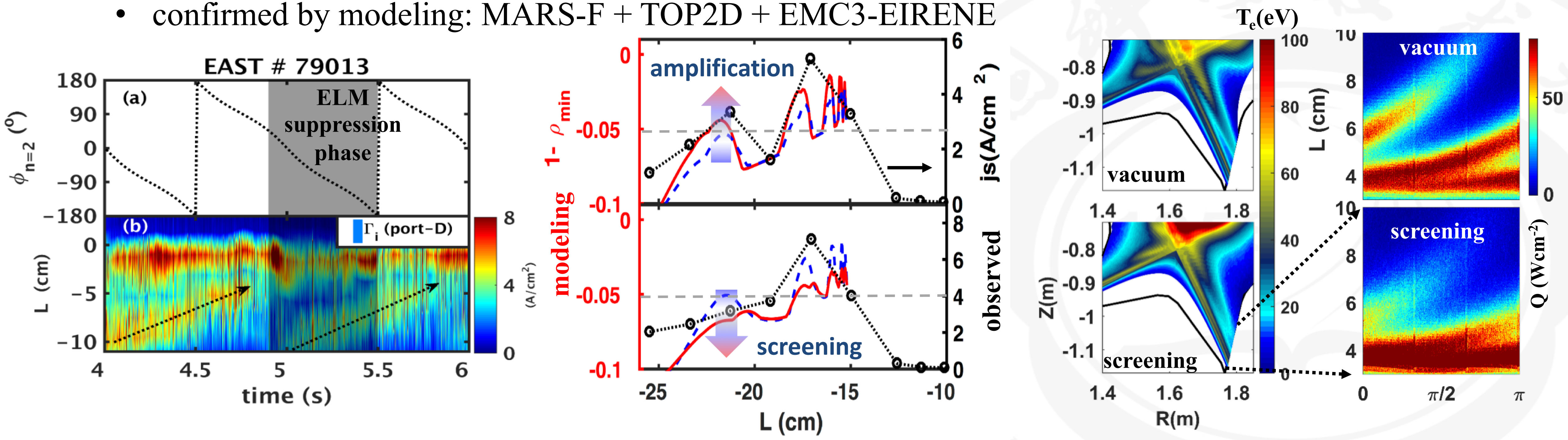

The process of active divertor flux control through a dynamic RMP fields on EAST is investigated

O19: RMP exp. [Ting Wu]

Effect of RMP on boundary plasma turbulence and transport on J-TEXT tokamak

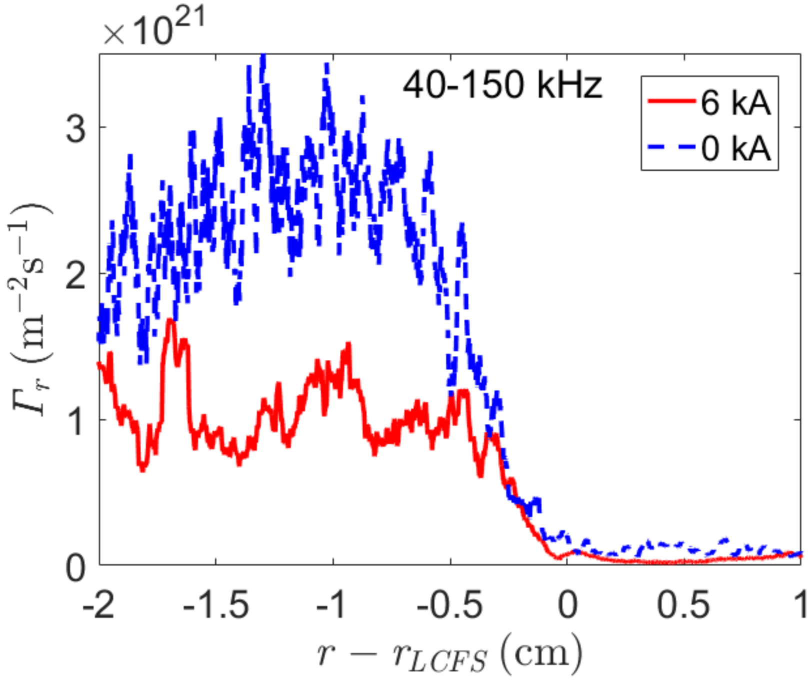

Fig. 1. Radial profile of turbulent flux.

With 6 kA RMP averaged flux Γ_r drops
Edge: about 38%
near SOL: about 43%

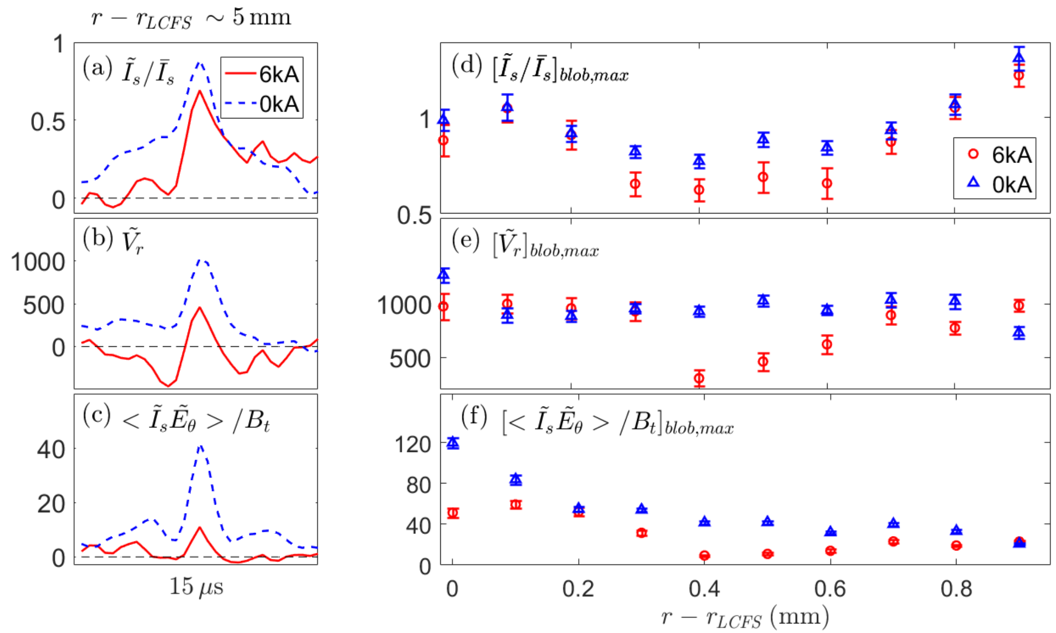

Fig. 2. Blob properties with conditional average method and the radial profiles of the maximal values of blob parameters.

In the SOL with RMP:
- ✓ The blob amplitude and radial velocity decrease;
- ✓ Turbulent flux of blob drops dramatically.

fluctuations in the edge/SOL region, particle flux and blob transport has been dropped clearly with RMP

Outline

- Contributions to MF
- Major Progresses
  - Major progresses of machines
  - ELM control and RMP
  - MHD and EP physics
  - Transport and confinement
  - SOL/divertor/PMI physics
  - Scenario/Integrated model
  - Discharge Control/Diagnostics/Disruption

I23: EP-Chirping Mode [Liming Yu]

Observation of High-frequency Chirping Modes Driven by Energetic Ions on HL-2A

The chirping modes locate on BAE and TAE gap, so called BAE-EPM and TAE-EPM. The nonlinear interaction between EPM and tearing mode/Long-lived mode are identified.

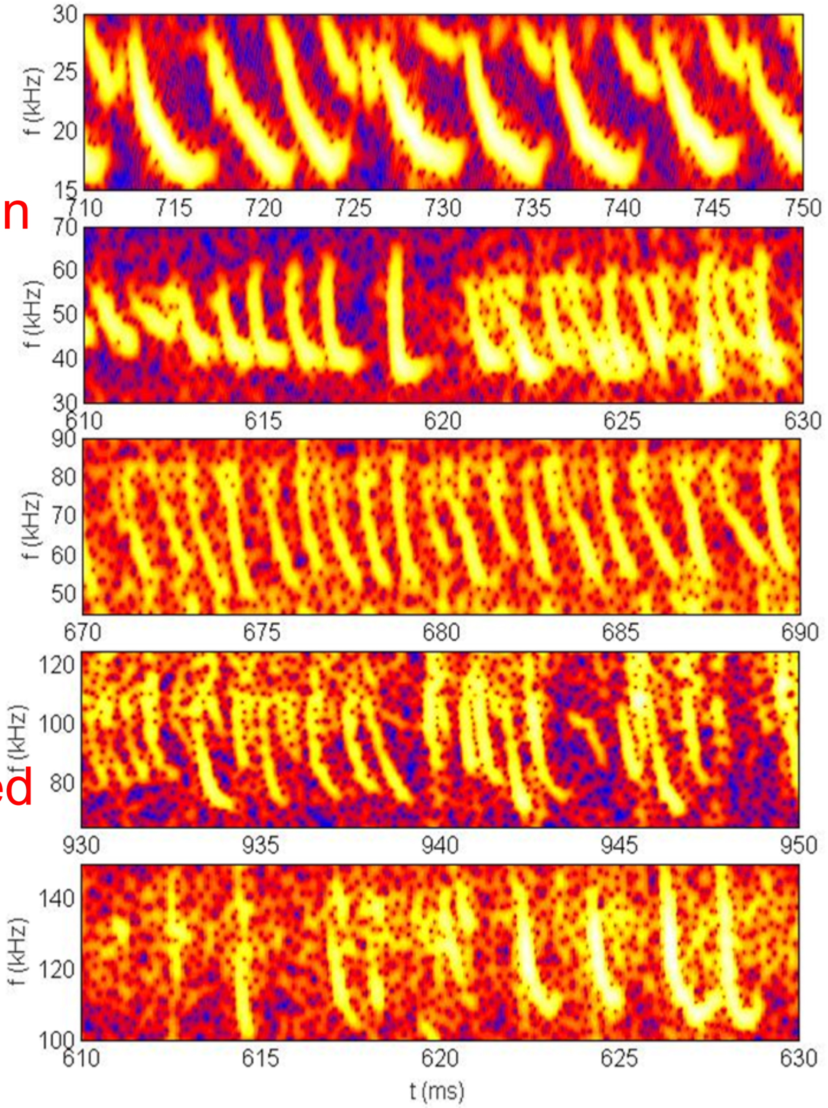

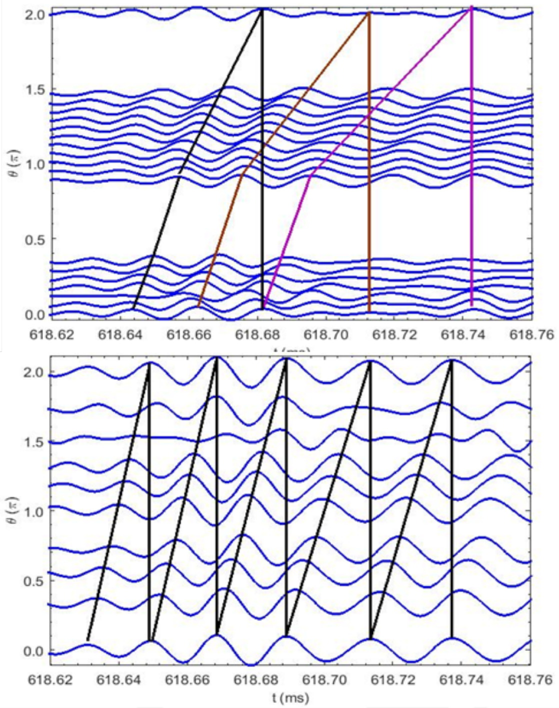

For 35-65 kHz EPMs

- n is always as n=1, but m changes from m=2 to 3, and then to 4 with the decreasing frequency;
- Energetic ions are exciting the EPM all the time at different positions in the progresses of being expelled.

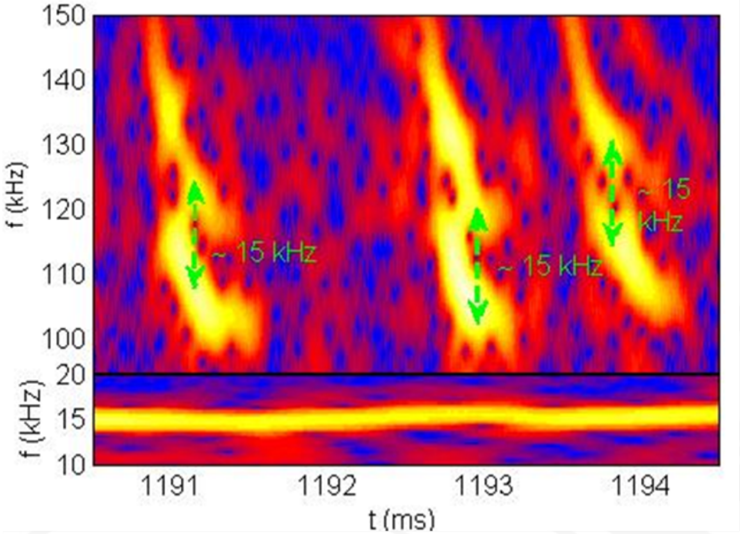

- Various frequency band (10-150 kHz) chirping modes during NBI heating are found in HL-2A;
- Several (3-4) different bands can coexist;
- Frequency scaling does not follow an Alfvén scaling;
- Nonlinear coupling between EPMs and low-frequency MHD modes are found.

I24: nonlinear AE [Wei Chen]

Nonlinear Dynamics of Alfvén Eigenmodes in HL-2A NBI Plasmas

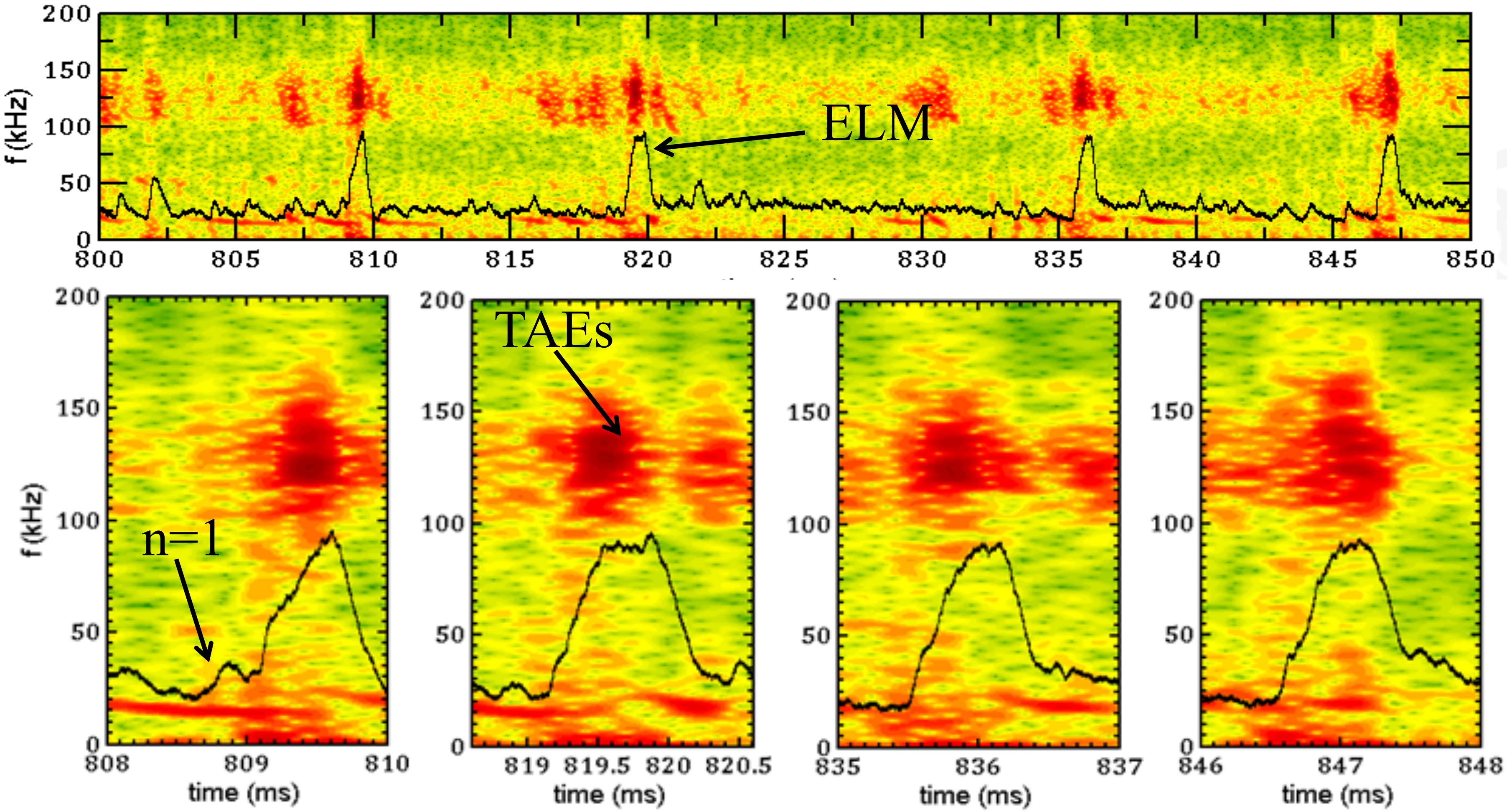

The nonlinear dynamics of TAEs, including nonlinear wave-particle and wave-wave interactions, have been observed in HL-2A NBI L- and H-mode plasmas.

The outer TAE with m/n=7-10/3 nonlinear dynamics triggers the onset of ELMs and pedestal collapse within several hundred Alfvén times, and they are correlated to the irregular ELM features.

O10: Transport Theory [Fulvio Zonca]

Gyrokinetic transport theory of phase space zonal structures

- Theoretical framework to address fluctuation-induced and collisional transport on the same footing for applications in collisionless fusion plasmas.

$$\frac{\partial}{\partial t}\overline{F_{z0}} + \frac{1}{\tau_b}\left[\frac{\partial}{\partial P_\phi}\overline{\left(\tau_b \delta \dot{P}_\phi \delta F\right)_z} + \frac{\partial}{\partial \mathcal{E}}\overline{\left(\tau_b \delta \dot{\mathcal{E}} \delta F\right)_z}\right]_S = \overline{C_{z0}} + \langle \bar{S} \rangle_S$$

$\bar{F}_{z0}$ contours

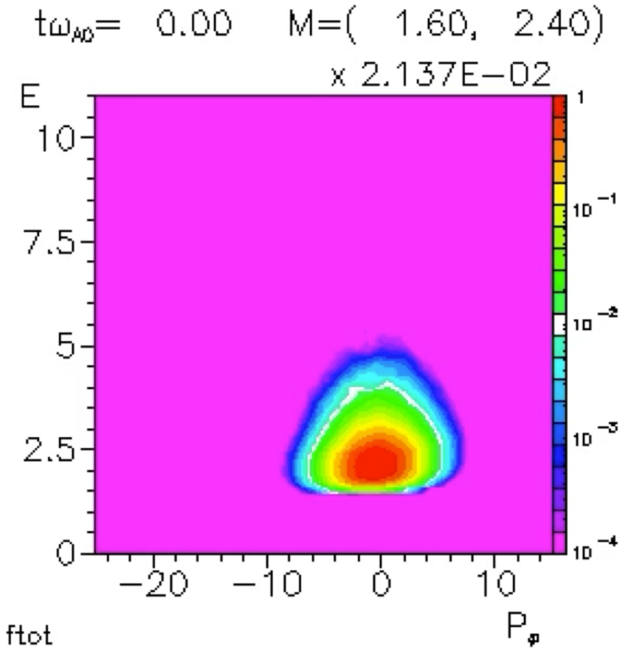

- Framework ready for implementation as collaboration between EUROfusion and ITER-CN Projects (EP Physics)

O30: Excitation of AE [Shuanghui Hu]

Excitations of Alfven Modes in Burning Plasmas

Vorticity equation

(with kinetic compression upon particles by analytical solution of gyrokinetic eq.)

$$\frac{\partial}{\partial\theta}\left(f\frac{\partial\tilde{\psi}}{\partial\theta}\right)+\alpha g\tilde{\psi}+\frac{\omega(\omega-\omega_{*P,Ci})}{\omega_{A0}^2/q^2}f(1+2\varepsilon\cos\theta)\tilde{\psi}+i\frac{\omega_{A0}}{\omega_{C0,Ci}}\frac{s(3-2s)}{\hat{\lambda}_{Ci}\varepsilon}\frac{\partial\tilde{\psi}}{\partial\theta}=G(\theta,\omega,\tilde{\psi})$$

Kinetic compression supported by wave-particle resonances upon the passing/trapped particles described by perturbed distribution function governed by gyrokinetic equation.

Preliminary efforts to detail kinetic compressions with resonance contributions upon trapped as well as passing particles with specific examples of kinetically excited Alfven waves.

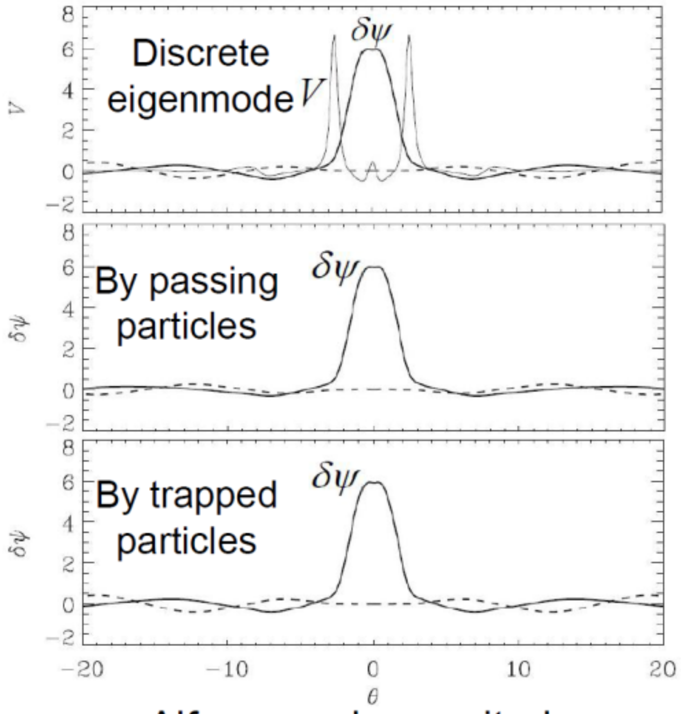

Alfven modes excited by energetic particles

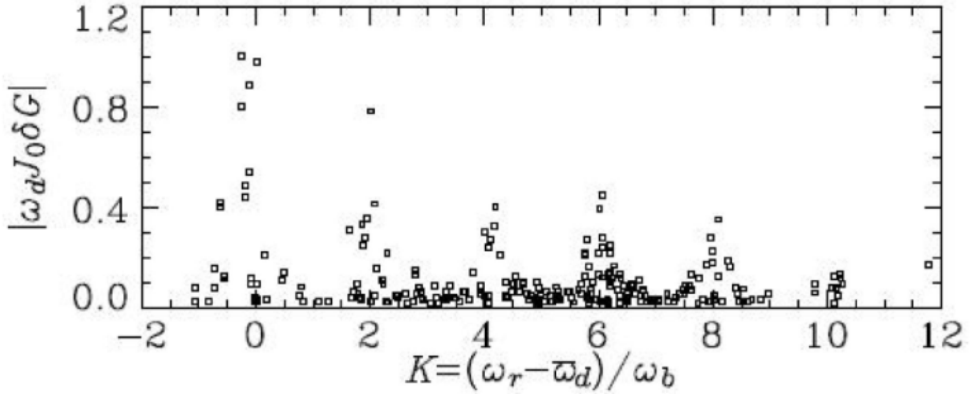

Kinetic excitation upon wave-particle resonances

O24: GAE [Hooman Hezaveh Hesar Maskan]

Modelling of a long range chirping global Alfven Eigenmode in tokamaks

A theoretical description has been developed to study the hard nonlinear evolution of a global Alfven eigenmode in resonance with energetic particles in an NBI scenario during the adiabatic frequency chirping

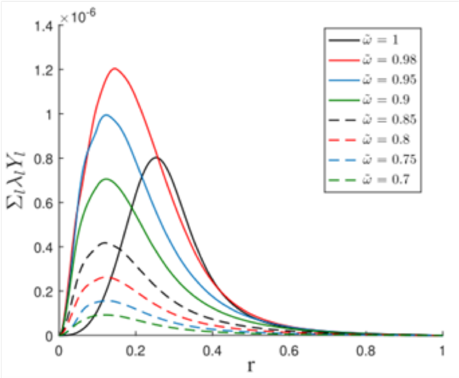

Fig.1 Evolution of the radial profile due to frequency chirping

The radial profile is expanded in finite elements and the nonlinear mode equation is derived by varying the total Lagrangian of the system with respect to the weight of basis functions. The peak of the initial profile will be shifted inward towards the center of the plasma and the mode becomes more localized close to the plasma center. This inward displacement is in compliance with the drift of EPs. In addition, it can be observed that the radial profile is broadened as the frequency moves away from the shear Alfven continuum.

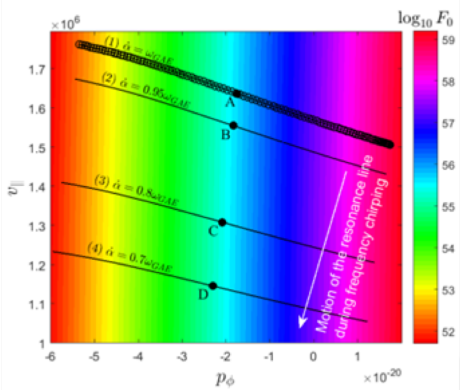

Fig.2 A slice $(\mu \approx 0)$ of the phase-space showing the equilibrium phase-space density and the resonance line at different frequencies.

As the frequency deviates from the initial value, the energetic particles, which are initially in resonance with the mode, will be carried to other regions of the phase-space. During the frequency chirping, appropriate constants of motion have been introduced to reduce the dynamics to 1D.

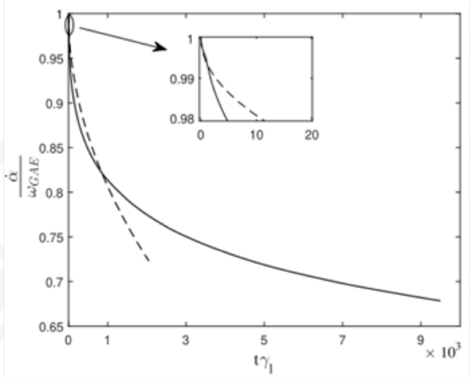

Fig.3 Time evolution of the mode frequency

The dissipated power via weak collisions into the bulk plasma should be equal to the power released by the phase–space structures energy. The chirping rate is derived using this energy balance. It is shown that the square root dependency holds for the very early stages of frequency chirping.

O2: Fishbone simulation [Wei Shen]

Hybrid simulation of fishbone instabilities with reversed safety factor profile

Fishbone instabilities with reversed safety factor profile have been investigated by M3D-K code. There are two types: dual resonant fishbone (DRF) with double q = 1 surfaces and non-resonant fishbone (NRF) with the minimum value of safety factor q_{min} a little larger than unity.

- When q_{min} increases from below unity to above unity, the fishbone transits from DRF to NRF, and the mode frequency of the NRF is higher than the DRF as the NRF is resonant with fast ions with larger precessional frequency.
- Nonlinear simulations show that the saturation of the DRF is due to MHD nonlinearity with a large n = 0 component. However, the saturation of the NRF is mainly due to the nonlinearity of fast ions, and the frequency of the NRF chirps down nonlinearly.

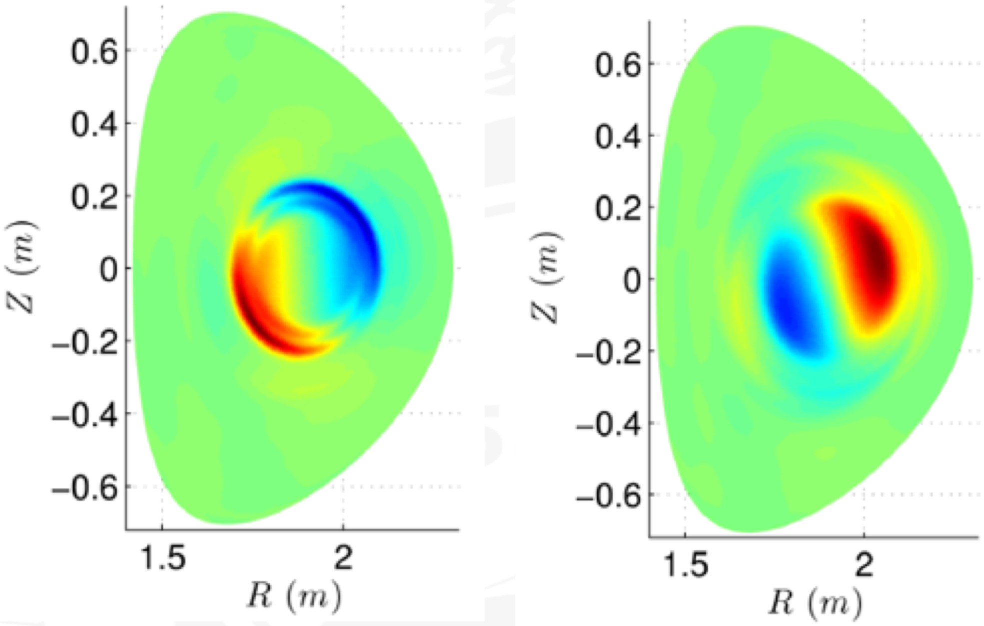

Mode structures of DRF(left) and NRF (right)

I44: EGAM [Ivan Novikau]

EGAM nonlinear dynamics in ASDEX Upgrade configuration

the dynamics of EGAMs is investigated with PIC code ORB5, the saturation mechanisms are identified by separating the wave-particle and wave-wave nonlinear dynamics, and the comparison with the experiments is discussed.

Exper. spectrogram versus ORB5 NL sim.

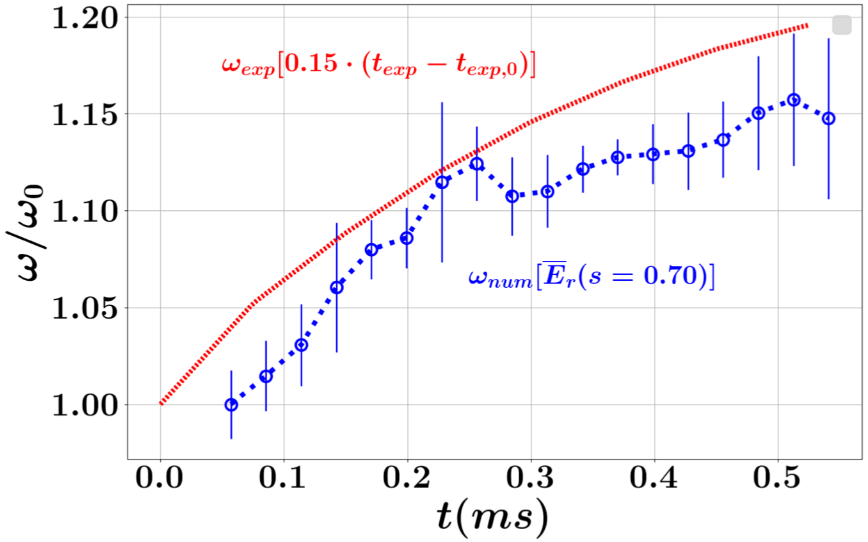

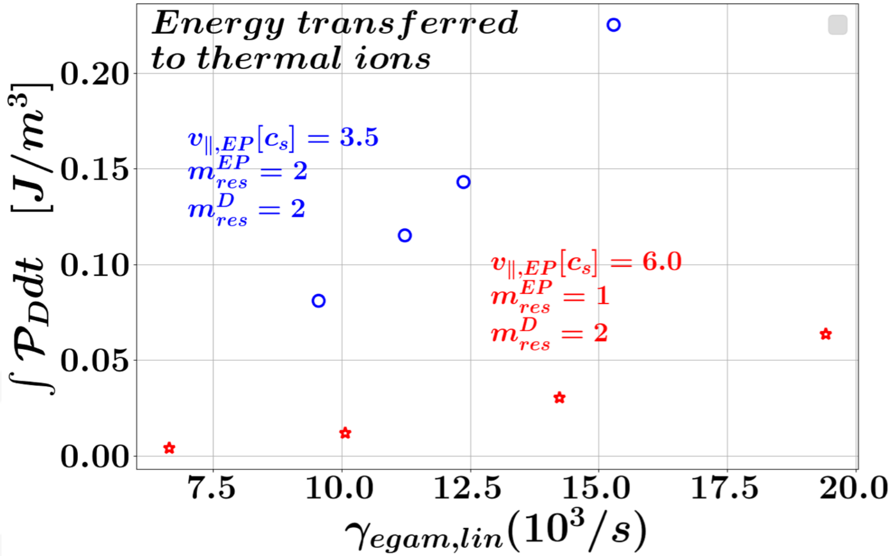

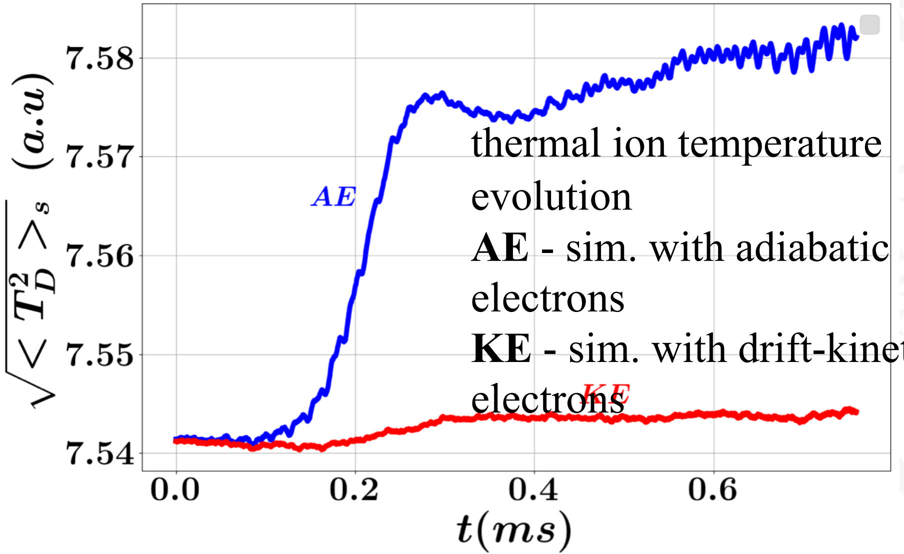

thermal ion temperature evolution
AE - sim. with adiabatic electrons
KE - sim. with drift-kinetic electrons

- reproduced **relative EGAM up-chirping** in NL ES simulations in the code ORB5.
- enhancement of the **EGAM channelling** in the plasma heating due to the high-order EGAM-bulk plasma resonances.
- reduction of the EGAM channelling due to the **electron dynamics**.

I45: EGAM [Hao Wang]

Nonlinear simulation of energetic particle driven geodesic acoustic mode channeling in LHD

The mechanism and other properties of EGAM channeling in LHD plasmas is systematically investigated with realistic parameters through MEGA code.

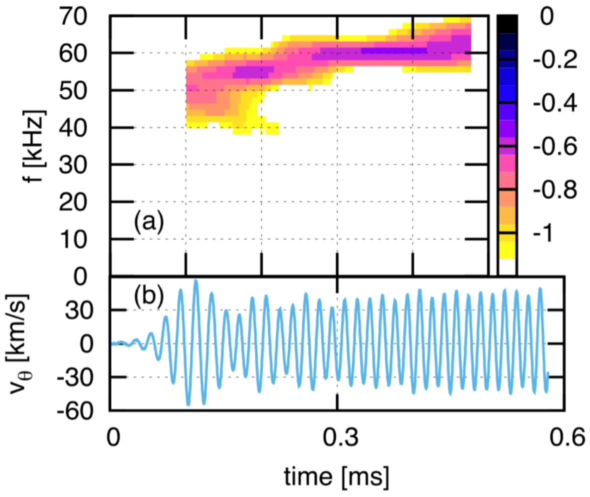

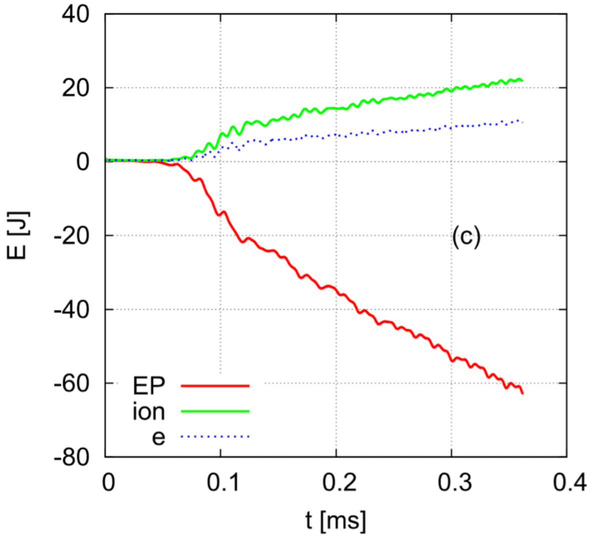

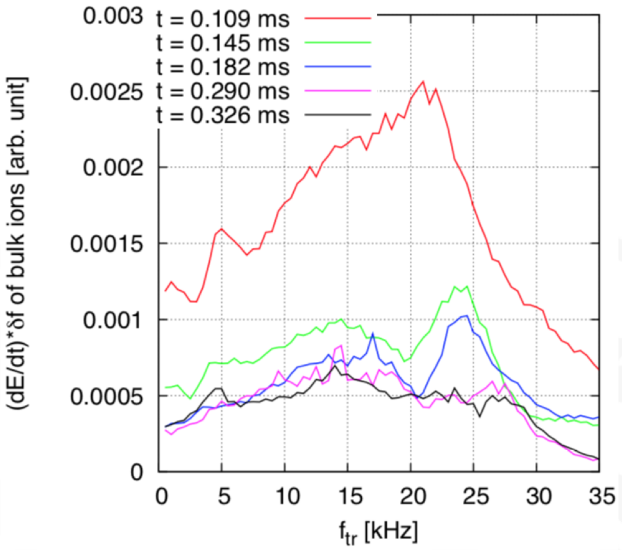

- The ions obtain energy when the energetic particles lose energy, and this indicates that an energy channel is established by the EGAM. EGAM channeling is reproduced by simulation with realistic parameters for the first time.
- The sideband resonance is dominant during the energy transfer from EGAM to the bulk ions, and the transit frequencies of resonant bulk ions are one-half of the EGAM frequency.
- The lower mode frequency, the higher energy transfer efficiency. The interaction between EGAM and bulk ions is stronger for lower frequency mode.
- In order to enhance the energy transfer efficiency, we suggest to increase EP pressure, decrease NBI energy, increase T_i, and increase pitch angle Λ.

I46: Plasmoid [Fatima Ebrahimi]

Plasmoid-mediated magnetic reconnection: From space to fusion plasmas

elongated current-sheets in toroidal geometry can result in a transition from slow reconnection to fast plasmoid-mediated reconnection;

The importance of reconnection physics during burst-like events in tokamaks, such as ELMs has been elucidated.

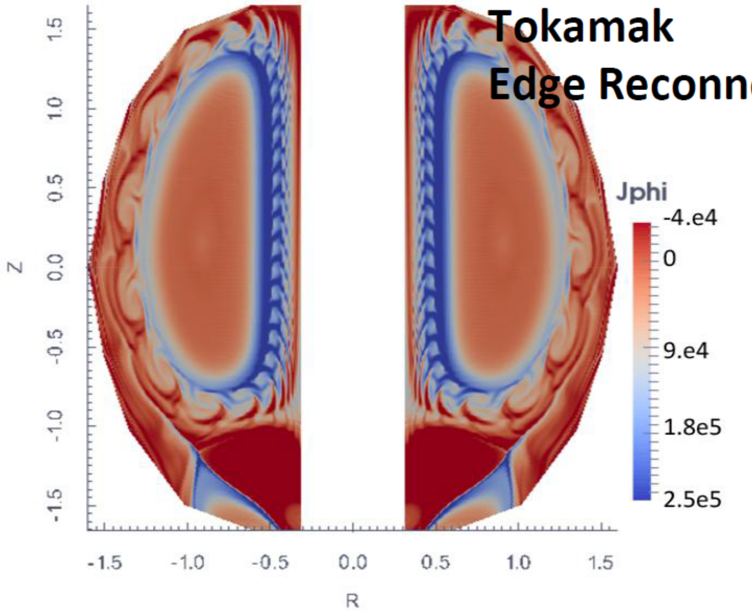

3-D MHD simulations shed light onto the role of reconnection in ELM nonlinear dynamics of a tokamak. The quasiperiodic dynamics of **peeling driven ELM filaments** are explained as reconnection events through a bi-directional emf dynamo term. Ebrahimi PoP 2017

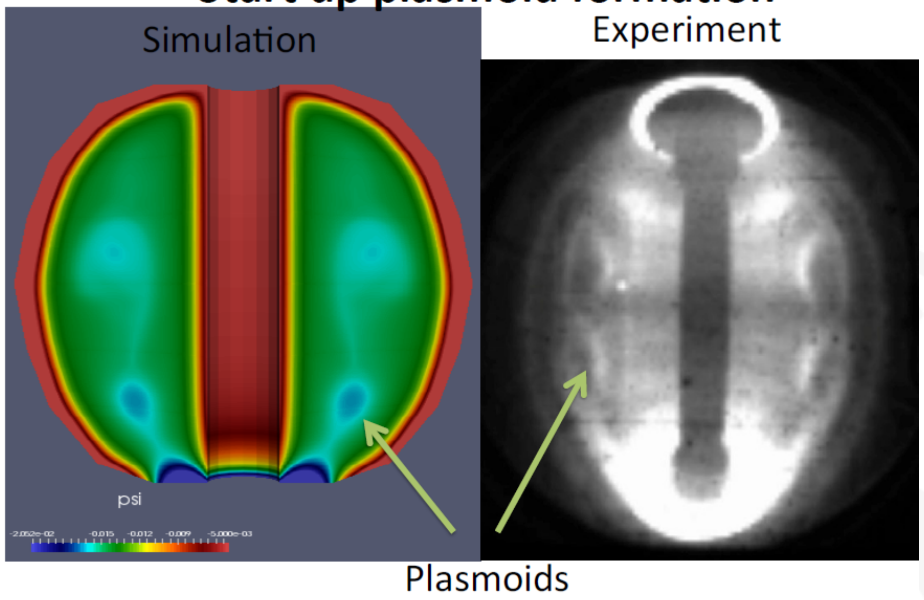

A transition to plasmoid instability has for the first time been predicted by simulations in a large-scale toroidal fusion plasma.
Ebrahimi & Raman, Phys. Rev. Lett (2015)

- 3-D MHD simulations have shown that system-size plasmoid formation can produce large plasma startup current in spherical tokamaks and a large-fraction conversion of injected open flux to closed flux. Ebrahimi&Raman Nucl.Fusion 2016, Ebrahimi PoP 2019

O34: Radial electric field; kink mode [Yi Zhang]

Dual role of radial electric field in edge MHD dynamics: Er-shear vs Er-curvature

Equilibrium flow

Equilibrium Er:

Most unstable region

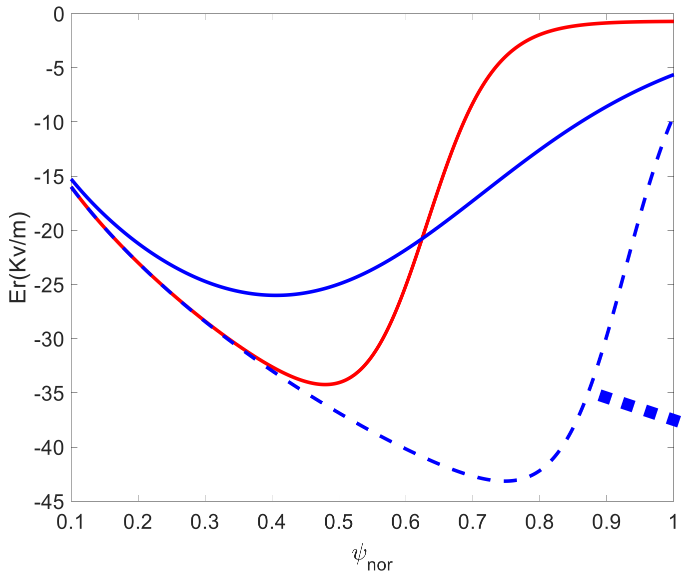

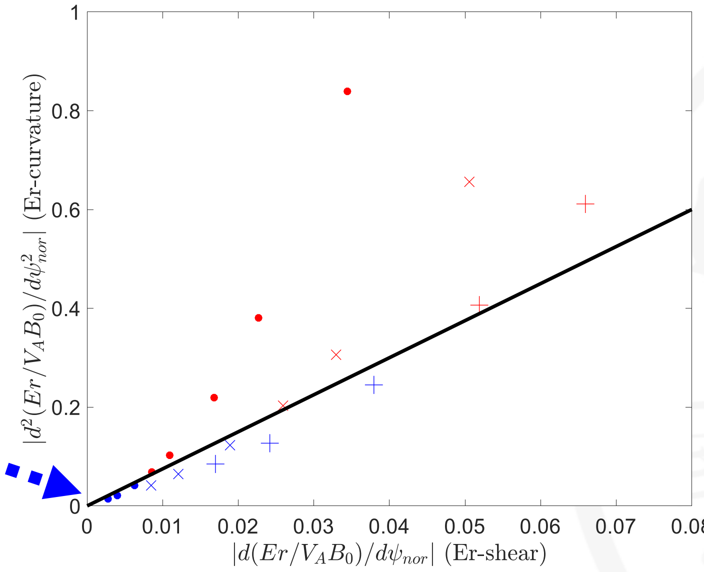

- Er-shear can stabilize the ideal linear kink mode, while Er-curvature is destabilizing. The actual stability depends on which is stronger or which can take the leading position.
- The Er-curvature destabilizing effect comes from the **Kelvin–Helmholtz instability**.

Outline

- Contributions to MF
- Major Progresses
  - Major progresses of machines
  - ELM control/simulation and RMP
  - MHD and EP physics
  - Transport and confinement
  - SOL/divertor/PMI physics
  - Scenario/Integrated model
  - Discharge Control/Diagnostics/Disruption

I10: I-mode [Tim Happel]

Overview of ASDEX Upgrade I-mode results and extrapolation to future devices

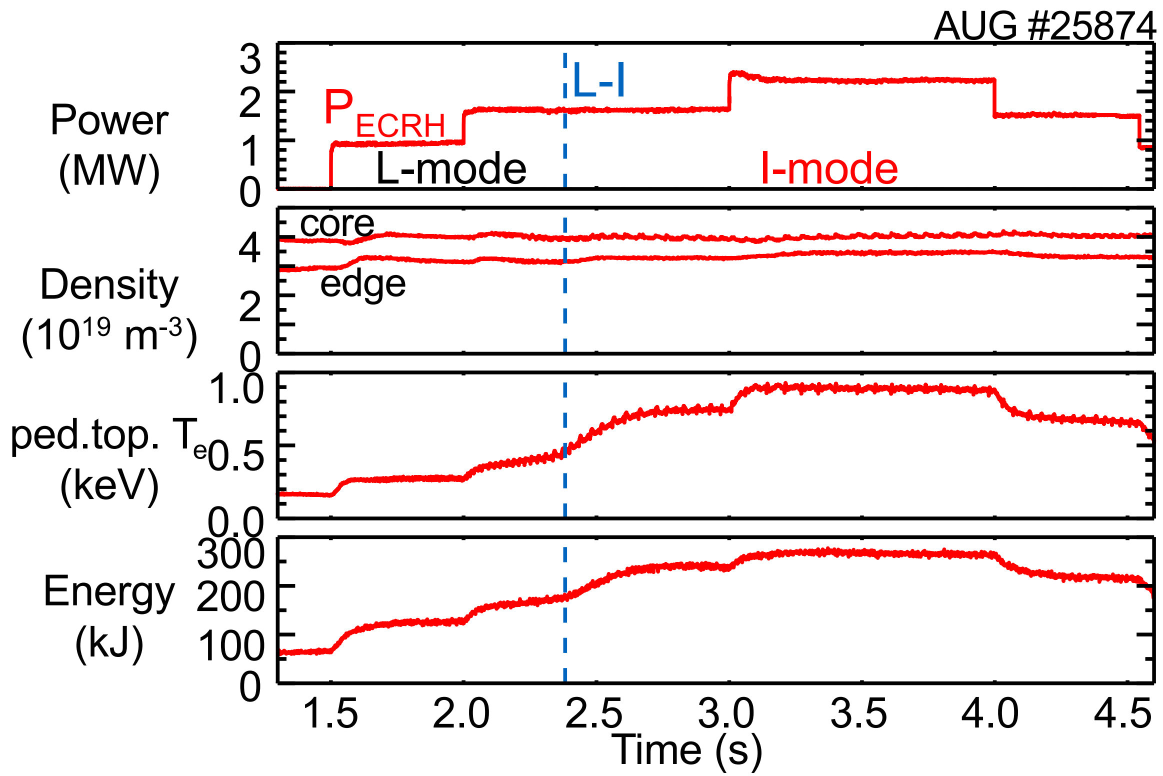

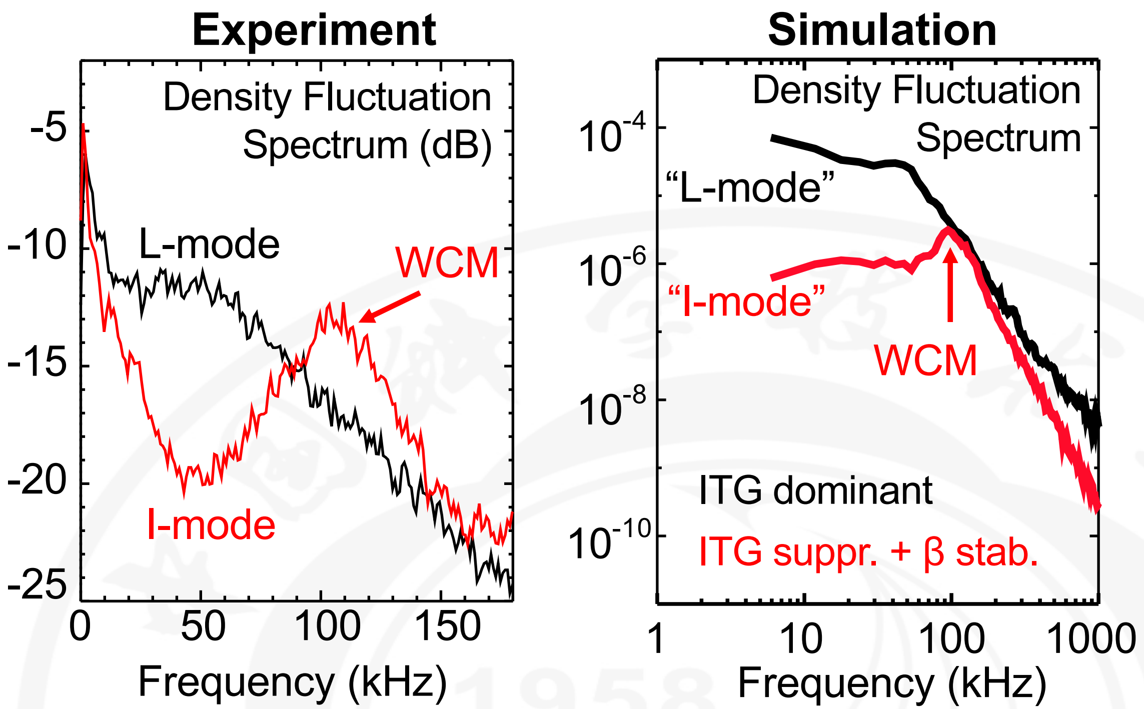

- I-mode is an improved energy confinement regime.
- Significant progress in stationary I-mode operation on ASDEX Upgrade.
- So far no detachment achieved in I-mode, experiments are ongoing.
- Understanding of I-mode edge turbulence: suppression of ITG yields drift wave, β stabilization gives weakly coherent mode (WCM).

I38: I-H transition [Jun Cheng]

interaction between oscillation flows and turbulence across a transition to H mode in edge plasma

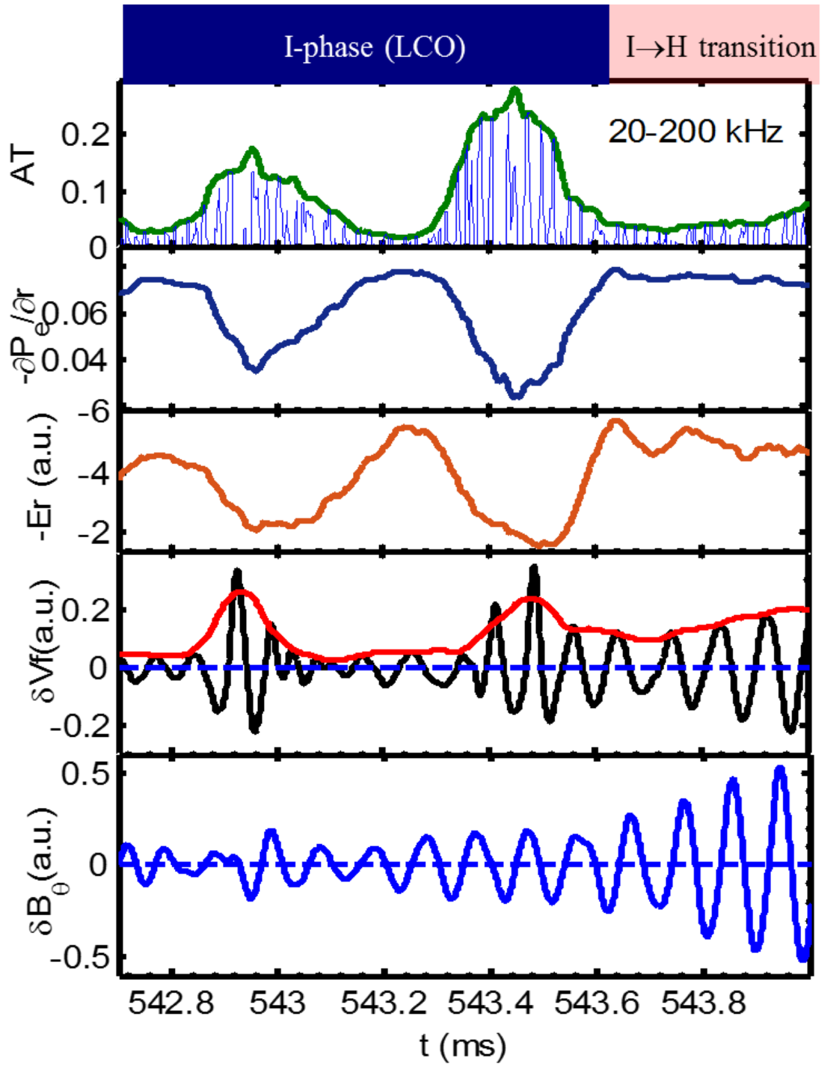

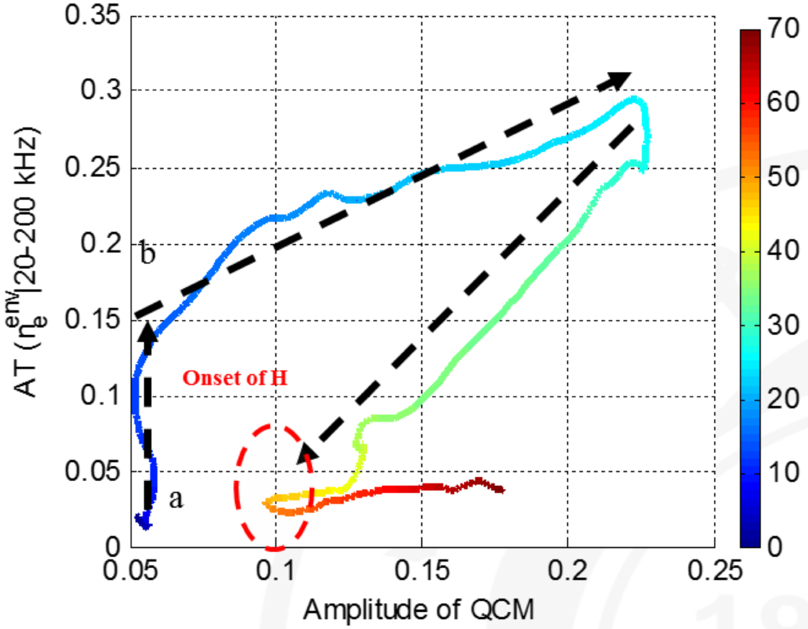

The dynamic progress during I-phase to H-mode has been investigated through Langmuir probes. The interactions between oscillation flows, QCM and turbulence across the transition is analyzed.

- Energy transfer from AT to QCM, consistent with the increasing b^2
- The magnetic oscillation gets energy from QCM and its amplitude begins to rise when AT reaches the minimal value
- AT is locked at a low level , plasma cross the bifurcation point, i.e., directly towards to H mode

I8: L-H transition [Linming Shao]

Recent progress of L-H transition physics and H-mode power threshold studies in EAST

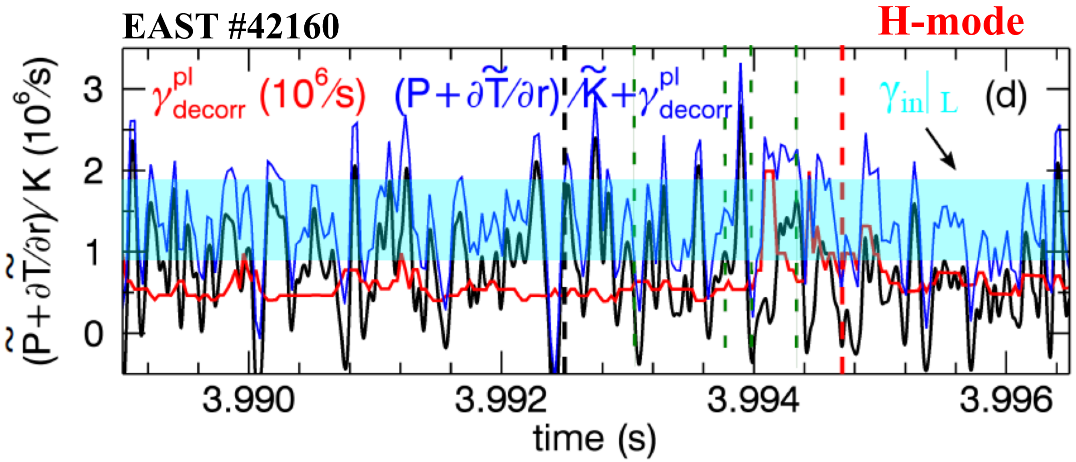

Both turbulent decorrelation rate and nonlinear energy transfer rate are found to play key roles on the turbulence quench.

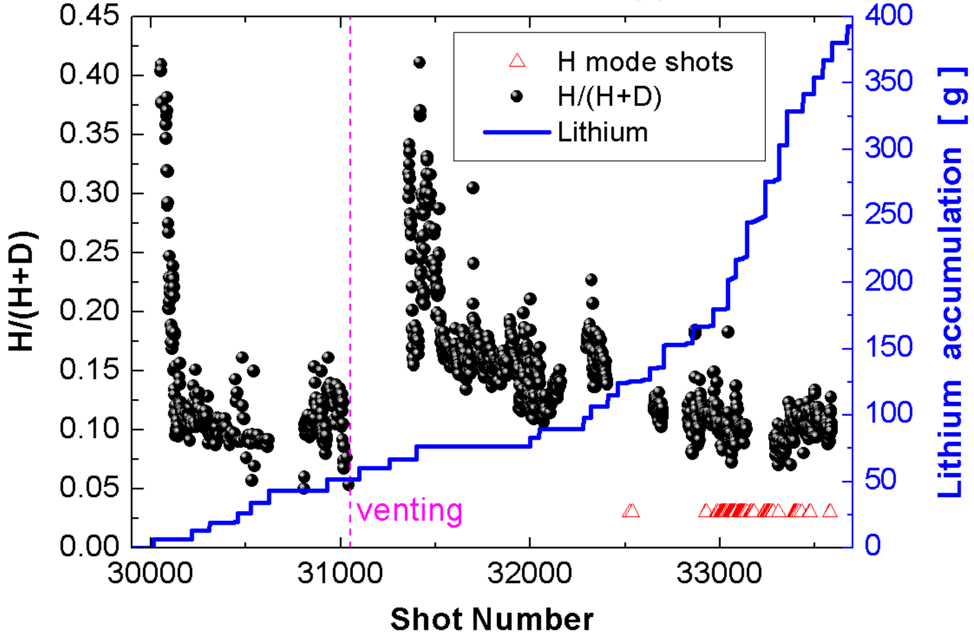

Reduced H/D+H by the lithium conditioning is the probable cause for the reduced $P_{\mathrm{L-H}}$.

Lower $P_{\mathrm{L-H}}$ is also observed in discharges with metallic divertor, favorable configuration and shorter outer leg length.

I42: L-H transition [Zheng Yan]

Role of turbulence and shear flow dynamics in the L-H transition and power threshold scaling

- **Rapidly increasing shear flow generated from turbulence prior to and triggering the L-H transition [1-4]**
  - Critical role of turbulence kinetic energy transfer between plasma turbulence and poloidal velocity flows in triggering the transition

- **Unifying observations of multimode turbulence structure in plasmas with lower P_{LH} [5, 6]**
  - Dual modes commonly observed in plasmas of deuterium (vs. hydrogen), at higher q_{95} (vs. lower q_{95}), and in favorable magnetic configuration (vs. unfavorable)
  - Associated with larger Reynolds stress and mode velocity shear

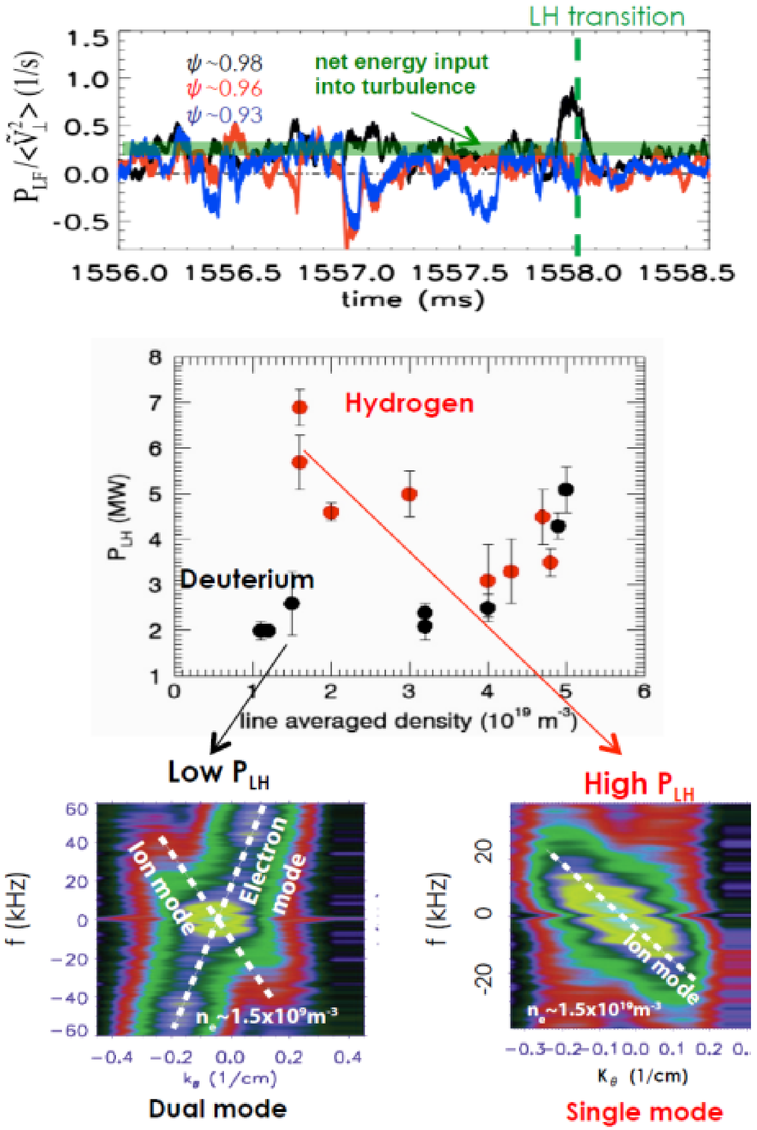

[1] Z. Yan, PRL, 2014
[2] G. Tynan, NF, 2013
[3] I. Cziegler, PPCF, 2014
[4] C.S.Chang, PRL, 2017
[5] Z. Yan, NF, 2017
[6] Z. Yan, PoP, 2019

I39: power law [Jeronimo Garcia]

On the validity of scale invariance and power laws for describing and predicting confined plasmas

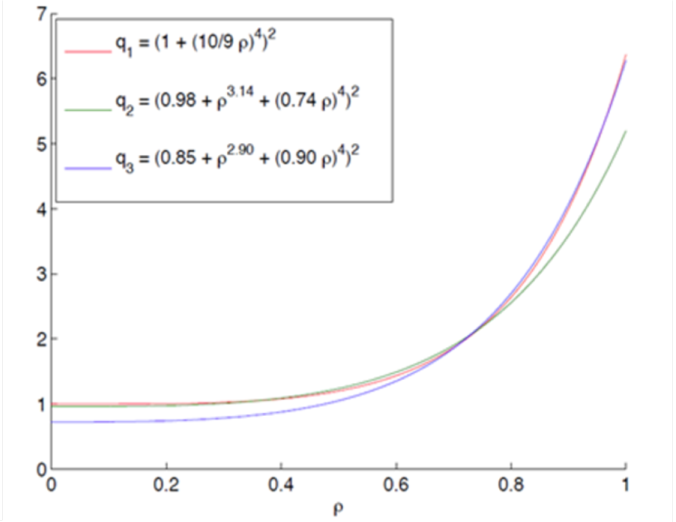

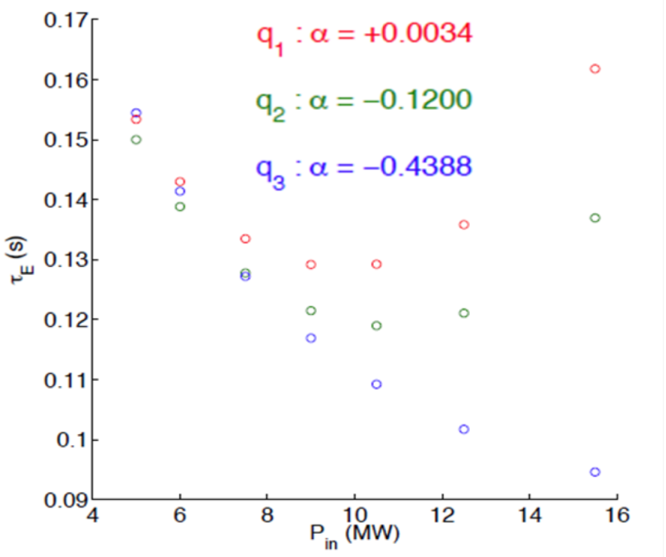

- Validaty of power law thermal energy confinement time dependence on input power, $\tau_E \sim P_{in}^{\alpha}$, studied for JET
- In conditions of transport reduction with collinear effects from input power and magnetic shear, deviations from power laws are obtained
- A power law approximation with a constant exponent covering a broad range of plasma conditions can lead to misleading results when…
- …Non-linear interplay between turbulence and input parameters is dominant
- Scale invariance can be broken in conditions of far from ion scale dominated plasmas
- In particular low ion transport obtained in high power plasmas

I29: ITB; Rotation; ITG/TEM [Kenji Imadera]

Effect of kinetic electron dynamics on ITB formation in flux-driven ITG/TEM turbulence are investigated through the comparison with adiabatic electron case

1. ITB formation in flux-driven ITG turbulence with adiabatic electron

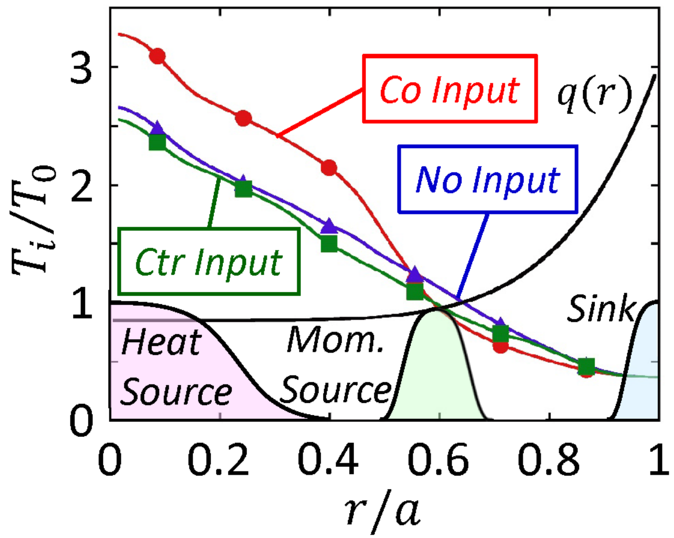

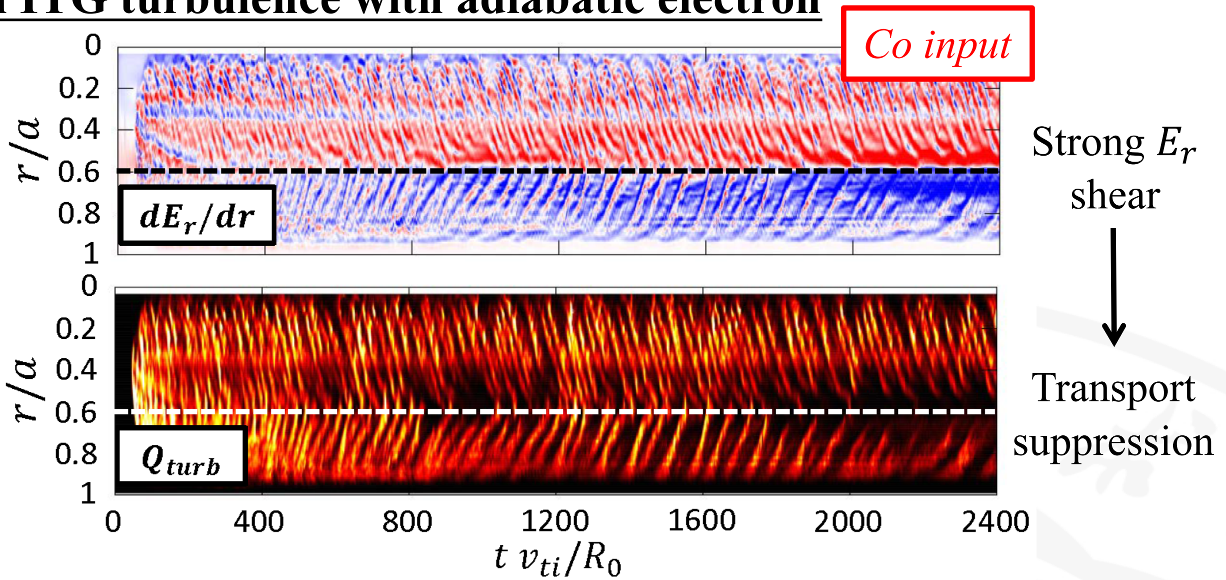

✓ Co-current toroidal rotation in weak/reversed magnetic shear plasma can enhance mean E_r shear (Right Fig.) through the radial force balance, leading to ITB formation (Left Fig.).

2. Effect of kinetic electron on ITB formation in flux-driven ITG/TEM turbulence

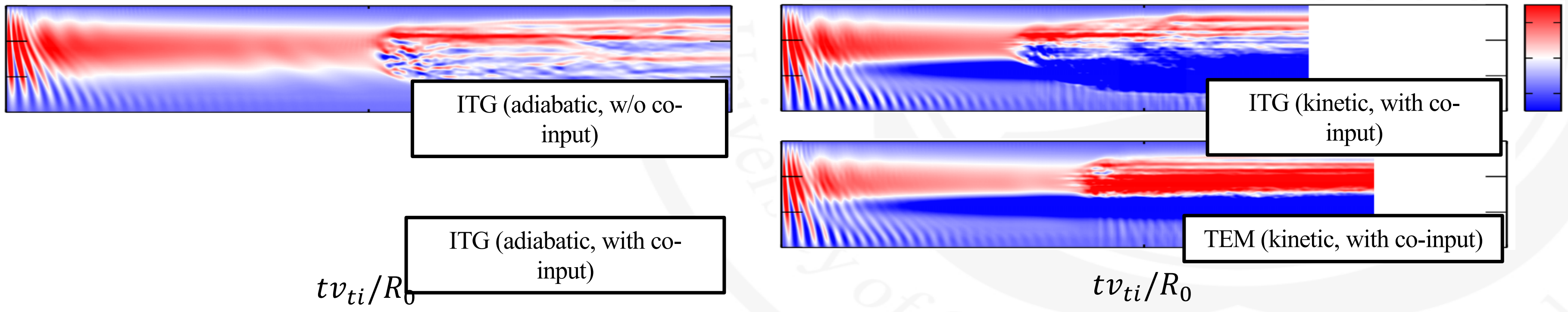

✓ Co-current toroidal rotation becomes more effective in TEM case by reversing mean E_r.

I34: Fast-Ion and ITG/TEM [Samuele Mazzi]

Impact of fast ions on microturbulence and transport: expectations for JT-60SA and ITER

- **Experimentally** → Detected **reduction** of **turbulent transport** respect to IPB98(y,2) scaling law in several devices
- **Numerically** → **Stabilization** found for **ITG-dominated** systems in **gyrokinetic simulations** [Di Siena NF(2018), Zarzoso PRL(2013), Citrin PPCF(2014), Garcia NF(2015), Doerk NF(2017)]

The impact of Fast-Ion on Turbulent Transport is investigated with GENE based on a JT-60U high-ß discharge and found that TEM-induced heat flux is not affected by Fast Ions.

Analysis of JT-60U TEM-dominated hybrid scenario with local version of GENE [Jenko POP(2000)]:

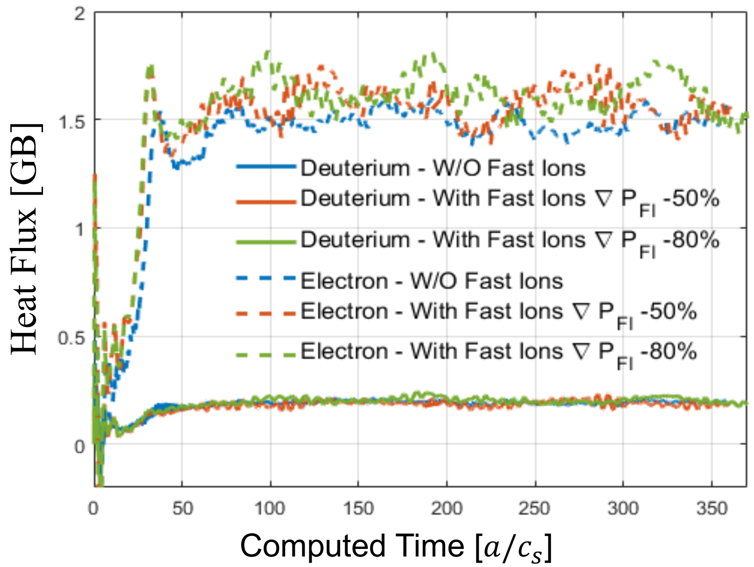

[S. Mazzi, *Nuclear Fusion*, 2019, submitted]

- **TEM**-induced **heat flux** is **not affected** by **Fast Ions**
- **Possible explanation** → **Weak** impact of **Zonal Flows** as **saturation mechanism** in ∇T**-driven TEM** [Merz PRL(2008), Ernst POP(2016)]

- **ITER predictive Hybrid Scenario** analysis [Garcia POP(2018)] : **Fast ions** (α**-particles** mainly) **reduce ITG**-driven turbulent **transport** (beneficial effect) → **Similarity** with **JET** and **ASDEX-U** cases
- **JT-60SA predictive Hybrid Scenario** preliminary analysis: **Inconsistency** between simplified electrostatic reduced models and GENE analyses → **Electromagnetic effects** must be taken into **account** in **reduced models**

O9: Staircase [Wenbin Liu]

Observation of multiple shear layers and long-range transport events on HL-2A tokamak

Based on the BES data on HL-2A, multiple shear layers and long-range avalanche-like transport events are observed, suggesting the existence of $E\times B$ staircase

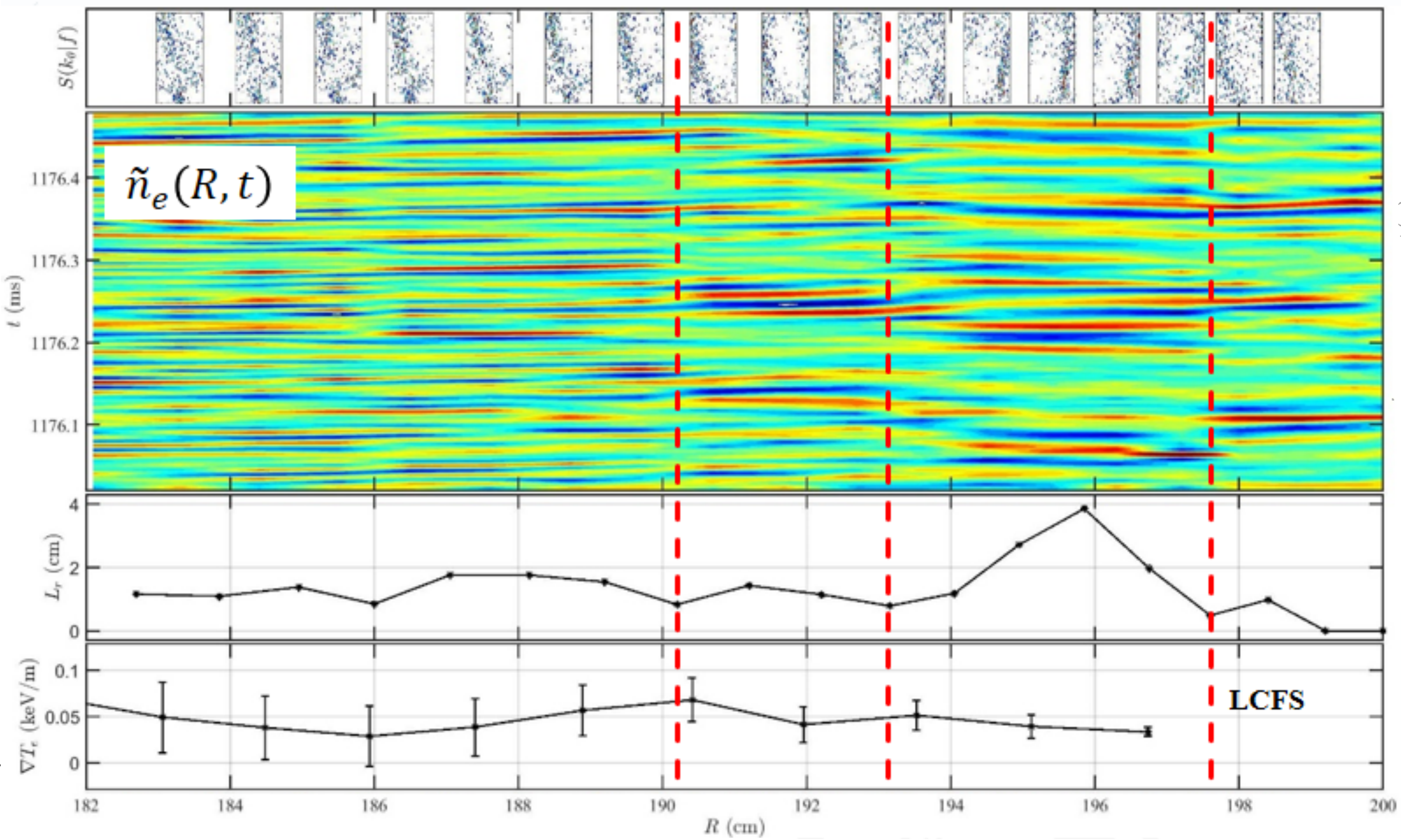

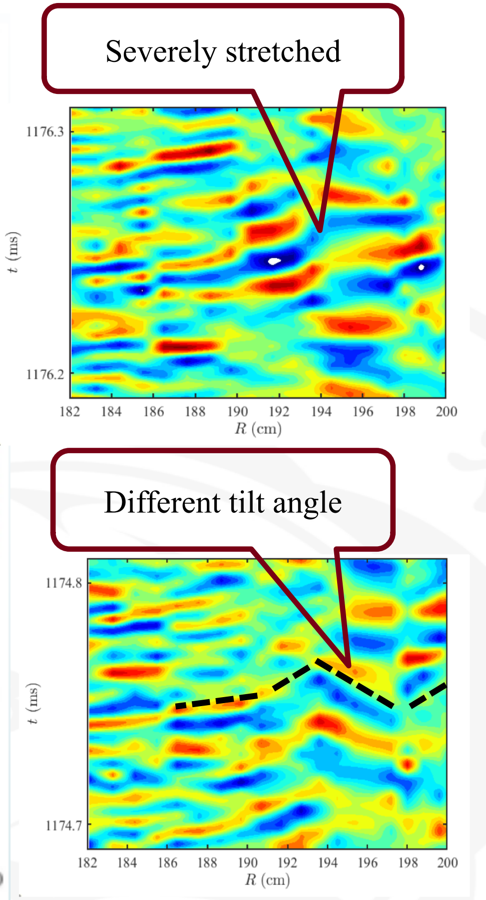

Evidence for the existence of $E\times B$ staircase:

- **observation of multiple shear layers** (red dashed lines):
  - Obvious changes of $S(k_\theta\,|f)$ such as the slope of dispersion curve $\omega(k)$, poloidal direction of turbulence;
  - Termination of radial extension from $\tilde{\boldsymbol{n}}_{\boldsymbol{e}}(\boldsymbol{R},\boldsymbol{t})$ or reduction of radial correlation from $\boldsymbol{L_r}(\boldsymbol{R})$;
  - Corrugation of $\boldsymbol{\nabla T_e}$ profile;
  - Eddies stretched and different tilt angles in the two sides of shear layers from $\tilde{\boldsymbol{n}}_{\boldsymbol{e}}(\boldsymbol{R},\boldsymbol{t})$.

$E\times B$ staircase dynamics:

- Long-range **Avalanche-like transport events** in-between transport barriers
- Semi-permeability (Strong disturbance is more likely to penetrate the barrier.)

I28: Zonal flow staircase; avalanche [Lei Qi]

Role of zonal flow staircase in electron heat avalanches in KSTAR L-mode plasmas

1. Non-diffusive avalanche-like electron heat transport events are observed in KSTAR L-mode plasmas in the absence of MHD instabilities
   - ✓ The power law scaling $|\delta T_e(f)|^2 \sim f^{-0.7}$ (*Fig. 1a*)
   - ✓ Corrugation scale in mean δT_e is $\Delta \sim 45\rho_i$ (*Fig. 2b,2d*)
2. Nonlinear gyrokinetic analysis shows consistent results with the experiments
   - ✓ The power law scaling $|\delta T_e(f)|^2 \sim f^{-0.7}$ (*Fig. 1b*)
   - ✓ Corrugation scale in mean δT_e is $\Delta \sim 40\rho_i$ (*Fig. 2a,2c*)
3. Nonlinear gyrokinetic analysis shows that zonal flow staircase is responsible to shear the avalanches
   - Corrugation scale in zonal flow staircase is $\Delta \sim 40\rho_i$, consistent with δT_e corrugation. (*Fig. 3a,3b*)
   - Zonal flow shears electron temperature gradient fluctuations. (*Fig. 4a, 4b*)
   - Zonal flow shears the turbulence radial correlation. (*Fig. 4a, 4c*)
   - Regulates the electron heat transport avalanches (*Fig. 3e,3f*)

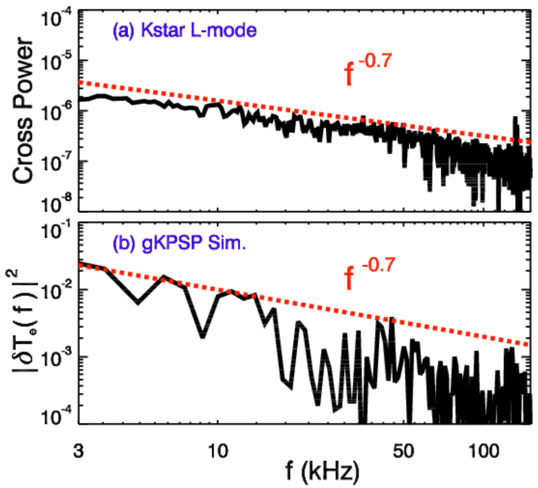

Figure 1

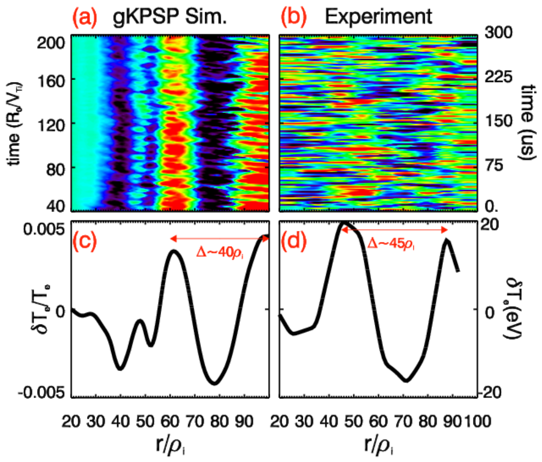

Figure 2

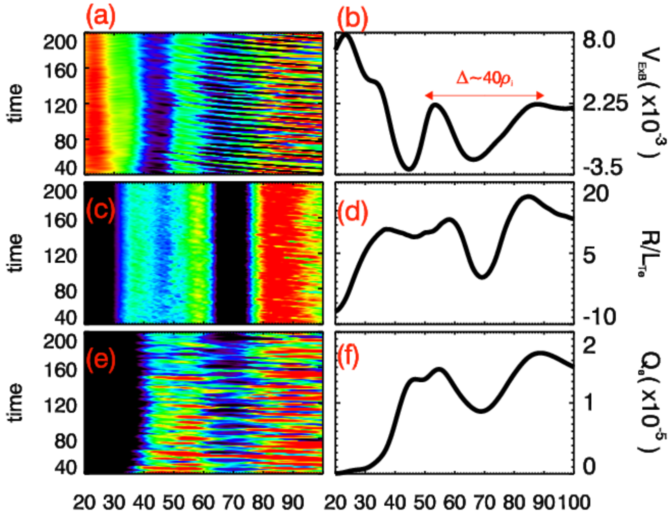

Figure 3

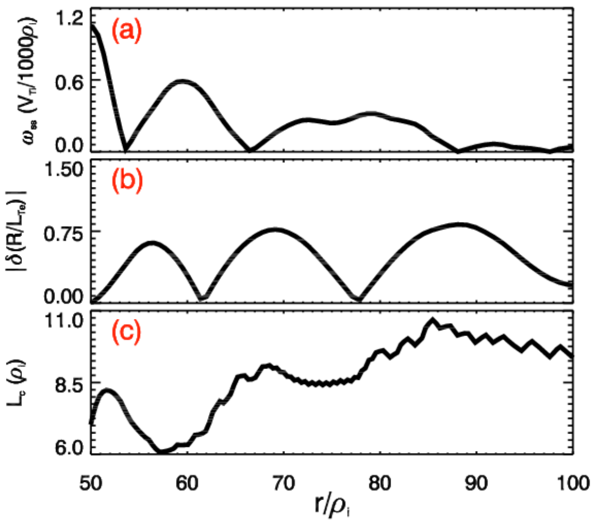

Figure 4

O20: KH instability [Chu Zhou]

Investigation of the Kelvin–Helmholtz instability in EAST

Based on the Doppler reflectometry measurement, a KH-like coherent mode triggered by velocity shear is observed at the EAST pedestal and the mode features, as well as the coupling with H-mode GAM are shown.

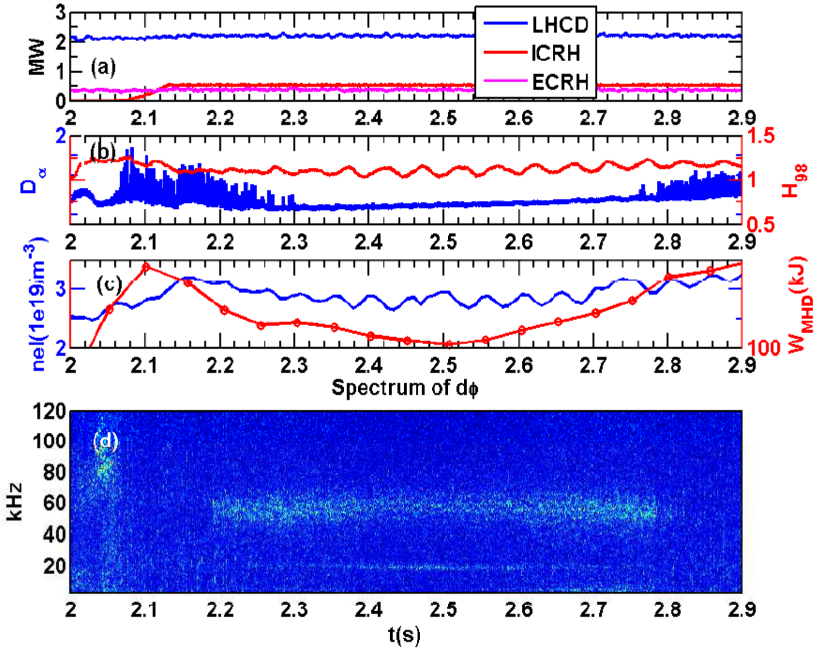

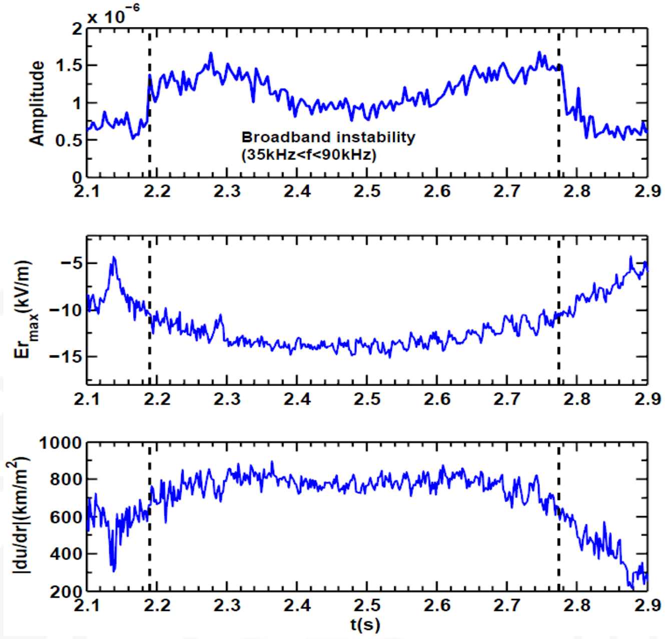

•After ICRH turns, the KH-like coherent mode appears, and then turns into the ELM-free operation;
•The density and energy decrease as this instability;
•GAM may accompany with this instability;
•When the edge velocity shear is large enough, the K-H like instability is aroused.

O44: turbulence and ICRF [Wei Zhang]

The interactions between ICRF and turbulence are Investigated on EAST. It is found that ICRF influences turbulence mainly by generating convective cells close to the antenna. While turbulence influences ICRF mainly by influencing the propagation of ICRF waves.

Influence of ICRF on turbulence

In the scrape-off layer:

Through radiofrequency (RF) induced convective cells

In the plasma core:

Through fast ions

Influence of turbulent on ICRF

On ICRF power coupling

By changing the width of fast wave evanescent layer

On ICRF wave fields

By changing the plasma dielectric properties in the filaments

Poloidal stretching and splitting of blobs by RF convective cells (#34676, measured by GPI)

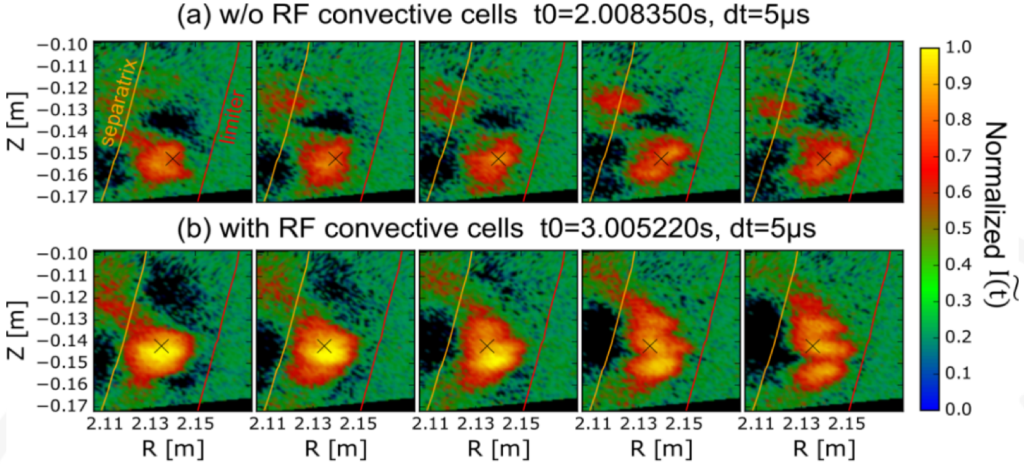

Scattering of ICRF wave fields by ELMy filaments (#33616, calculated by JOREK+RAPLICASOL)

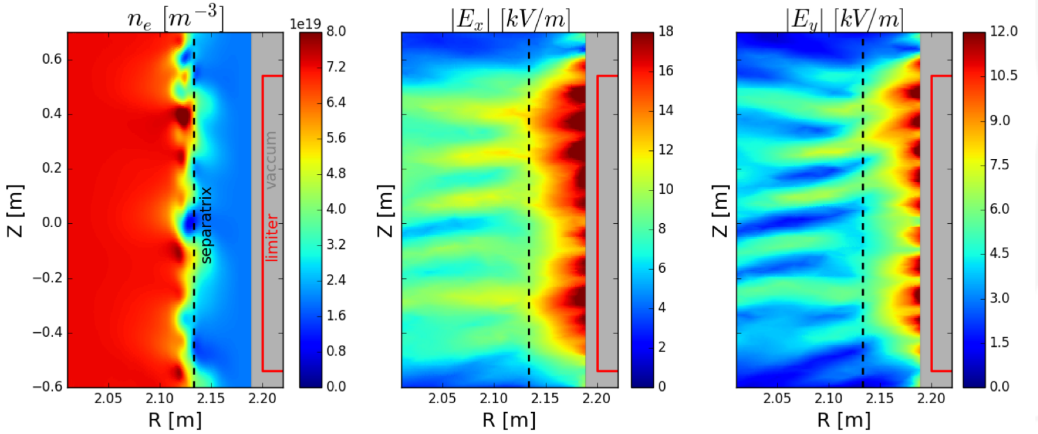

I30: Rotation; LHCD [Bo Lyu]

Overview of experimental investigation of LHCD's effect on plasma rotation on EAST

- **Plasma rotation change induced by the 4.6GHz LHCD on EAST were studied to characterize its behavior and dependence on various plasma parameters;**
- **For LHCD plasmas, co-current rotation increment was observed and increased with LHCD power. Rotation change was closely correlated with current density profile and inductance;**
- **Momentum transport analysis indicated a strong pinch in rotation, supported by intrinsic torque measurement with relatively co and large value the edge**

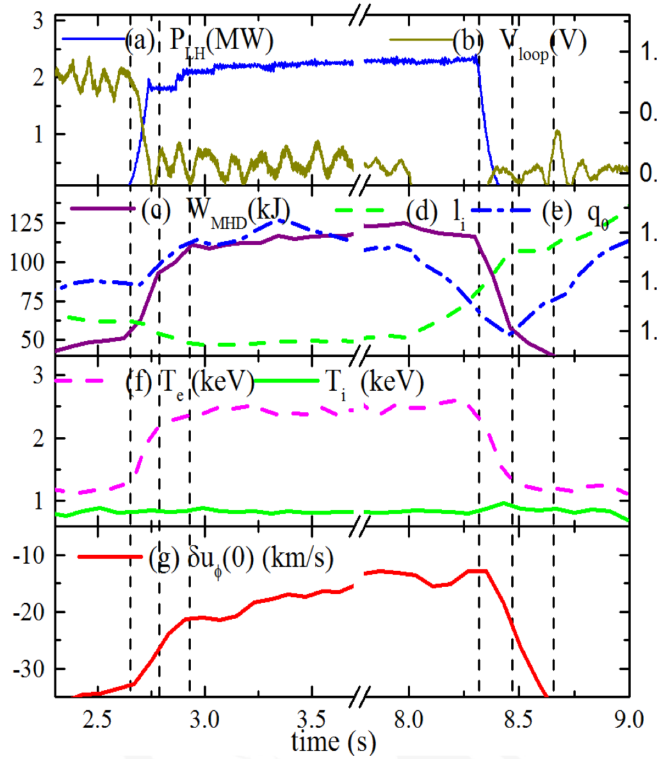

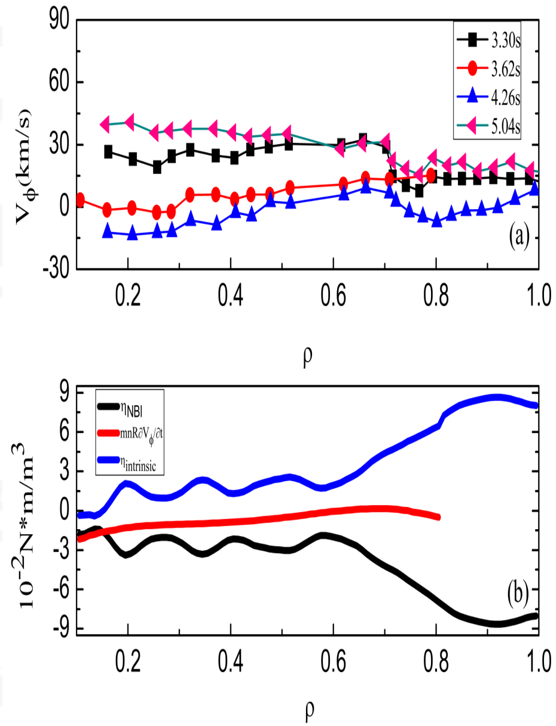

O43: magnetic coherent mode [Xingquan WU]

The drift kinetic effects of the magnetic coherent mode in the H-mode pedestal of EAST

experimental MCM (magnetic coherent mode)

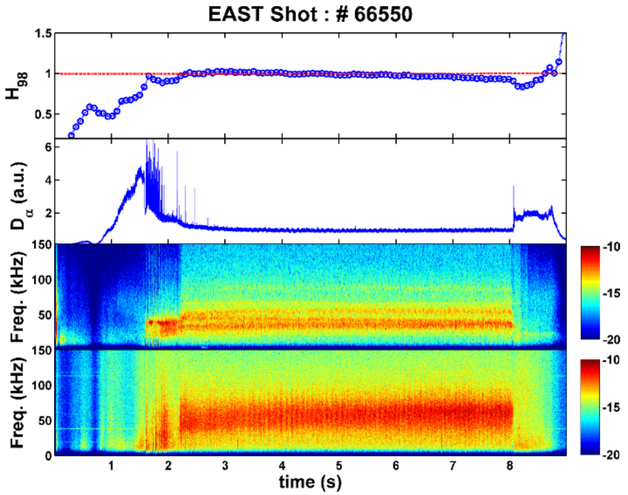

MCM appearance is independent of:

- Heating
- Wall coating
- Wall materials
- This may rule out the possibility of energetic particle driven mode.

Model analysis of MCM

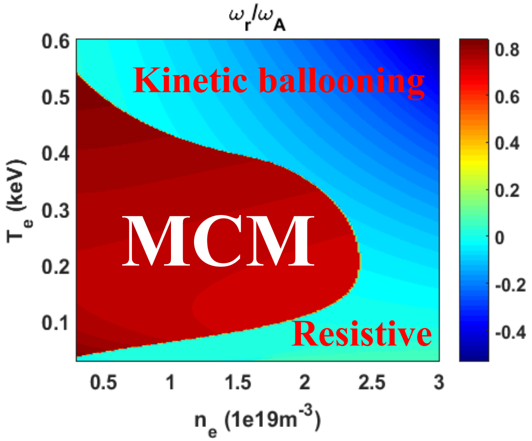

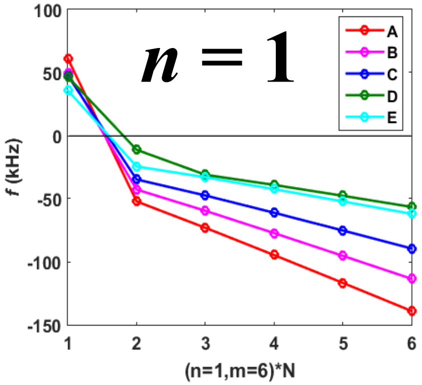

- A Magnetic Coherent Mode (MCM) is frequently observed in the EAST H-mode pedestal.
- Observations suggest that it is pressure-gradient-driven mode, but may rule out the possibility of energetic-particle-driven mode.
- An two-fluid model with drift kinetic effects successfully predicts a mode destabilized by the trapped electron bounce resonance. Its characteristics and parameter space are consistent with MCM.
- Model predicts that this mode could appear in the H-mode pedestal of future fusion reactors, such as CFETR.

O37: EAST coherent mode [Yanqing Huang]

Nonlinear simulation and energy analysis of the EAST coherent mode

The coherent mode in the edge region is a potential candidate to solve the high heat flux issue for EAST long-pulse high-performance operation.

- In simulations, n=5 mode is dominant. Compared to experiments, $k_\theta = 0.5(exp.) \rightarrow 0.2(sim.)cm^{-1}, n = 15(exp.) \rightarrow 5(sim.)$.

- Coherent mode is driven by the DAW and Peeling-Ballooning mode in the linear phase of nonlinear simulation.

Three-wave interaction and bispectral analysis get

1. In the process of mode coupling, energy transfer: medium-n → low-n modes,
   dominant modes: medium-n → low-n modes.
2. The mode coupling effect : Saturation phase > early phase; $T_e > N_i$

- The turbulence extracts more energy from density profile than electron temperature.

- The energy transfer rates prove that the coherent mode is electrostatic dominant.

O12,P12: Neural-network on transport [Emi Narita]

Quasilinear turbulent transport modeling with semi-empirical and mixing-length-like saturation rules

□ The neural-network based transport model DeKANIS has been constructed.

- Quick prediction of quasilinear kinetic fluxes
- Bringing information on the diagonal and off-diagonal terms

Quasilinear kinetic fluxes

$$\bar{\Gamma}_{\mathrm{e}} = \bar{D}\left(\frac{R}{L_{n_{\mathrm{e}}}} + C_{\mathrm{T}}\frac{R}{L_{T_{\mathrm{e}}}} + C_{\mathrm{P}}\right)$$

$$\bar{Q}_{\mathrm{e}} = \bar{\chi}_{\mathrm{e}}\left(C_{\mathrm{N}}\frac{R}{L_{n_{\mathrm{e}}}} + \frac{R}{L_{T_{\mathrm{e}}}} + C_{\mathrm{HP}}\right)$$

The fluctuation amplitude

How to estimate the coefficients

- ➢ C_{T}, C_{P}, C_{N} and C_{HP}: Gyrokinetic code linear calc.
- ➢ $\bar{D}$: **Two different saturation rules**
  - Semi-empirical rule -> DeKANIS-1
  - Mixing-length-like rule -> DeKANIS-2
- ➢ $\bar{\chi}_{\mathrm{e}}$: The Onsager symmetry

- ✓ DeKANIS predicts $\bar{\Gamma}_{\mathrm{e}}$ and $\bar{Q}_{\mathrm{e}}$ with a neural network, which has learned the coefficients estimated for JT-60U experimental data.
- ✓ The two models based on different saturation rules reproduce $\bar{\Gamma}_{\mathrm{e}}$ and $\bar{Q}_{\mathrm{e}}$ for unknown plasmas to a similar degree.

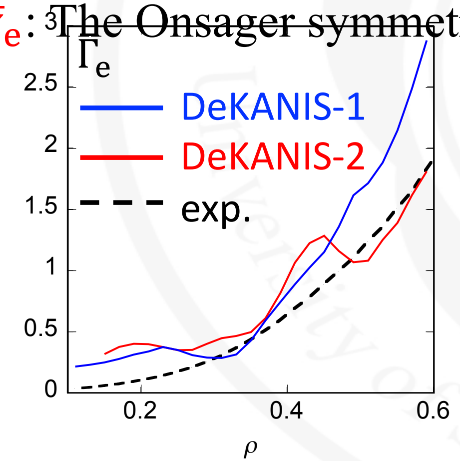

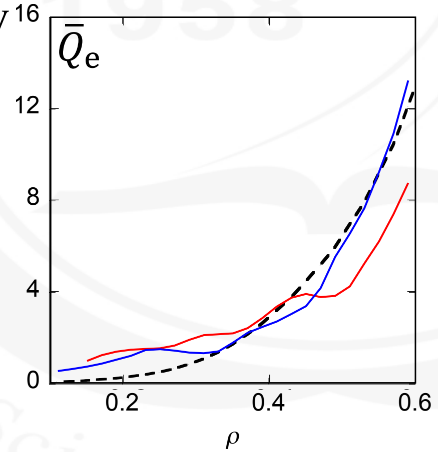

O33: Code integration [Dongrui Zhang]

Self-consistent simulation of transport and turbulence by coupling SOLPS-ITER and BOUT++

- The method and the procedure of coupling the fluid plasma/neutral 2D transport code SOLPS-ITER and the fluid 3D turbulence code BOUT++ are reported. SOLPS-ITER can provide the background profiles of density, ion, and electron temperature to BOUT++. In turn, BOUT++ can provide the corresponding radial transport coefficients to SOLPS-ITER.

- After several steps of iteration, the profiles of density, ion, and electron temperature show fluctuations, and the differences of the changes between two consecutive profiles are getting smaller and smaller. Finally, the self-consistent solutions of turbulence and transport can be obtained.

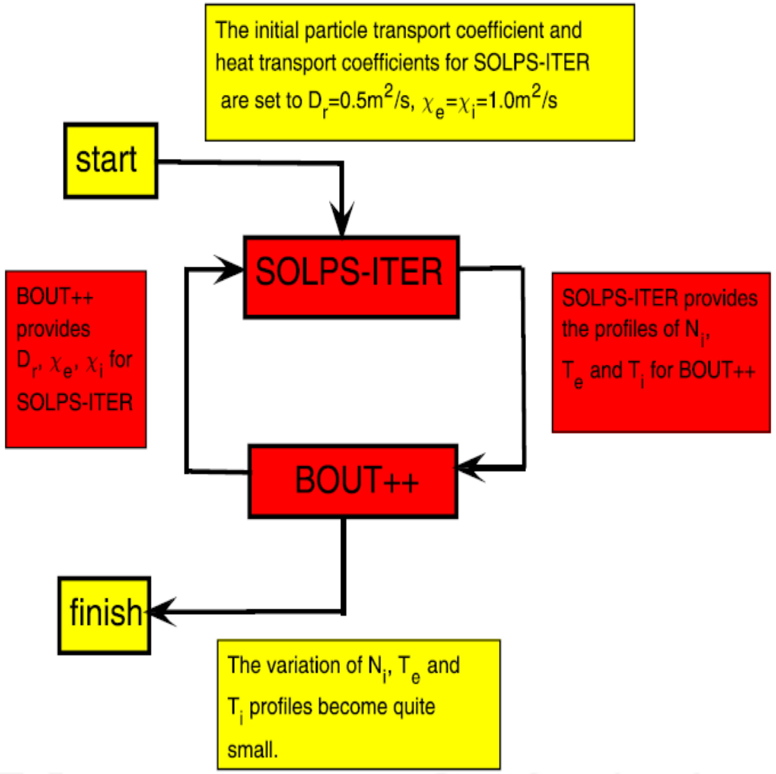

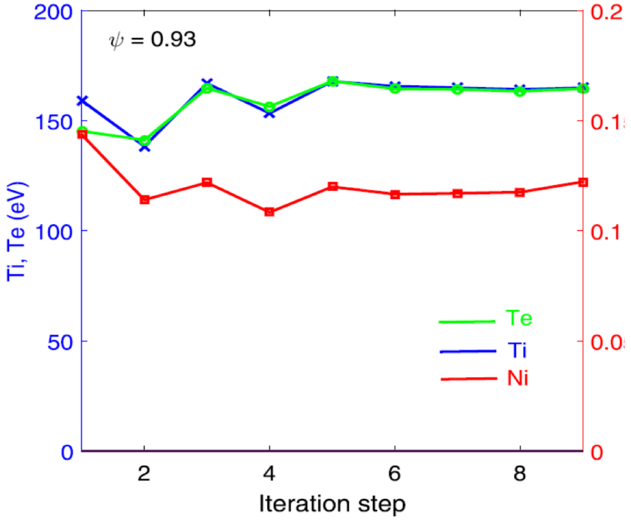

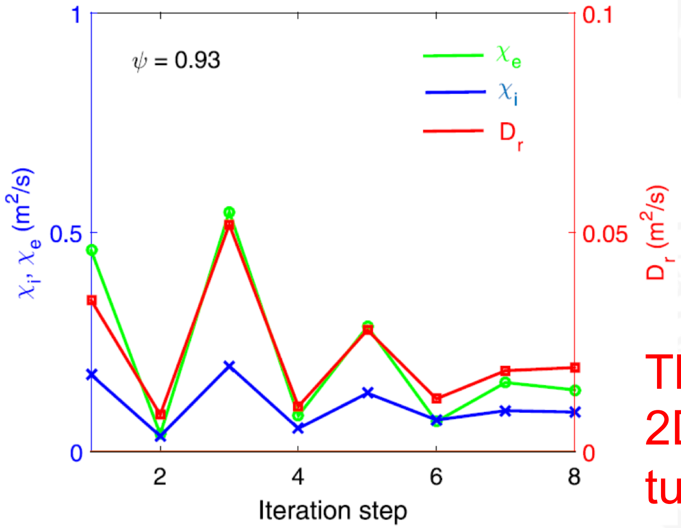

The method and the procedure of coupling the 2D transport code SOLPS-ITER and the fluid 3D turbulence code BOUT++ are reported.

O17: Core-edge integrated [Hai Xie]

Core-edge simulations of impurity behavior for the CFETR advanced scenarios

- **The impurity behaviors for the CFETR advanced scenarios have been analyzed by core-edge integrated simulations;**
- **The simulations are performed by different seeding impurities (Ne, Ar, Kr) with W divertor;**
- **Simulations show that impurity behaviors for the steady state and hybrid scenarios are similar;**
- **If W concentration in the core region is higher than 7×10^{-5}, power to SOL will be smaller than the L-H transition threshold and thus H mode cannot be sustained.**
- **Ne and Ar seeding is useful to reduce the heat load on divertor with high performance on core plasma;**
- **The operational window for Kr seeding is smaller, which requires higher density at separatrix or SOL diffusion coefficient.**

OMFIT

TGYRO (Turbulent and neoclassical plasma transport)
EFIT (Equilibrium)
ONETWO (source and sink for energy, momentum and particle)
EPED (Pedestal properties)

Plasma density and temperature profiles → Core plasma parameters

COREDIV

Plasma transport in the core region (1D)

$\Gamma, Q_{e,i}$ ↓ ↑ n_i, n_Z, T_e, T_i

Plasma transport in the SOL region (2D)

Outline

- Contributions to MF
- Major Progresses
  - Major progresses of machines
  - ELM control/simulation and RMP
  - MHD and EP physics
  - Transport and confinement
  - SOL/divertor/PMI physics
  - Scenario/Integrated model
  - Discharge Control/Diagnostics/Disruption

I1: Small Angle Slot Divertor (SAS) [Dan M. Thomas]

Closure, Detachment, and Energy Dissipation Studies Using the DIII-D SAS Divertor

The DIII-D SAS divertor provides a useful testbed for detailed modeling-experiment studies in a closed divertor.

In this system, the combination of enhanced neutral buildup and ExB drifts can significantly increase power dissipation and decrease heat flux to < few eV across the divertor target, necessary for future high duty factor reactor designs. Pedestal improvement is also seen.

Our ability to control drift directions and strike point locations, perform detailed in-slot measurements with novel localized diagnostics, and conduct constrained drift-dependent modeling are all key components of this research.

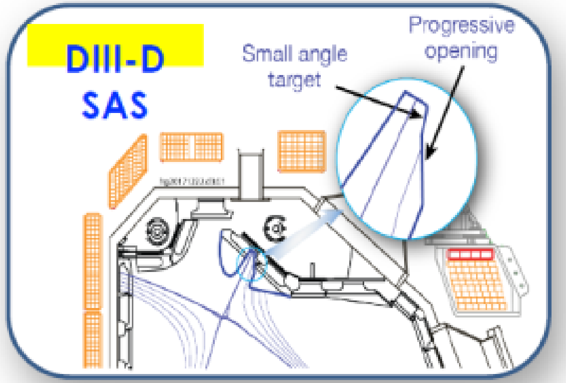

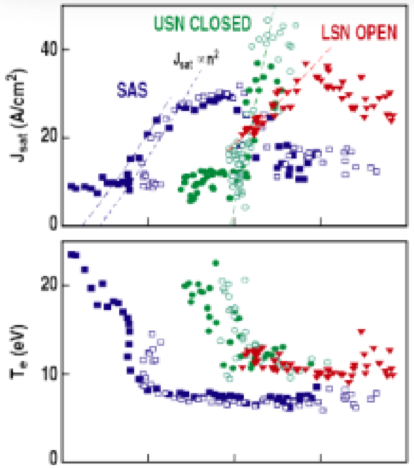

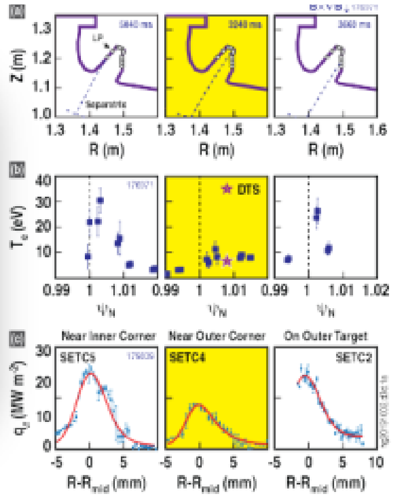

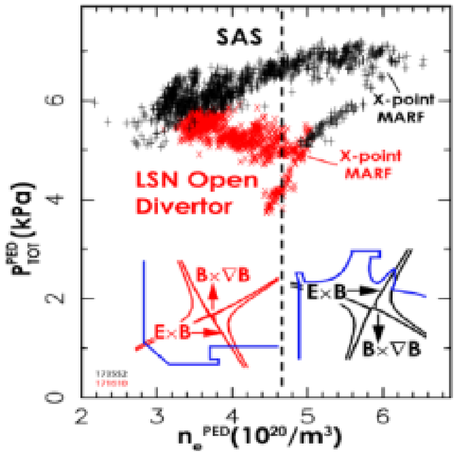

SAS operation has resulted in a confinement enhancement factor H_98Y2 up to ~30% better than the open divertor at the onset of detachment, as well as delaying the degradation in confinement due to enhanced radiation to significantly higher (~30%) pedestal densities.

O6: Detachment [Kedong Li]

Radiative divertor study for detachment in the grassy ELMy H-mode in EAST

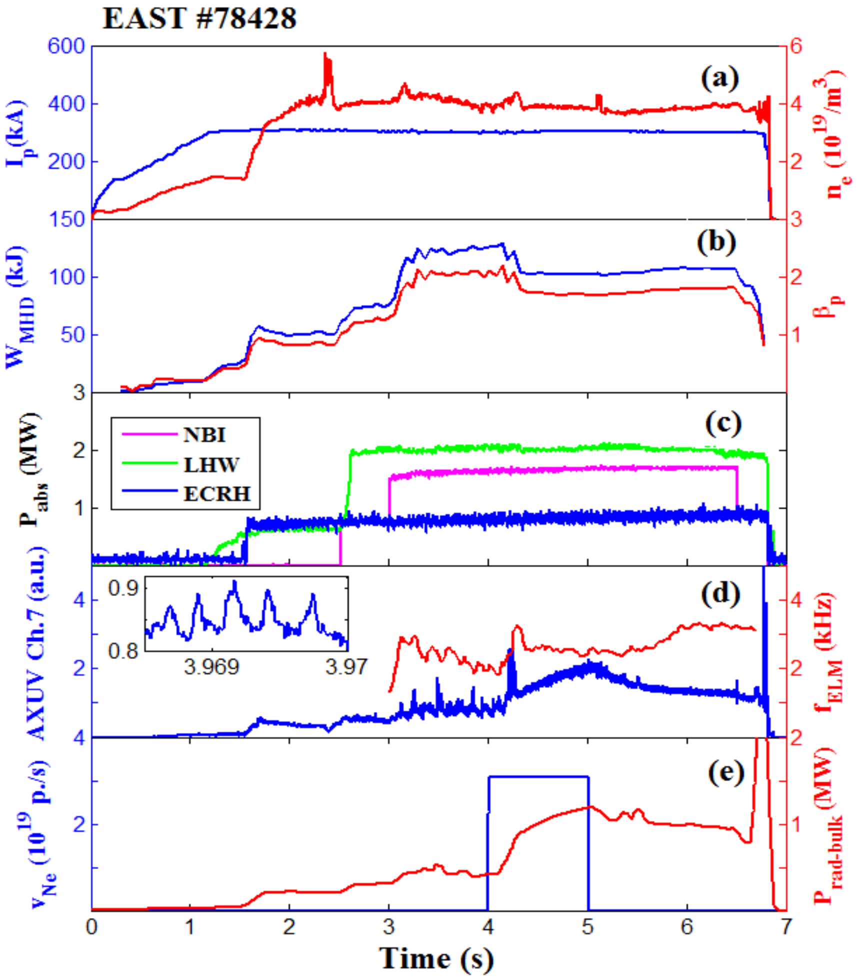

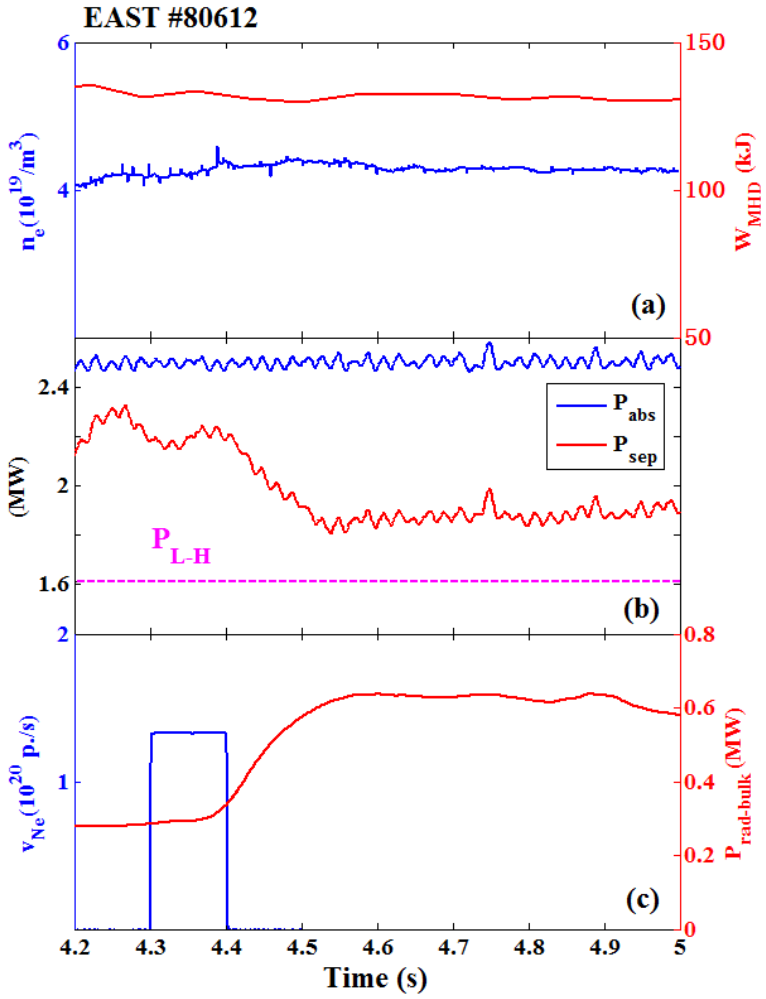

The combination of grassy ELMy regime and radiative divertor operation was proposed and performed in EAST

- ◆ Stable deep partial detachment
- ◆ Patial detachment without confinement degrade

I6: PWI [Dmitry Borodin]

Plasma-surface interaction studies in preparation of JET-ILW TT and DT operation

- **Plasma-wall interaction studies are an integrated part of JET exploitation**
  - ***Be/W ITER-like wall***
  - ***H, D, T isotope and DT***
- **Be and W impurity sources, Be migration, T retention are interconnected. ERO2.0 simulations give an insight on the interplay of various processes**
  - ***interpretive as well as predictive modelling***
- **Dedicated experiments are used for code and data validation.**
  - ***ERO2.0 used both in situ (spectroscopy, QMB) and post mortem measured data.***
- **The lessons learned at JET-ILW are extrapolatable for ITER:**
  - ***The improved sheath model and Y_{eff} procedure tested at JET impact ITER life time predictions***
  - ***Suppression of CAPS, CX and self-sputter contributions, effect of ICRH sheaths and molecular processes can impact ITER similarly to JET-ILW***
- **ILW contributed already to the ITER research plan (e.g. decision on W divertor) and will continue this in future with the isotope campaigns and DT operation**

presents the general understanding of the PWI picture at JET in Be/W environment, gives an overview of key JET experiments including the outlook for TT/DT and modelling efforts

I33: Impurity flow; SOL [Cameron Samuell]

Two absolutely calibrated Doppler Coherence Imaging Spectroscopy diagnostic systems are employed on DIII-D for direct measurement of ion flows, and the first imaging of 3D flows in a tokamak is estimated.

Velocity Imaging for Understanding Particle Transport in the Boundary of Magnetically Confined Plasmas

- Detailed investigations of physics driving 2D and 3D features in impurity velocities are now possible
  - Enabled by absolutely calibrated 2D imaging of ion velocities
- Estimation of convective heat transport points towards significant transport from cross-field drifts
- 2D UEDGE comparisons indicate need for more ion data to complement electron diagnostic (eg T_i)
- First imaging of 3D flows in a tokamak

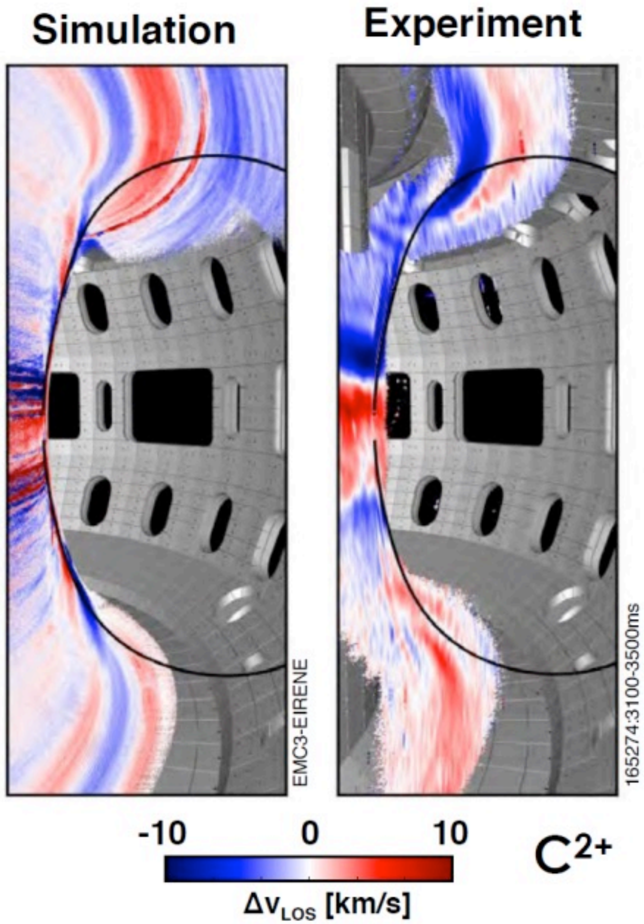

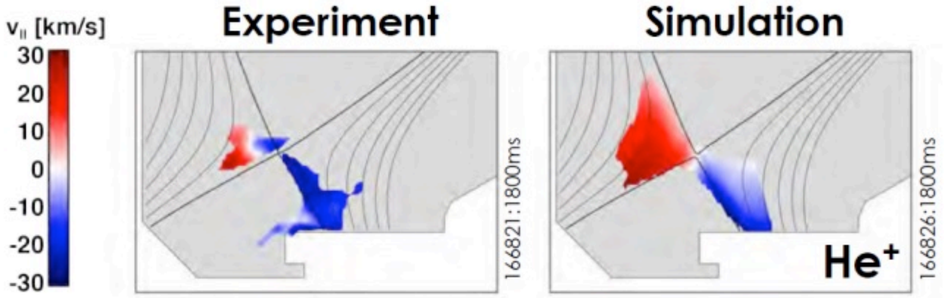

I18: Impurity seeding [Zhongshi Yang]

Experiments and simulations for power exhaust by impurity seeding on EAST and future devices

- Mitigation of high heat flux is a critical issue for ITER and future fusion reactors with high performance and long-pulse operation.
- The divertor plasma detachment can be achieved by Ne/D_2 and Ar/D_2 mixture seeding with different ratios and the heat flux and particle flux onto the target can be reduced dramatically.
- Multi-pulsed method could effectively avoid excessive impurities entering the plasma core region and causing contaminations there.
- The active radiation feedback control experiments were successfully realized on EAST.
- The simulations for Ar/Ne seeded radiative divertor experiments in EAST basically agreed well with the experimental results.

I35: SOL simulation [Fabio Riva]

Comparison of three-dimensional plasma edge turbulence simulations in realistic double null tokamak geometry with experimental observations

How to simulate scrape-off layer plasma turbulence with the STORM code? How do the numerical result compare to experimental observations?

➔Simulations of L-mode MAST plasma discharge with STORM [Riva *et al.*, 2019]. Simulations contain drift physics, turbulence, filaments, parallel flows, and sheath losses.

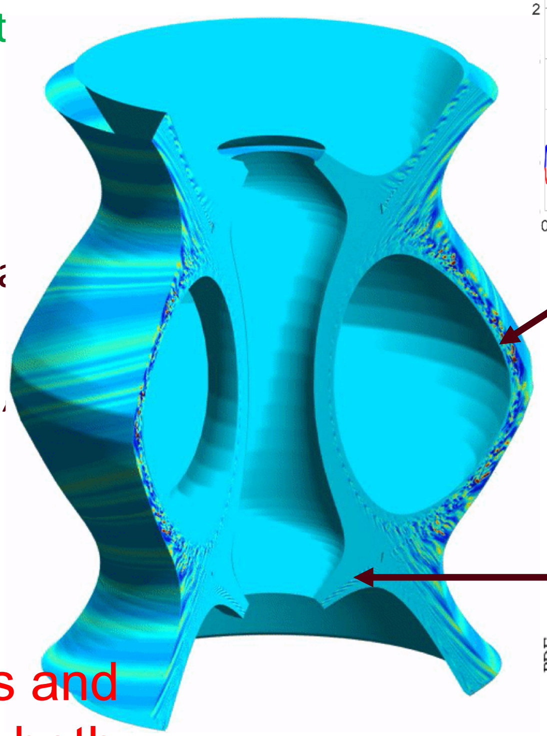

Good qualitative agreement between STORM simulations and experimental measurements both at the outer mid-plane and in the divertor legs is shown.

Outer mid-plane:

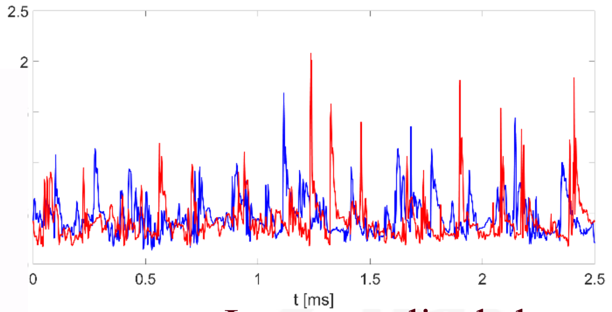

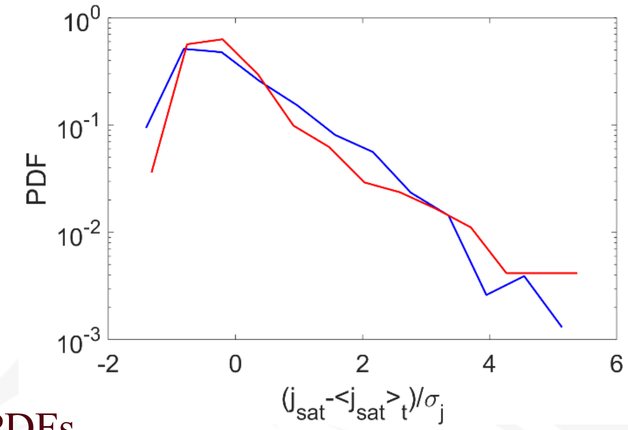

- Large amplitude bursts
- Skewed and flattened PDFs

Divertor legs:

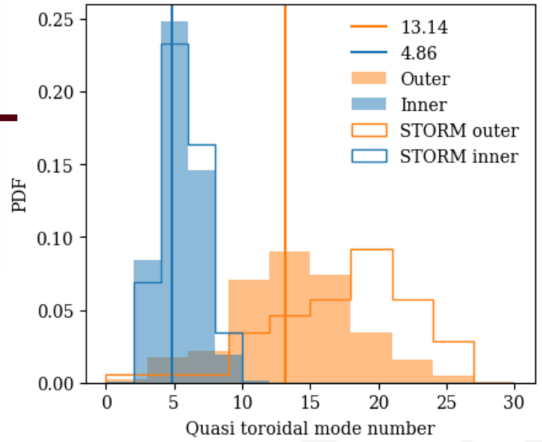

- Near separatrix: interchanges modes in inner legs, drift-waves and Kelvin Helmholtz in outer legs
- Asymmetry in quasi toroidal mode number between inner and out legs

O1: SOL-Divertor [YiPing Chen]

Simulations of SOL-Divertor Plasmas in EAST by using SOLPS-ITER

1. The edge plasma simulation code **SOLPS-ITER has been used for the simulation of SOL-Divertor plasmas on EAST tokamak**.

2. The effort has been made to simulate the SOL-divertor plasmas in the experimental shots on EAST tokamak for the comparison between the simulation results and the experimental measurement.

3. **The agreement between the code results and experimental measurement can be found** in the profiles of plasma parameters **at the inner and outer target plates**.

4. The simulation of the tungsten impurity transport has been carried out by using the code and the density distribution of the tungsten impurity has been obtained.

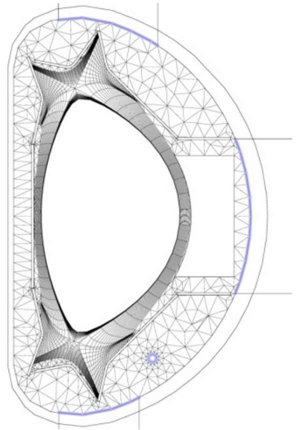

The computational meshes

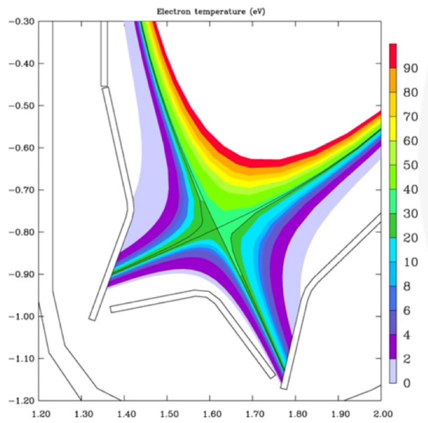

The profile of plasma temperature

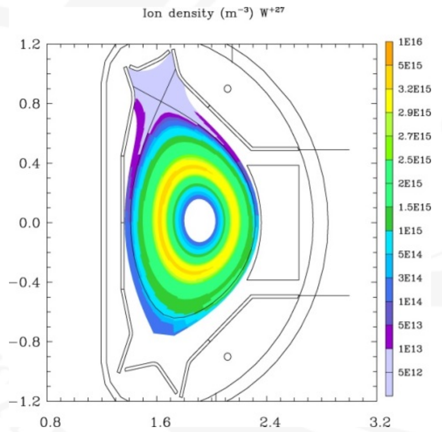

The density distribution of the tungsten impurity

I4: Flowing liquid lithium limiter [Guizhong Zuo]

Improvement of plasma performance with flowing liquid lithium PFCs in EAST

FLiLi can signifanctly improve high power H mode plasma performance.

Shot 81510 without FLiLi

Shot 81637 with FLiLi R_{FLiLi}=2.35m

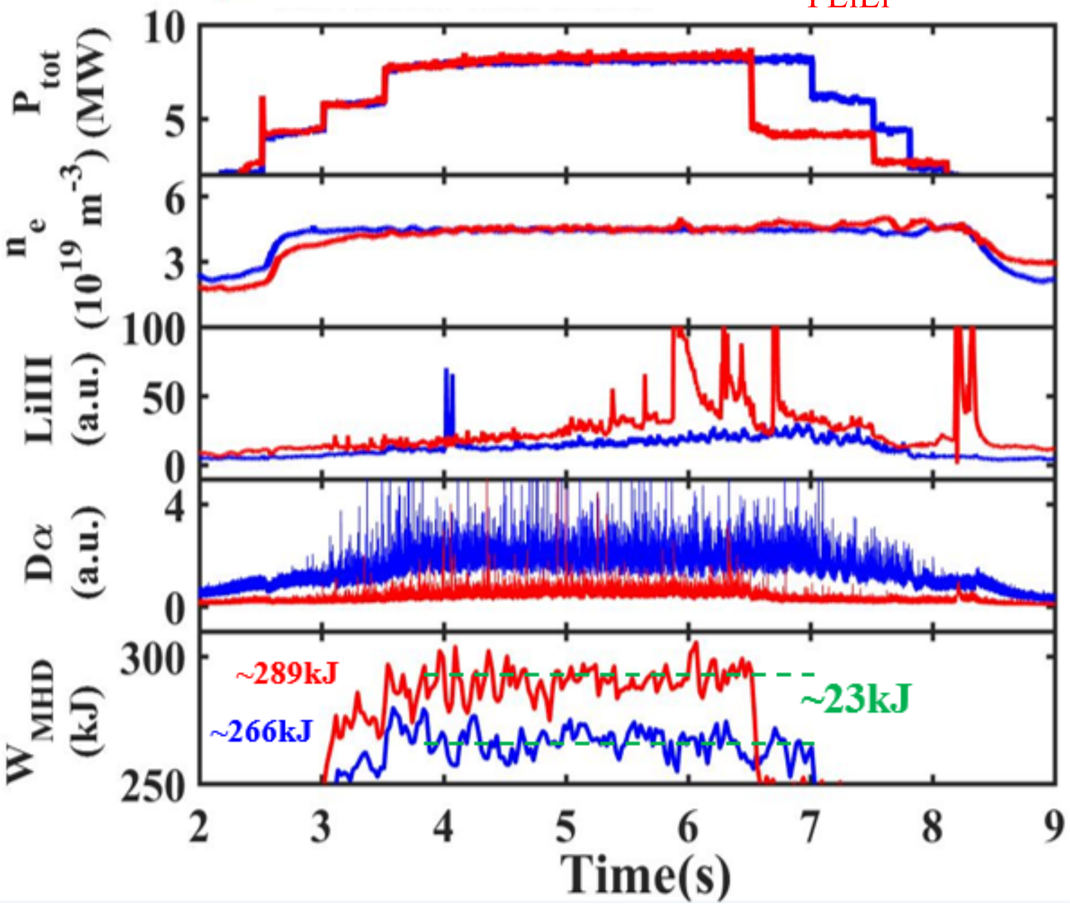

- ❖ **Compatible with high power plasmas!**
- ❖ Heating power: ~8.3MW
- ❖ Similar plasma parameter
- ❖ n_e and I_p=0.55MA
- ❖ **Strong Li emission**
- ❖ **Low particle recycling**
- ❖ **Large ELM mitigation**
- ❖ **Increased plasma stored energy**
- ❖ **Max. Stored energy: > 280KJ**

O32: Liquid Lithium [Daniel Andruzyk]

Liquid Lithium/Metal Research for Fusion

Liquid Lithium/Metal research for magnetic fusion at the University of Illinois is introduced in details

- **Liquid Lithium material testing**
  - Thermo-electric properties
  - Wetting properties
  - Corrosion studies
- **Flowing Liquid Lithium Limiters**
  - LiMIT
    - A flowing concepts, self pumping, has been developed.
    - Control of the wetting is possible
  - Flowing Lithium Limiter
    - Flowing liquid lithium limiters are progressing.
    - Constant low recycling surface is available during a plasma.
    - On 3rd generation of FLiLi.
    - Next tests preparing for LiMIT, Mo plate with TEMHD trench system.
- **CPMI and HIDRA**
  - HIDRA
    - up and running.
    - Magnetic flux surface have been measured.
    - Operation and first plasma experiments started and co
    - Material Analysis Test-stand (HIDRA-MAT)
  - MEME
    - Liquid lithium limiter-EAST integration
    - Plug-and-Play.
  - Distillation Column
    - Hydrogenic species removal
    - Eventual loop design for fuel/impurity extraction

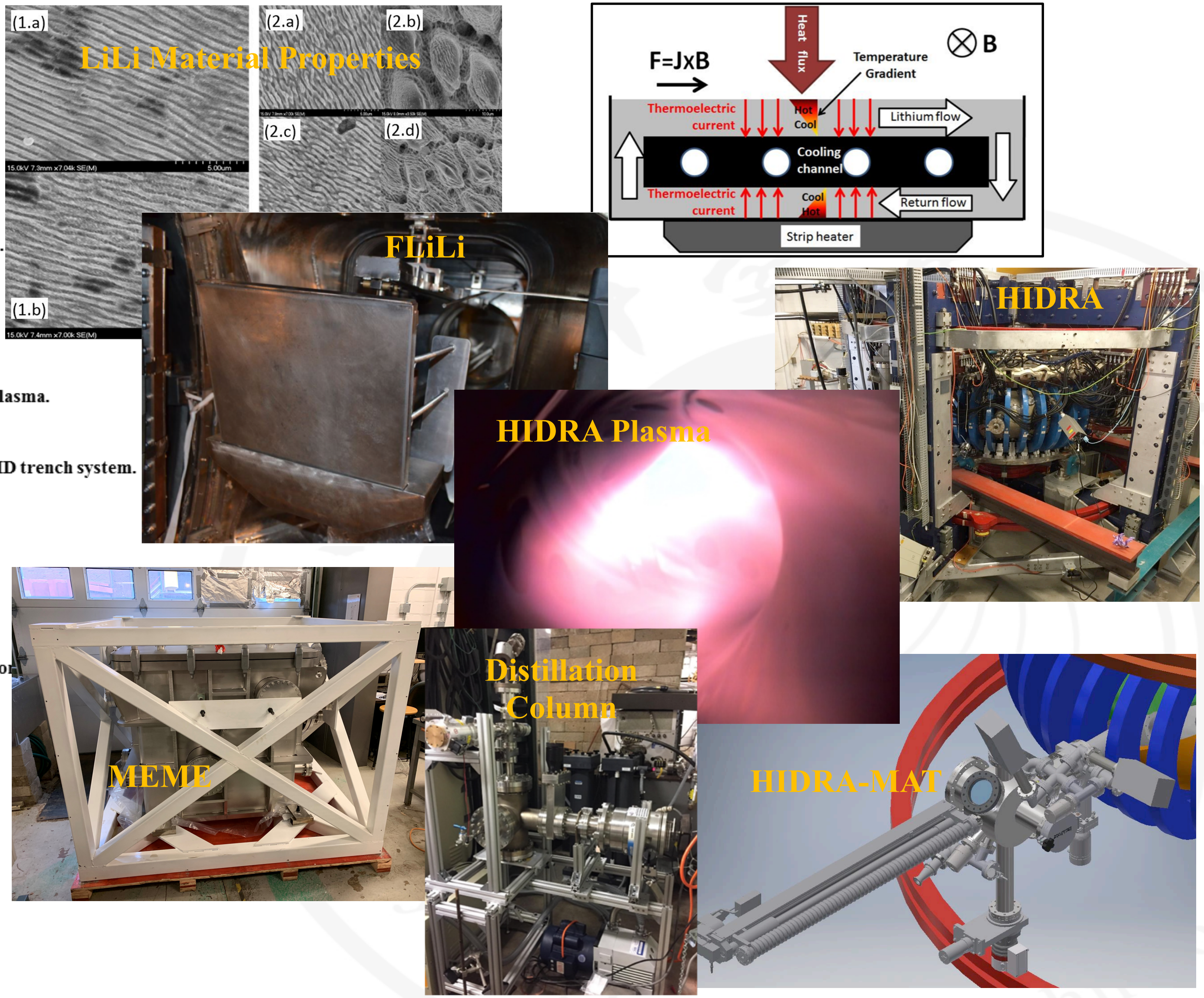

O35: Heat flux sim. [Tianyang Xia]

Simulations on the transient heat fluxes for the RF wave heating H-mode on EAST through BOUT++ are shown.

LHW:

- LHW can drive the helical current filament (HCF) in SOL, which changes the edge topology.
- A modeled HCF with force-free form in SOL is added into BOUT++ as the extra magnetic flutter.
- SOL width λ_q is indeed broadened by HCFs.
- The splitting of strike point behavior is reproduced

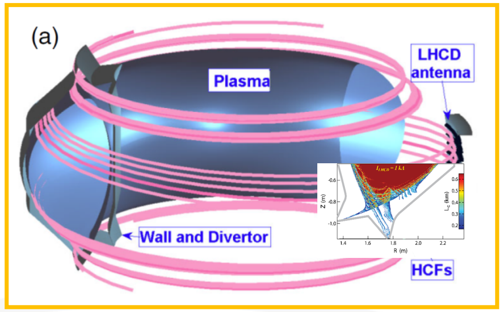

Weak filament align magnetic field line

Strong filament by HCF

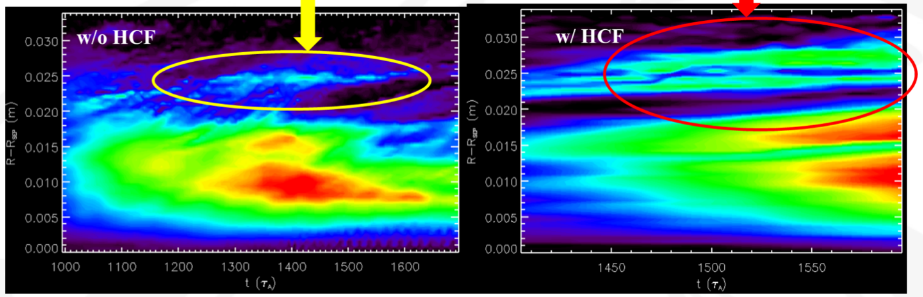

Splitting of the strike point is reproduced within HCF

ICRF:

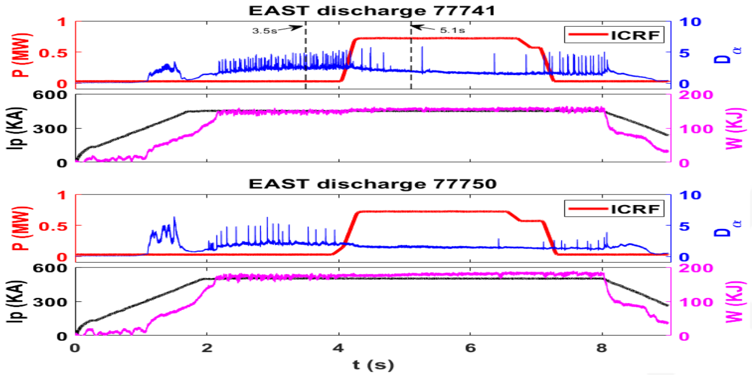

- ELM is able to be suppressed by ICRF on some EAST exps..
- The RF sheath is found the necessary factor to reproduce this effects
- Other effects, such as shear flow, turbulence, impurities…, are not practical.
- The RF sheath generates the strong flow shear near the separatrix, which leads to the widely nonlinear mode coupling.

Bicoherence analysis for RF sheath effects

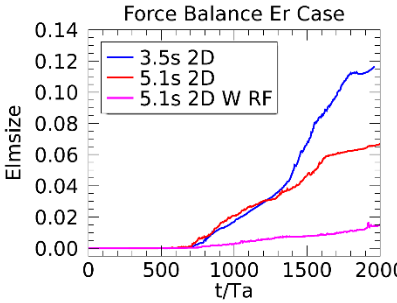

ELM size is decreased effectively by RF sheath

- 5.1s Er_Force:
- 5.1s RF sheath Er :

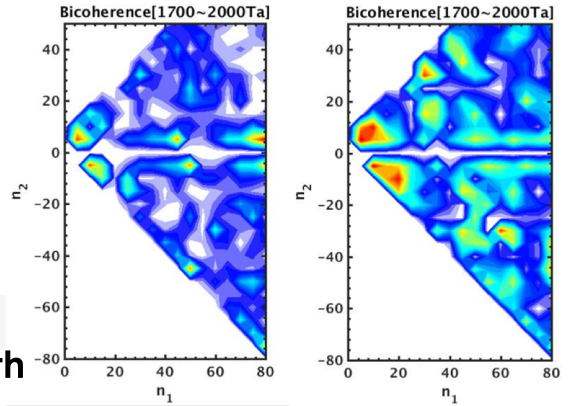

O16: Heat flux, CFETR [Feifei Nian]

Modelling of heat flux on CFETR first wall

Parameters	Steady-State (SS)	Hybrid	ITER (Q=10)
P_{fus} (GW)	1.0	0.92	0.5
$P_{heat}=P_\alpha+P_{aux}$ (MW)	305	251	173
P_{rad}^{core} (MW)	86	73	70
P_{sep} (MW)	219	178	103
P_{sep}/R (MW/m)	30	25	17

Larger P_{sep}/R, more risk on PFCs including blankets and divertor.
Estimation of heat load is becoming urgent

Design parameters for CFETR

The heat flux deposited on the first wall of CFETR with 1GW power is investigated by coupled modelling of SOLPS-ITER and PFCFLUX

SOLPS-ITER

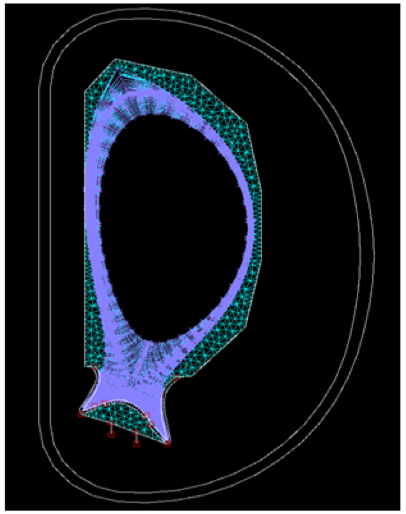

PFCFLUX

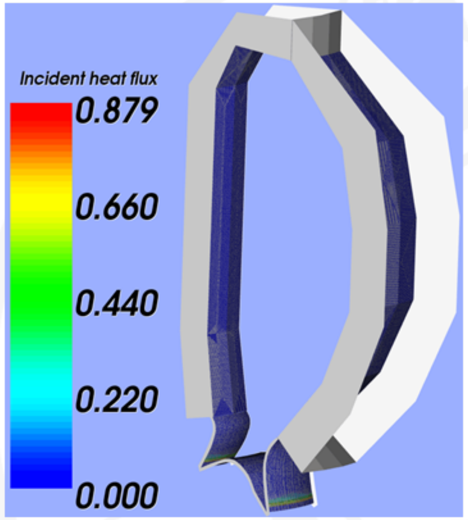

Coupling two codes

Radiation heat flux

Charged particle heat flux

A relatively complete heat flux

B2.5 & EIRENE, Plasma computation grid not extended to first wall

Through energy and parameters analysis from SOLPS, It provides a consistent input power and decay length for PFCFLUX.

Field tracing algorithm & exponential decay model

O31: Carbon deposition inside gaps [Qian Xu]

Simulation of carbon deposition inside gaps

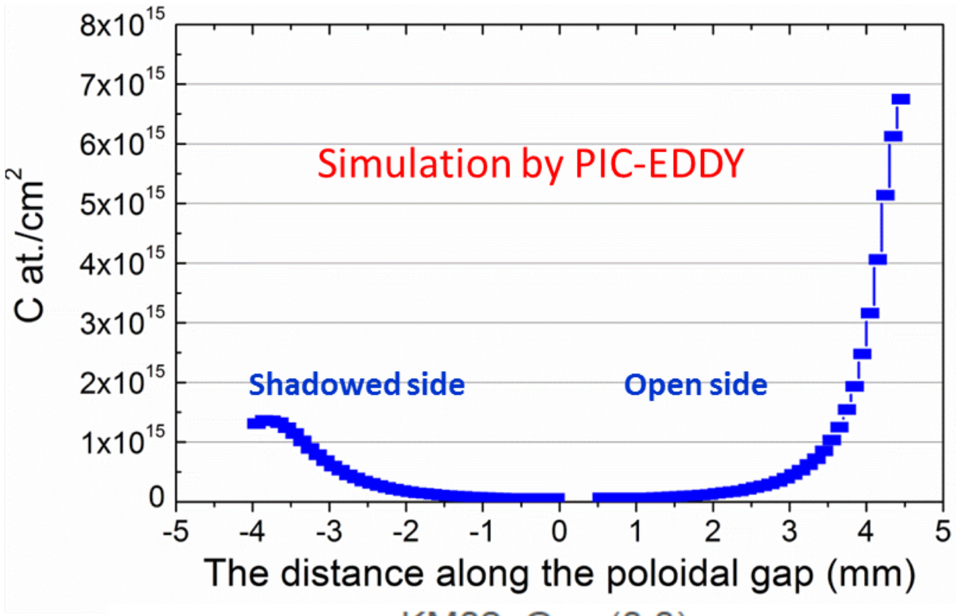

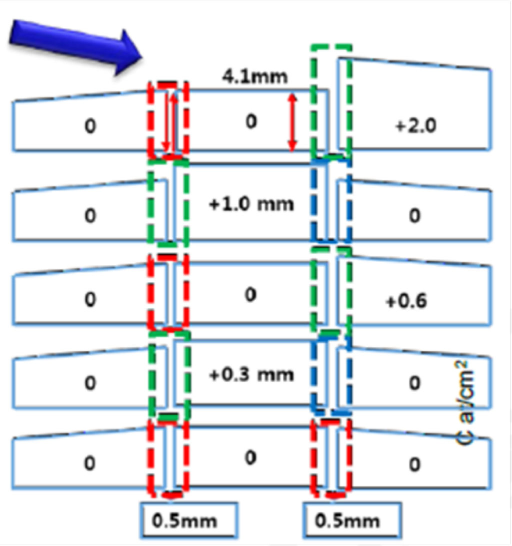

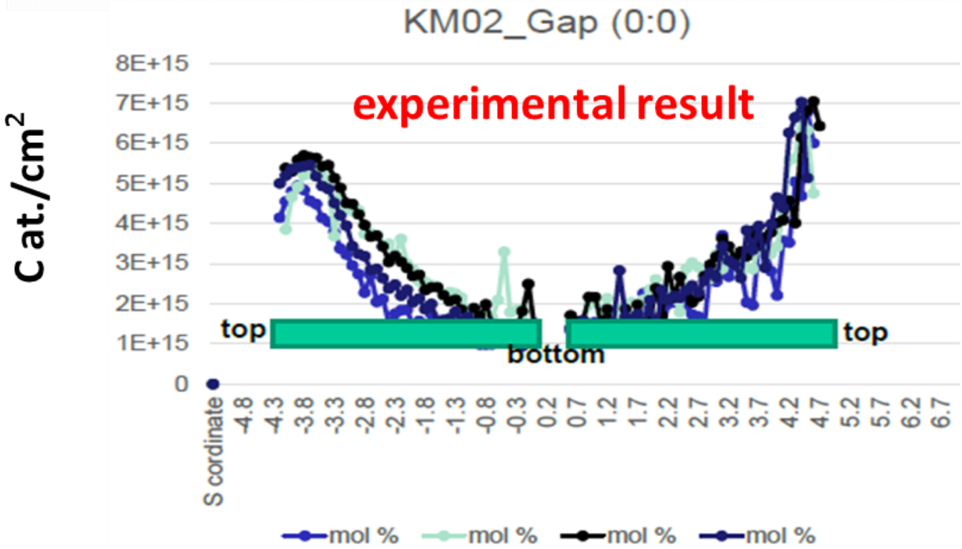

- The peak deposit amount is 7*10^{15} at/m^2.
- It's consistent with experimental result for deposition on the open side but on the shadowed side.
- CHx neutral molecules generated from chemical sputtering and A&M processes in the plasma may be one reason.
- The experimental results were obtained after a campaign, that means the divertor tiles experience many difference discharges

The deposition mechanisms inside gaps of castellated blocks with different shapes by comparison with results from KSTAR through 3D Monte Carlo code PIC- EDDY

Outline

- ➲ **Contributions to MF**
- ➲ **Major Progresses**
  - ☞ **Major progresses of machines**
  - ☞ **ELM control/simulation and RMP**
  - ☞ **MHD and EP physics**
  - ☞ **Transport and confinement**
  - ☞ **SOL/divertor/PMI physics**
  - ☞ **Scenario/Integrated model**
  - ☞ **Discharge Control/Diagnostics/Disruption**

PL19: Compact pilot plant [Richard Buttery]

An Attractive Compact Pilot Plant is Possible *when Advanced Tokamak Physics Principles are Applied*

- **High β_N & high density enable high bootstrap current to reduce recirculating power**
  - **Mitigates divertor heat flux & neutron loads**
  - **Operation at high safety factor without disruptions**

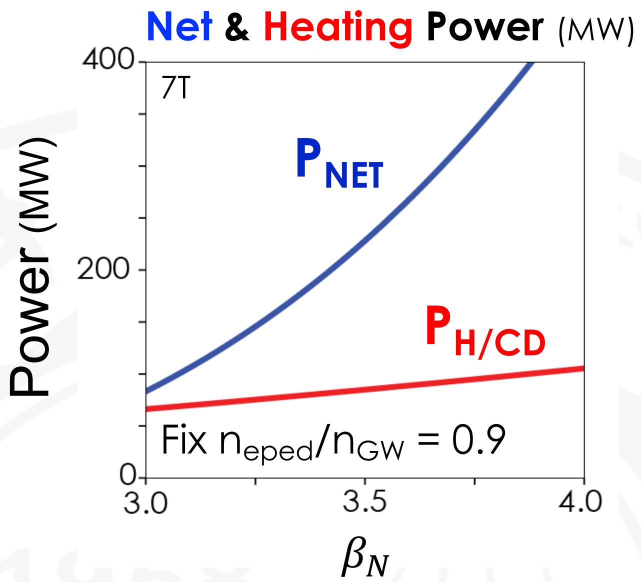

	6T	7T
I	9.5	8.2
q	5.7	7.1
β_N	4.3	3.5
H_{98}	1.3	1.5
Q	10	13
P_{heat}	74	51
P_{fus}	750	640
Neut.	1.9	1.7

- **200MW net electric at R=4m B=6-7T**
- **Sets research challenge for community:**

Validate AT physics: high β_N, high density, transient-free

Develop efficient current drive and steady state **divertor solution**

Technology: High T superconductors, reactor materials, engineering

Compact AT fusion device could realize net electric and nuclear research missions

I41: Enhanced pedestal [Devon Battaglia]

Enhanced Pedestal (EP) H-mode Regime on NSTX

EP H-mode on NSTX features a wide pedestal with improved energy and momentum confinement with a beneficial decrease in the impurity accumulation relative to a standard ELM-free H-mode; Largest normalized energy confinement on NSTX observed in EP H-mode;

- EP H-mode: edge ∇T_i increases while edge density decreases
  - Due to reduced neoclassical transport at low ν_i^* where $\chi_{i,neo} \propto Z_{eff} n_e$
  - $H_{98y,2} > 1.5$ operation in an ELM-free regime
- Recovery from large ELM can result in new pedestal solution with larger $\chi_{i,anom}$ and smaller $\chi_{i,neo}$
  - At low ν_i^*, can get improved thermal confinement while increasing particle transport

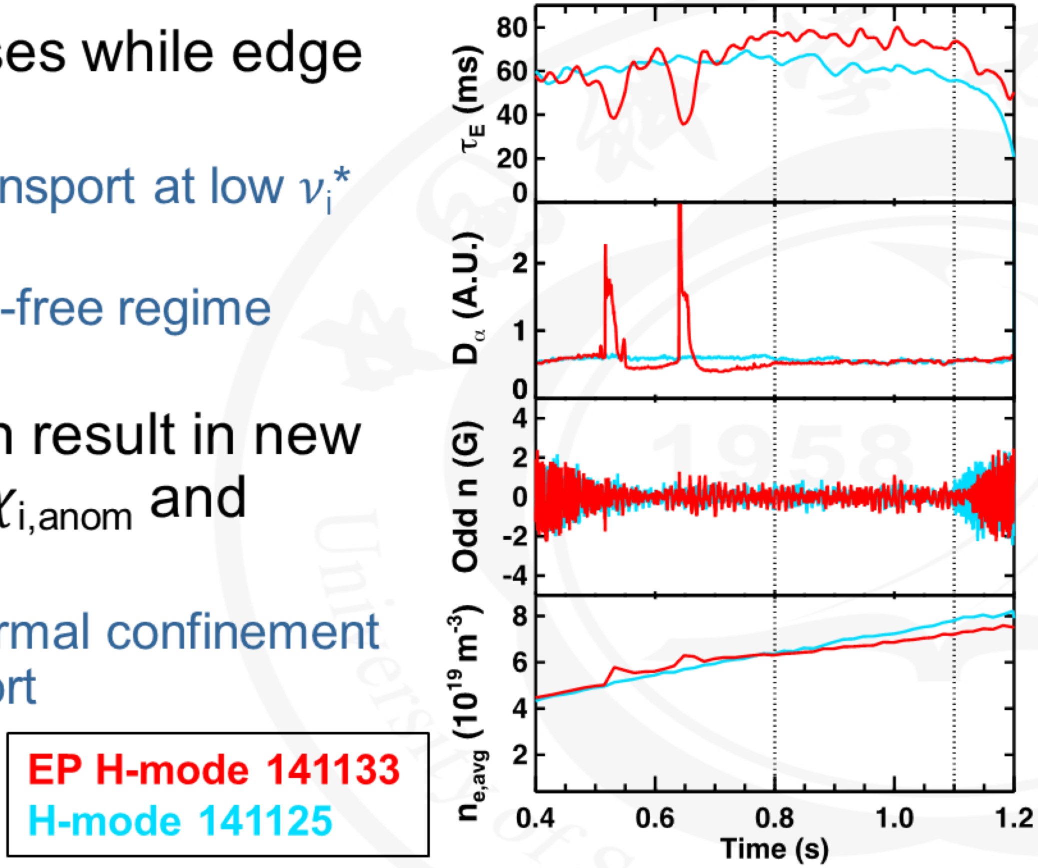

I13: Anisotropy impact [Matthew Hole]

The impact of anisotropy on ITER scenarios and ELMs

- New tools to study impact of anisotropy on equilibrium / stability
  - ➢ HELENA+ATF / remapping tools for equilibria with anisotropy for same J_{ϕ}, W_{th}
  - ➢ MISHKA-A – studies continua, global modes with anisotropy and FLOW
- First application to ITER-scenario remapping show shift of pressure and density relative to flux surfaces is possible

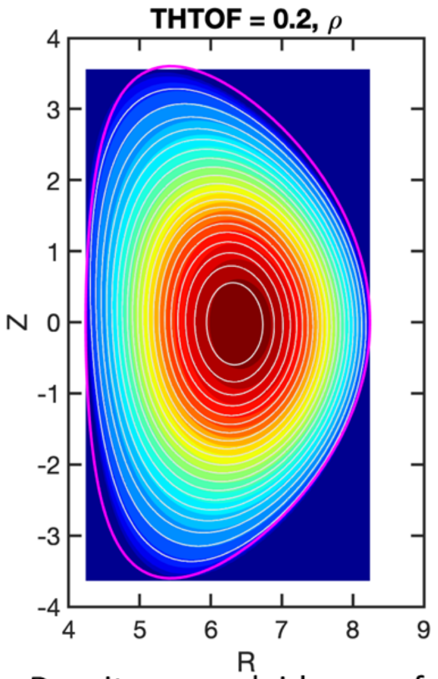

Density ρ overlaid on surfaces of constant flux (white) for ITER cross-section

- Impact of anisotropy on the compressional continuum substantial

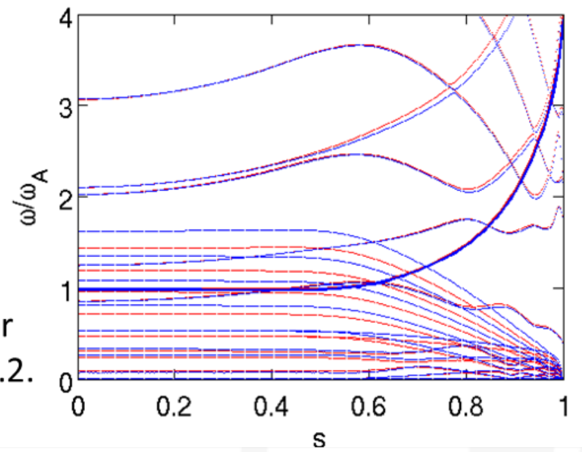

Compressional continuum for n=1 and $T_{||}/T_{\perp}=0.8$, $T_{||}/T_{\perp}=1.2$.

- First application to stability of n=30 ballooning mode. [PPCF 60 (2018) 065006]

γ^2/ω^2 increases with increasing $p_{\perp}/p_{||}$.
$\Rightarrow$ *increasing* $p_{||}/p_{\perp}$ in the pedestal region might lead to higher ELM-free performance

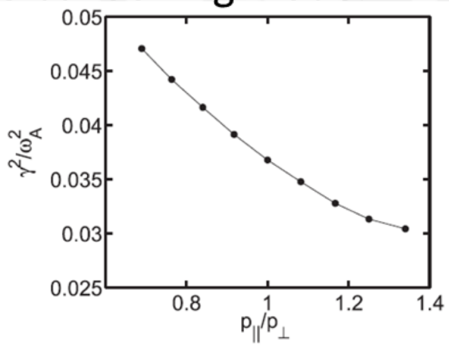

New tools are developed to study the impact of anisotropy on equilibrium / stability and firstly applied to ITER-scenario, as well as the impact of anisotropy on ballooning mode.

I20: NT High confinement [Max Austin]

Confinement and stability in DIII-D negative triangularity discharges and relevance for reactor devices

- Growing database of DIII-D NT discharges shows
  - H-mode confinement w/ L-mode edge
  - Significant β_N, ~3, without disruption
  - Appreciable bootstrap current w/ good alignment
- Bodes well for an NT reactor in low collisionality regime (TEM dominant)

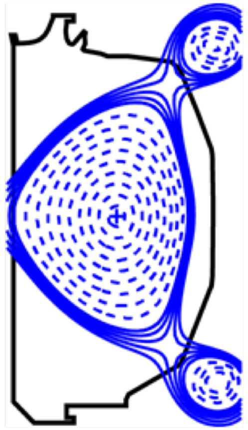

All discharges L-mode edge, no ELMS

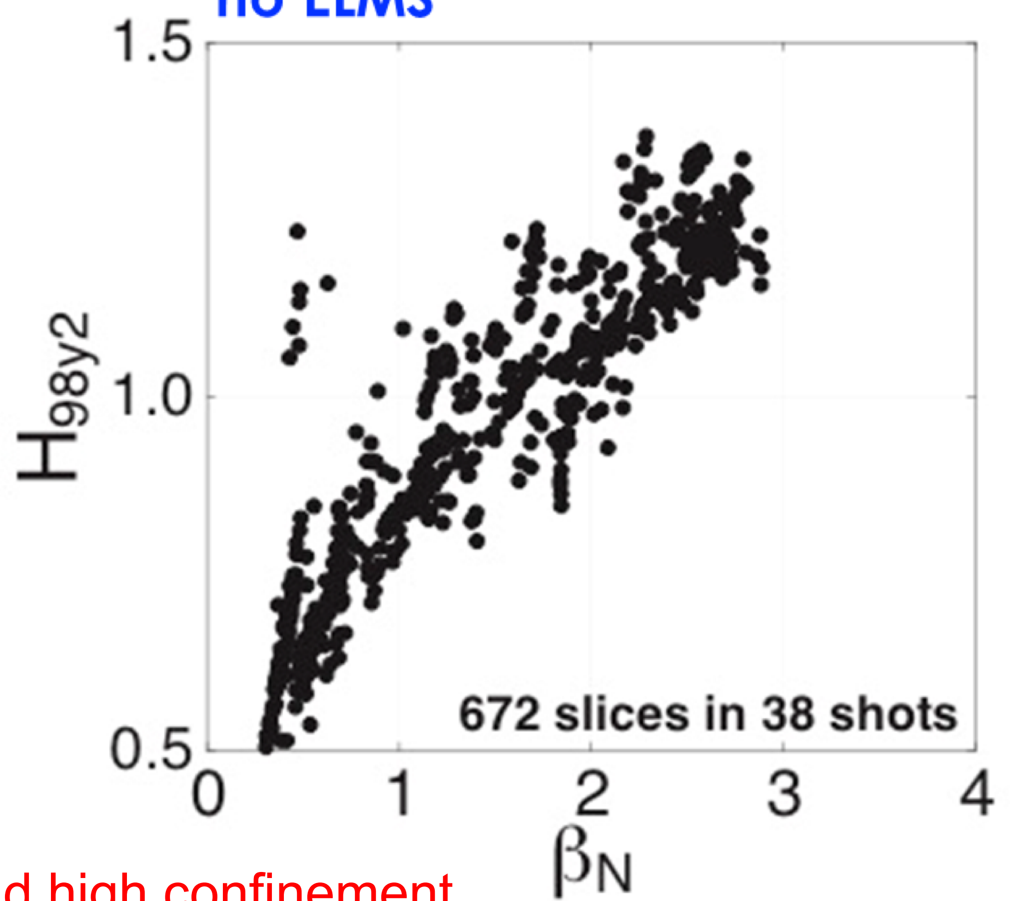

These good properties of NT, no ELMs, L-mode edge and high confinement without disruption, make it an attractive scenario for a reactor

O36: NT study [Laurie Porte]

Experimental Studies of Negative Triangularity on TCV

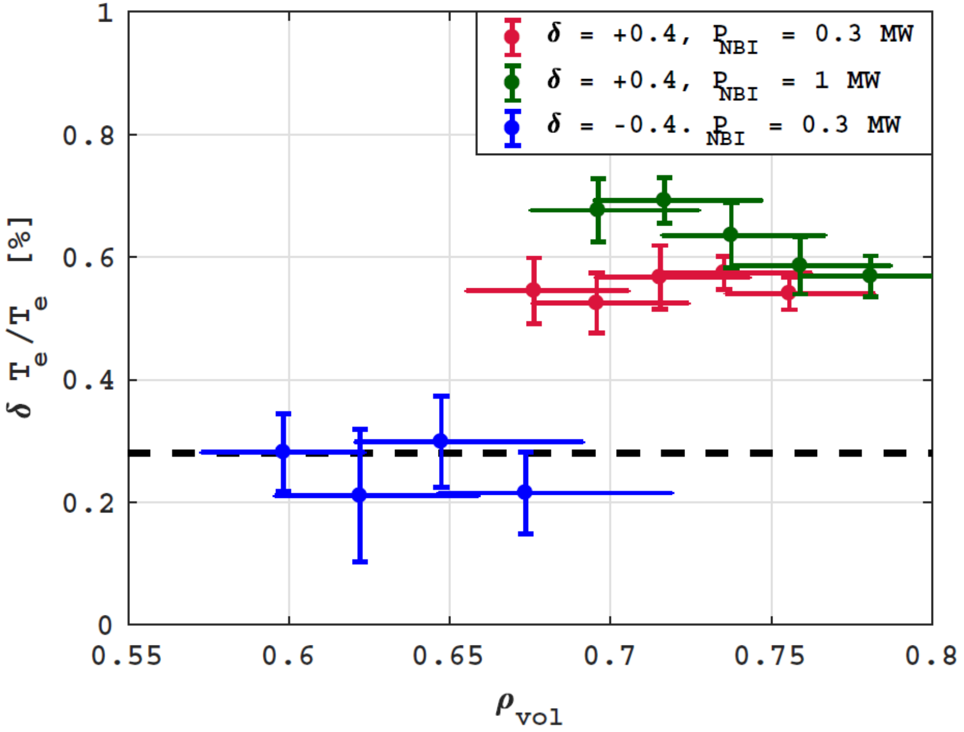

- Exceeded ITER reference β_N=1.7, exceeded $H_{98(y,2)}$ with 0.5 MW NBI
- q_{95}<3 poses no problem

Shot 63321, δ=-0.2

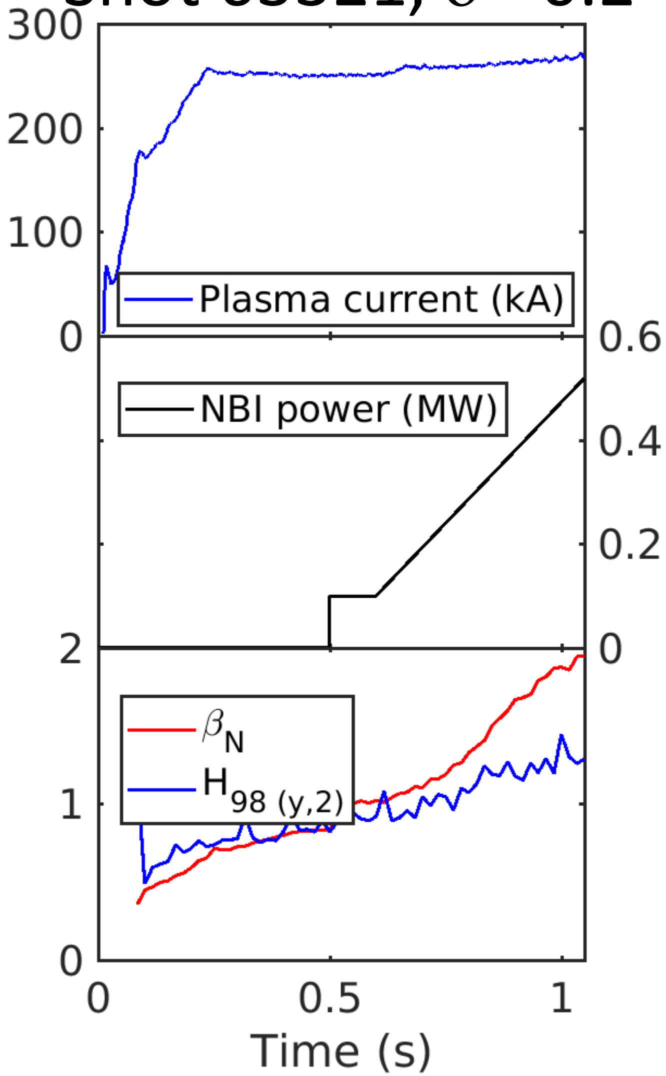

- With NBI and high collisionality, similar decrease of fluctuations at δ<0 is observed as at low collisionality with ECRH or Ω’ic heating

I36: NTT [Mitsuru Kikuchi]

Advances in physics basis of L-mode edge negative triangularity tokamak reactor

L-mode edge NTT (Kikuchi, NF2019) is reactor concept for power handling
Key is : Avoiding L-H transition, experimental and theoretical investigation of GAM/zonal flow in NT is crucially important

ITER Physics Basis, P_{LH} (MW) scales as $P_{LH} = 0.042\, n_{20}^{0.73}\, B_t^{0.74}\, S^{0.98}$.
Here n_{20}, B_t and S are electron density (10^{20} m^{-3}), TF (T), and surface area (m^2), respectively.

P_{heat}/P_{LH}~6.7 for DIII-D PT(limiter H-mode) and NT(stay L-mode edge).

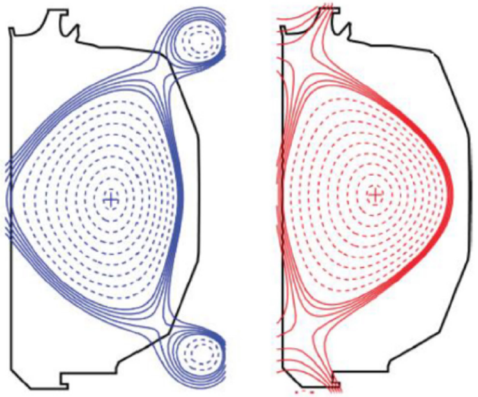

DIII-D (a_p=59cm,B_t=2T)

Austin, PRL2019
What changes L-H transition?

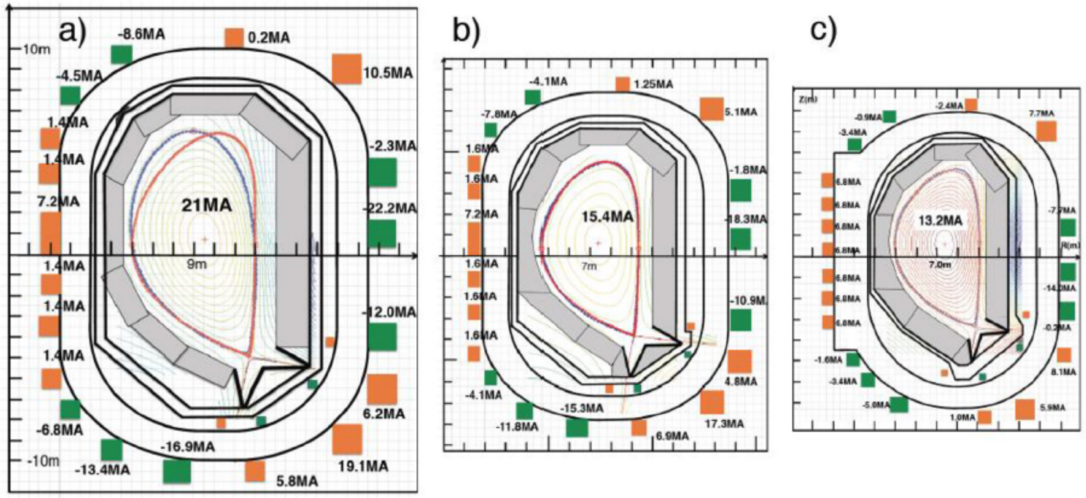

P_{heat}/P_{LH}~3.5 **P_{heat}/P_{LH}~ 2.2** **P_{heat}/P_{LH}~2.6**

O29: Scenario design [Jiale Chen]

Progress in Design of CFETR Plasma

- **Both hybrid and steady-state scenarios are developed to meet the missions of CFETR with long pulse and high fusion plasmas.**
- **Core-pedestal coupled integrated modeling simulations are performed to provided solutions with consistent current drives including .**
- **For hybrid scenario a flattened q profile in the deep core is obtained with good confinement with high density. For steady state scenario a local reversed shear is sustained to significantly reduce the transport at mid-radius which is similar to the high β_P and high density scenario developed in DIII-D/EAST joint experiment.**
- **Both scenarios is expected to be compatible with small ELMy or grassy ELMy pedestal.**

"0 D table"	Hybrid	Steady State
Pfus (MW)	940	955
Q	9.39	11.17
β_N(thermal/total)	2.06/2.28	2.41/2.72
fbs	0.45	0.68
H_{98Y2}	1.11	1.29
Pfus(MW) (NB/EC/Helicon)	100 (40/35/25)	86 (30/31/25)
Ip(MA)	13	11
<n>/nGR	1.08	1.16
Zeff	2.51	2.0
q95	5.82	7.32

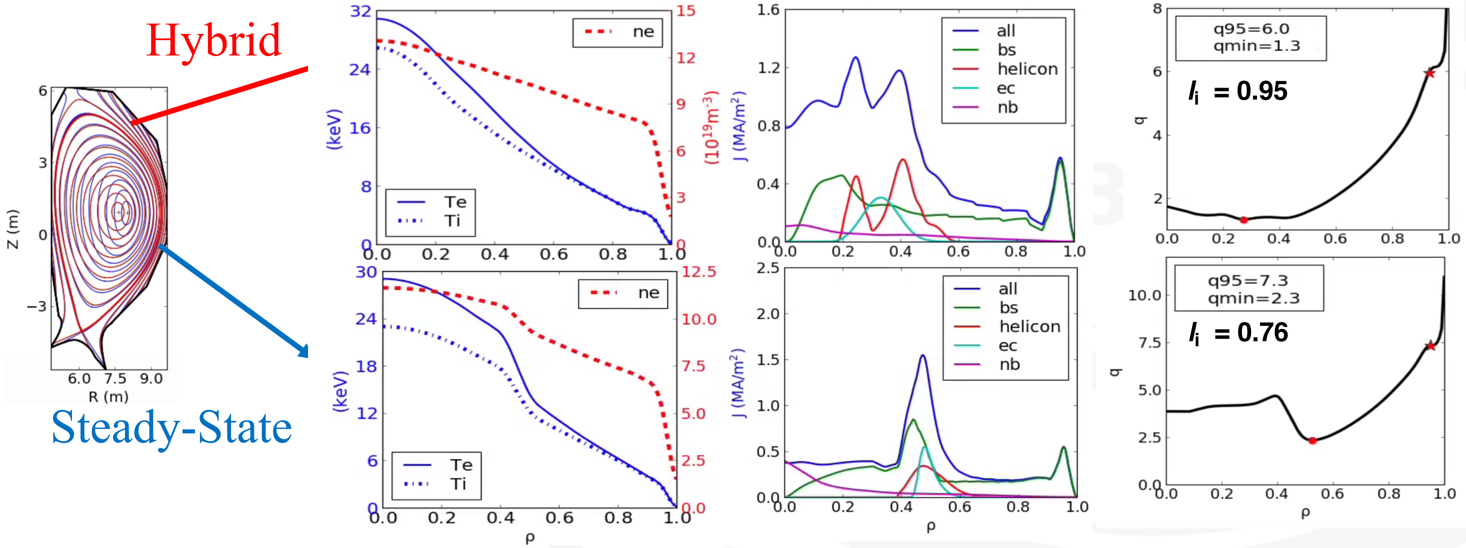

Figures: Equilibrium and profiles

O28: Scenario design [Lei Xue]

Integrated scenario analysis for HL-2M high-performance operation

- Thermal stored energy could reach 5 MJ
- β_N = 2.5 below the expected no-wall β limit (4xl$_i$=3.4)
- $T_e(0)$ = 11 keV. $T_i(0)$=8.4 keV

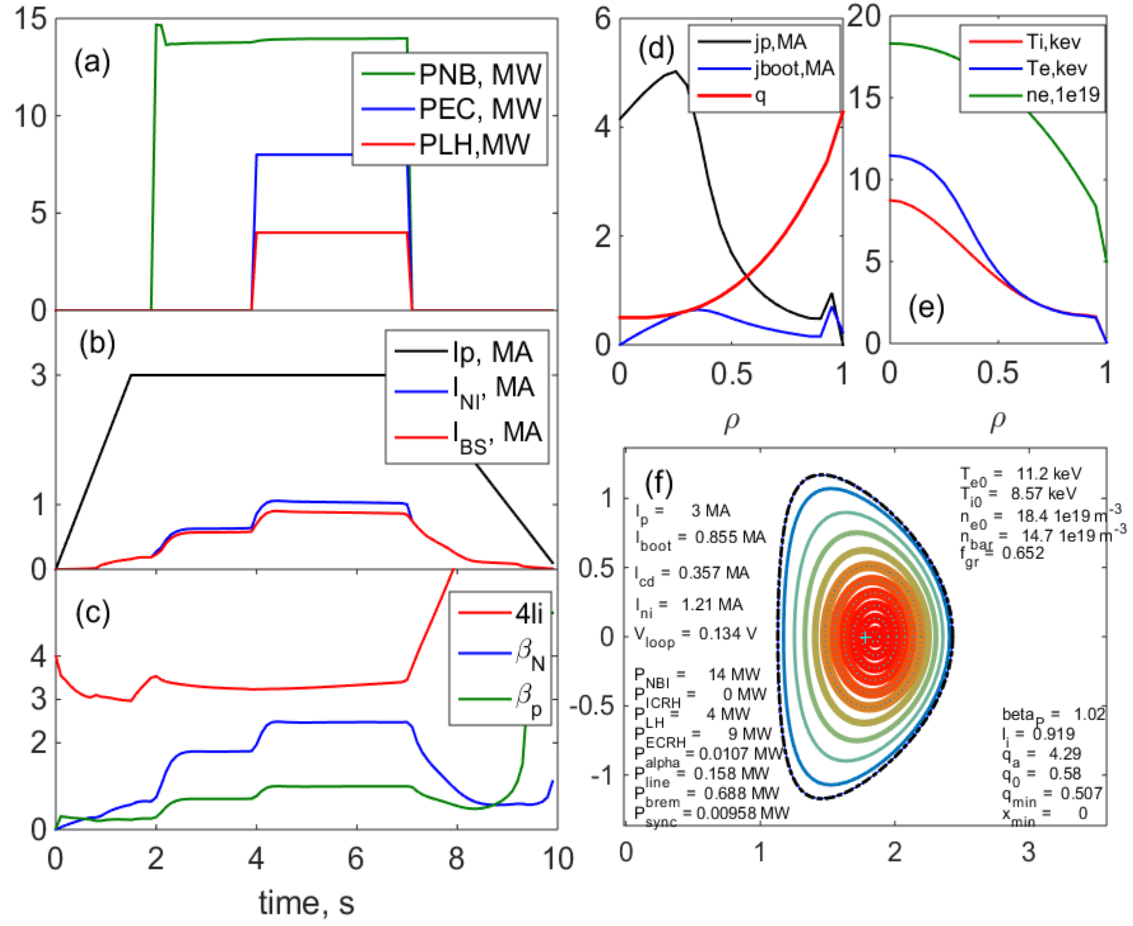

Ip(MA)/ Bt(T)	3/3
κ/δ	1.8/0.5
a/R(m)	0.65/1.78
f_G	0.65
$P_{NBI}/P_{EC}/P_{LH}$ (MW)	15/8/4
X_{EC}/X_{lh}	0.3/0.1
q_{95}	3.4
β_p	1.0
β_N /4li	2.5/3.4
f_{BS}/f_{ni}	0.28/0.34
Te0/Ti0 (keV)	11/8.4
Teped/Tiped (keV)	1.6/1.6
neped/nesep (1e19)	8.4/5
Pped (Pa)	4.0e4
W_{th} (MJ)	5
$H_{98}(y,2)$	1

The expected discharge regimes (Baseline, Hybrid and Steady-state) of HL-2M based on the integrated suite of codes METIS are presented

O26: Startup [Jiaxian Li]

Preliminary analysis of breakdown and startup conditions for the first plasma of HL-2M

$E_\phi B_\phi / B_p \geq 1000\, V/m$

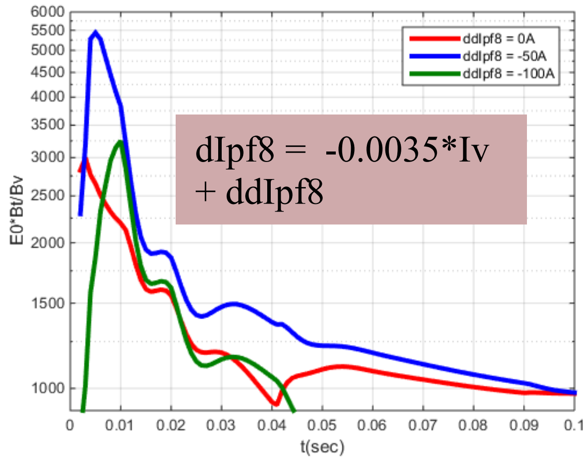

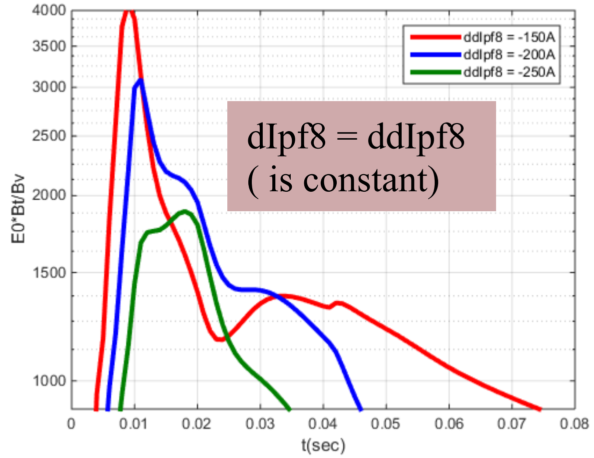

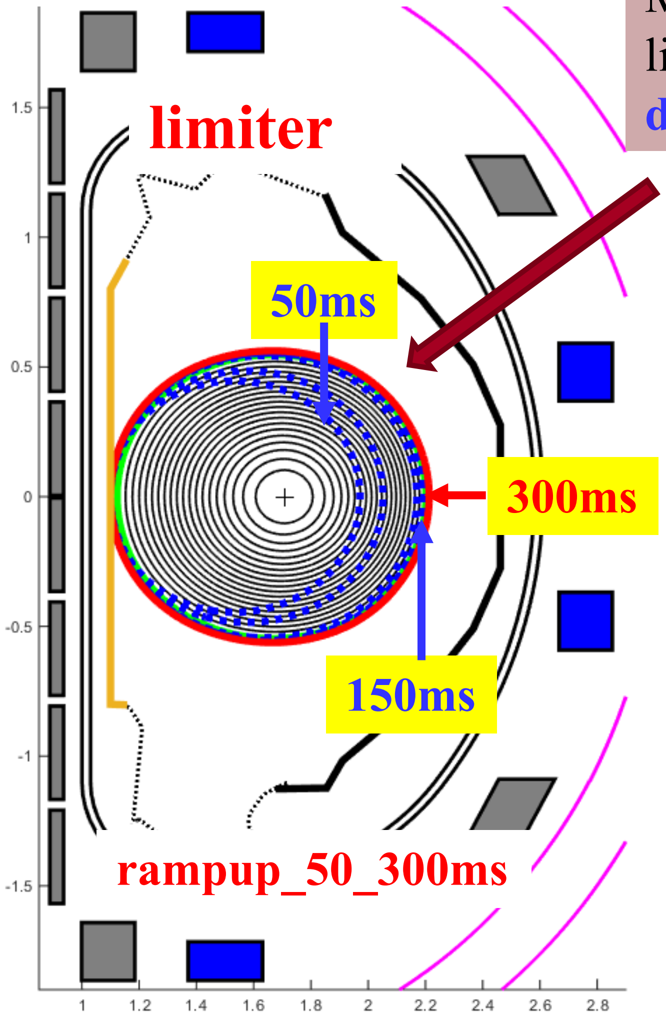

Magnetic surface evolution of limiter configuration with **dIpf8 = -0.0035*Iv - 150A**

Discharge waveform

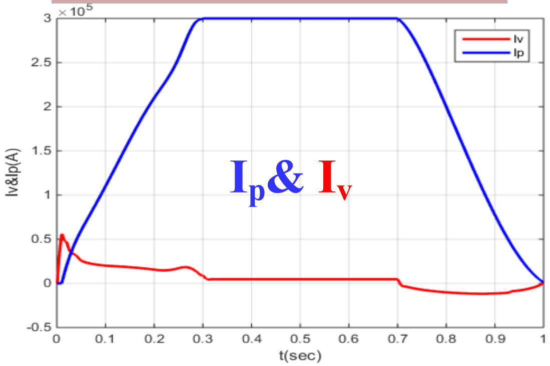

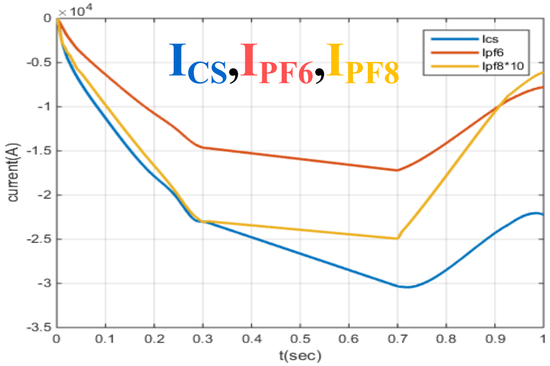

- Constraining the limiter configuration using the minimum coils (**CS, PF6 & PF8**)
- PF8 compensates the stray magnetic fields by eddy currents(I_v). Both schemes (compensation current dI_{PF8} changes with I_v or fixed value) can maintain enough time for **breakdown conditions.**

Outline

- ➲ Contributions to MF
- ➲ Major Progresses
  - ☞ Major progresses of machines
  - ☞ ELM control/simulation and RMP
  - ☞ MHD and EP physics
  - ☞ Transport and confinement
  - ☞ SOL/divertor/PMI physics
  - ☞ Scenario/Integrated model
  - ☞ Discharge Control/Diagnostics/Disruption

I17: Heat load control [Qiping Yuan]

Achievements of active feedback control of divertor heat load in EAST Plasma Control System

- EAST achieves heat load reduction by advanced divertor configuration (QSF), radiation power control, and radiative divertor induced detachment control.
- Active feedback control via particle flux, Te, or Te+Prad with D_2 fueling or divertor impurity seeding has been achieved successfully, with excellent compatibility with the core plasma performance.

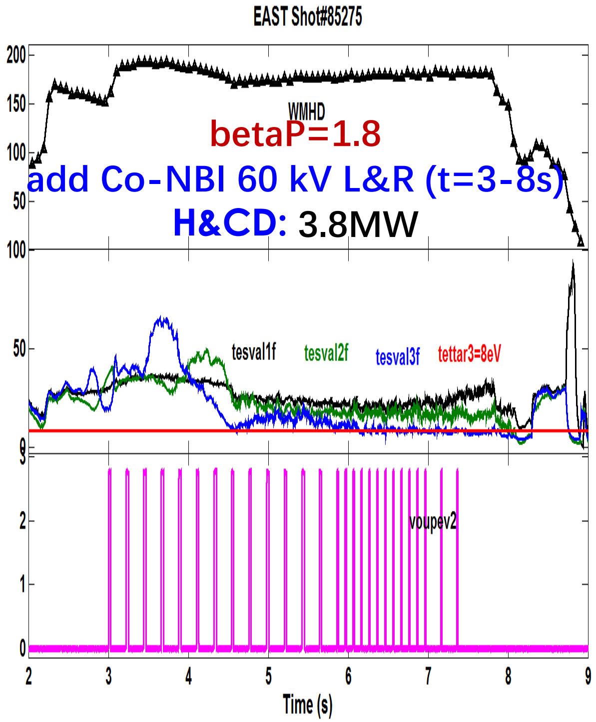

Te control: compatible with high betaP scenario

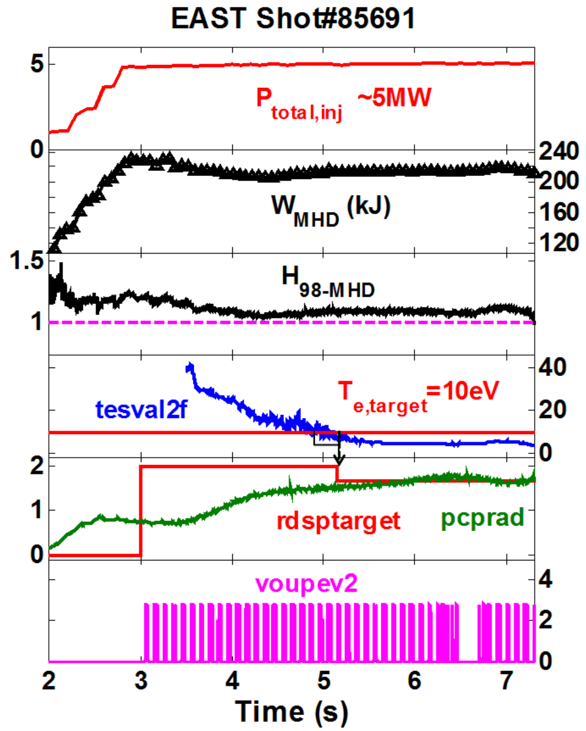

Te+Prad control: Success at high heating power P_{inj} ~ 5MW with good confinement

O39: Recycling control [Yaowei Yu]

Fuel recycling control for long pulse H-mode operation in EAST superconducting tokamak

- Various methods for recycling control in EAST
  - Baking and discharge cleaning provides a basic clean wall condition
  - Lithium coating/injection is more powerful than silicon
  - Gradual decreasing of recycling by enhanced desorption of lithium from first wall/tile gaps during long pulse operation
- 101.2 s H-mode plasmas obtained with low fuel recycling by combined recycling control methods

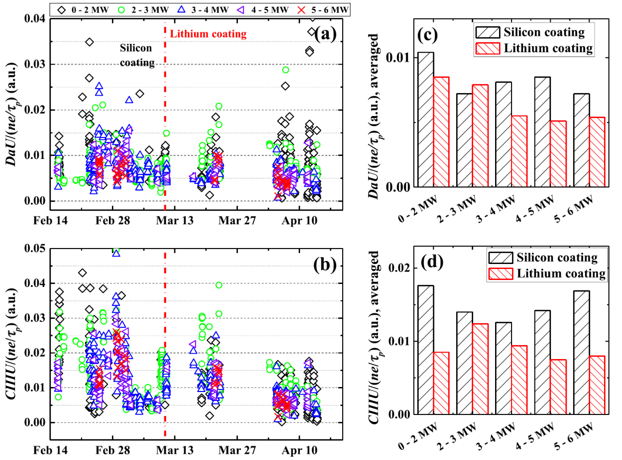

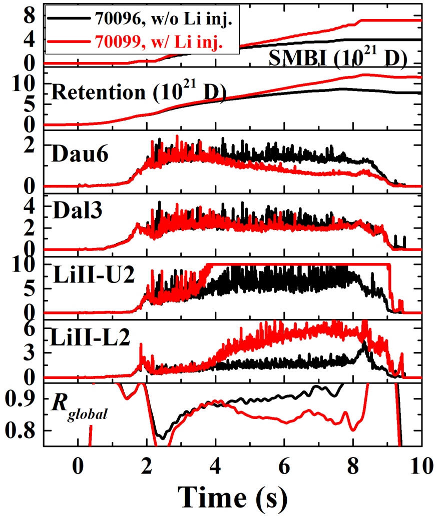

Effect of Lithium Aerosol Injection

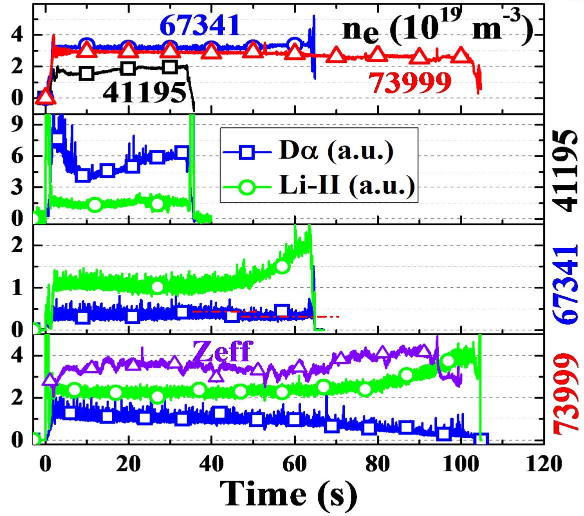

Lithium desorption for recycling control during long discharge

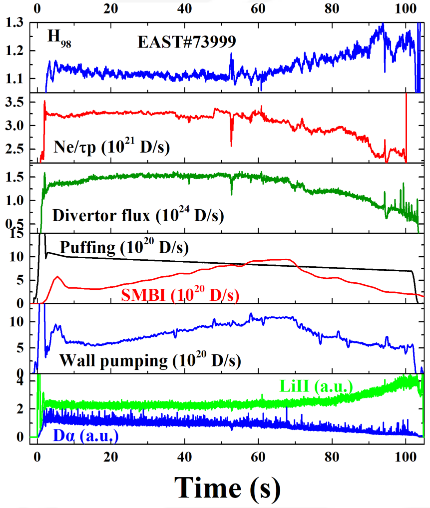

101.2 s H-mode with controlled recycling

I15: System-on-chip [Jo-Han Yu]

Revolution in Microwave Imaging of Magnetic Fusion Plasmas

Electron Cyclotron Emission Imaging

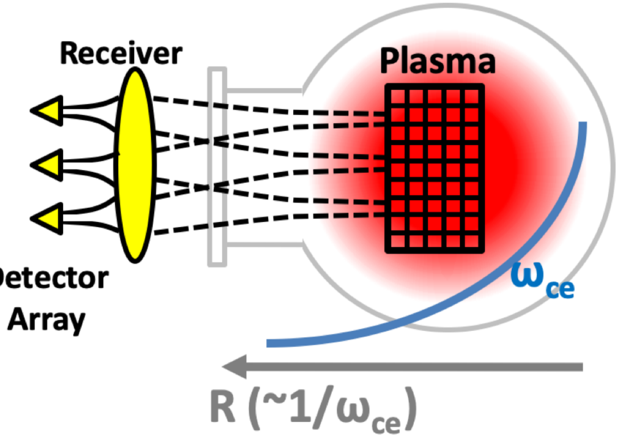

Microwave Imaging Reflectometer

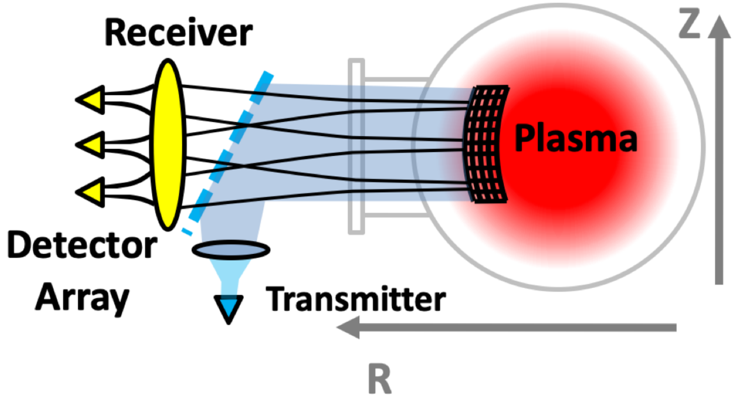

~ 10^{-3} meter

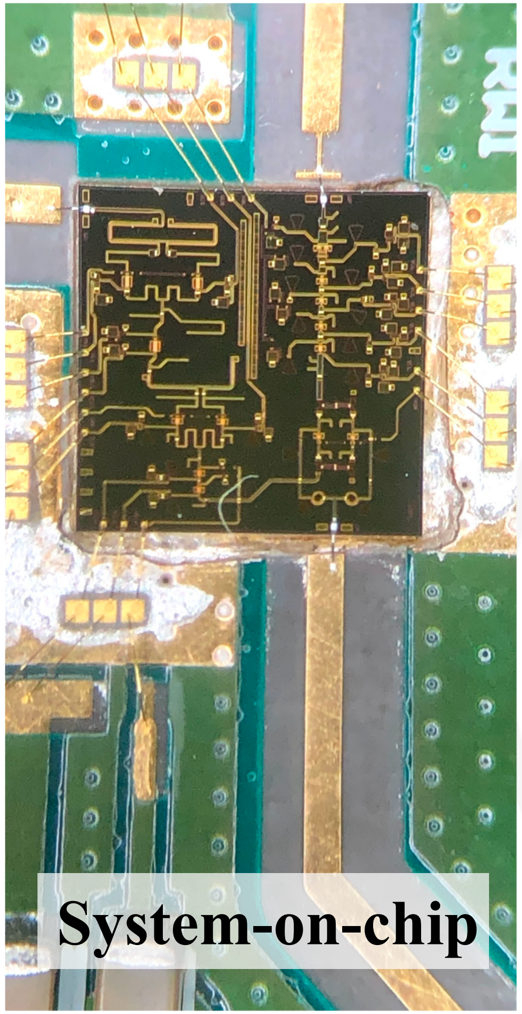

monolithic millimeter wave integrated circuit (MMIC) technology makes possible system-on-chip (SoC) solutions for Millimeter-wave plasma diagnostics

Current technology has been widely applied on a number of major tokamaks and has provided important contributions on sawtooth, Alfven eigenmodes, ELMs, etc.

Limitations:

- ❖ Noise temperature limitations
- ❖ EMI shielding performance issues
- ❖ Difficulties for repair/replacement
- ❖ High cost

✓ **Customized mm-wave chip/module design**
✓ **System integrated into individual module**
✓ **3,000 K noise temperature base line**
✓ **Employ on DIII-D tokamak in mid 2019**

O15: MW Interferometer [Bili Ling]

The design of 1mm microwave interferometer with high stability and wide dynamic range for EAST is introduced

- Microwave interferometry is an effective and reliable way to measure line integrated plasma electron density on tokamaks；
- Prototype design of a microwave interferometer for EAST has been finished on SUNIST；
- The bench test data and plasma electron density measurement result on SUNIST have verified the interferometer’s excellent phase linearity, precision and resolution；
- The extremely low noise heterodyne interferometer has been routinely operated in SUNIST;
- Plan of 1mm microwave interferometer for EAST has been decided and the key components are available.

O41: Disruption prediction [Tatsuya Yokoyama]

Data-driven study of high-beta disruption prediction in JT-60U using exhaustive search

Key parameters of high-beta disruption in JT-60U

- Results of feature extraction using exhaustive search, one of sparse modeling techniques
- Key parameters which seem to be relevant to high-beta disruption: $\beta_\mathrm{P}, q_{95}, \kappa, f_\mathrm{GW}, T_\mathrm{i}$

Disruption likelihood

- Power low like decision function: boundary between disruptive and non-disruptive

$$f_\mathrm{exp}(\boldsymbol{x}) = e^{7.45}\beta_\mathrm{P}^{5.39} q_{95}^{-8.29} \kappa^{7.40} f_\mathrm{GW}^{4.50} T_\mathrm{i}^{-0.120}$$

- Disruption likelihood against $f_\mathrm{exp}(\boldsymbol{x})$ and operational parameter region

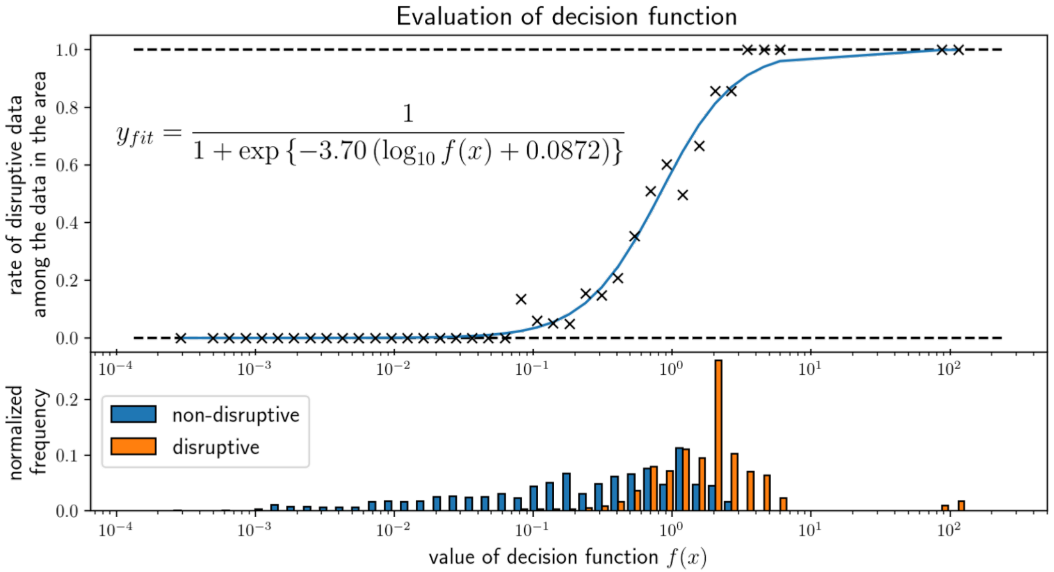

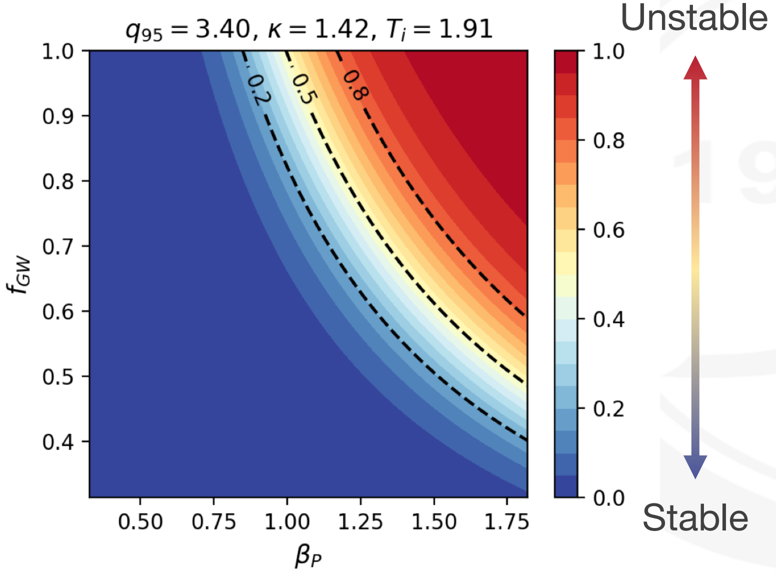

A disruption predictor model has been developed by using a support vector machine (SVM) based on high beta experiment data in JT-60U. The result will be useful to design a secure operational regime and develop control systems of fusion reactors.

Thank you!

谢谢！